CHAPTER SEVEN

CRYSTAL GROWTH IN BARIA-SILICA GLASSES

7.1 DEVELOPMENT OF CRYSTAL MORPHOLOGY IN BARIA-SILICA GLASSES

7.1.1 Optical microscopic examination of $BaO2SiO_2$ spherulites

The general appearance of crystalline particles in baria-silica glasses resembles the well known spherulites that are common in amorphous materials, such as organic polymers[138], gels and volcanic rocks[139]. The structure of the spherulite can be readily discerned by optical microscopy. Examples of optical micrographs are given in Figure (7.1). The spherulites are composed of very fine and densely packed fibrils radiating from a centre separated from one another by uncrystallized melt.

The observations agree closely with the descriptions of the crystal morphology made by Peddle[140] in a dense barium crown optical glass. It is interesting to note that Peddle, Bowen[142], and Holland and Preston[141] have described also the presence of large flat plate crystals. These may correspond to the lath-shaped crystals described by MacDowell[16] and Burnett and Douglas[15].

An alternative possibility to a radial arrangement of fibrils in the sphere is a 'wheatsheaf' arrangement of fibrils, as described by Morse and Donnay[139]. However no evidence of sheaves was observed in glass 35, either in the structural arrangement of fibrils or in general outline. By contrast, Peddle[140] and Bowen[142] have reported the existence of X-shaped crystals in dense barium crown glasses, each consisting of a sheaf of minute hair-like crystals.

The microstructure of the surface layer is similar to the spherulites in appearance. Impingement of the surface layer with internal crystals prevents the spherulitic growth from proceeding in baria-silica glasses, but in certain low nucleating glasses the spherulites can be grown to a size visible to the naked eye.

Since the cross sections of the crystals are always circular, it can be deduced that the crystals are spherical. However, less well developed

crystals are more irregular in shape and often consist of a few randomly orientated fibrils (see Figure (7.1B)). Sometimes small circular centres can be seen,particularly in high nucleating glasses (such as glass 35 see for example Figure (7.2)).

The microstructure of glass 35 heat treated at 700°C at 38, 55, 70, 87, 96 and 116 hours is shown in Figures (7.2). Small spherical particles and fibrils occur. The proportion of fibrils to spheres increases with time. At times of less than 70 hours, although numerous specks are visible, they are too small for their shapes to be discerned (i.e. whether they are spheres or fibrils).

7.1.2 Electron microscopic examination of $BaO2SiO_2$ spherulites

More detailed information is available from the electron micrographs. First to appear on the replicas are small circular particles (Figure 7.3)). In Figure (7.4) the corresponding thin section shows spheres that are composed in some cases of radiating strands of crystallites or fibres about 100 Å in diameter. In other instances the spheres appear mottled in appearance as though the radiating crystallites are protruding in a direction perpendicular to the thin film surface. In such cases the outer surface of the spherulite is probably being observed whilst in the former case the interior structure of the spherulite is probably being revealed by the thin sectioning.

The next stage in the development of the crystals starts after about 40 hours at 700°C (see Section 7.1.4) and involves nucleation and growth of spikes from the initial spheres (see Figure (7.5). The spike consists of a central spine that grows very rapidly outwards from the sphere. Radiating at right angles on each side of the spine are numerous crystallites similar in appearance to those existing in the central sphere (Figure 7.11)).

Figure 7.1A Optical micrograph of glass ABS_2 heated at 860°C for 3 hours
Mag x60

Figure 7.1B Optical micrograph of glass ABS_2 nucleated at 735°C for 8 hours and grown 834° C.
Mag x600

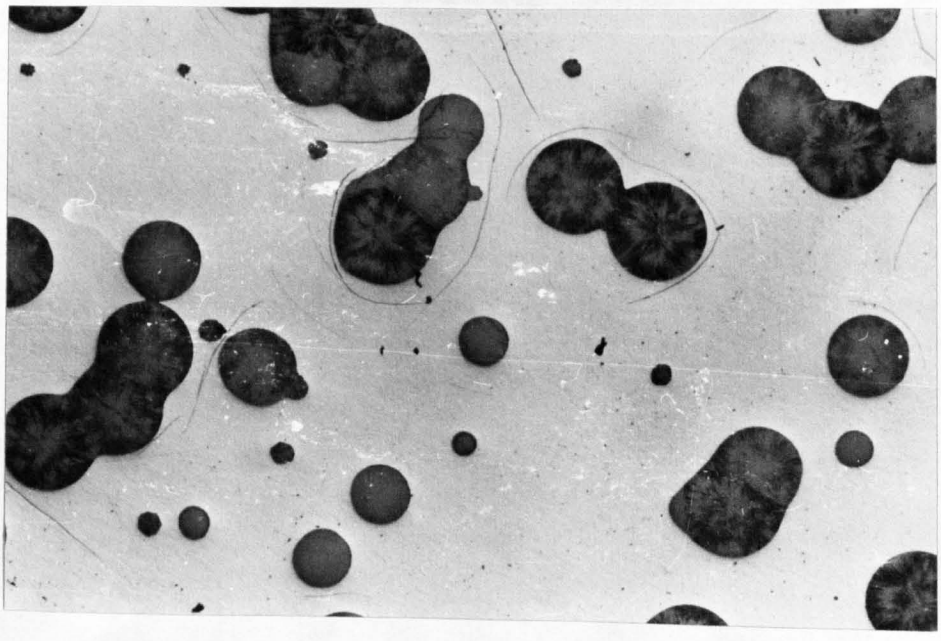

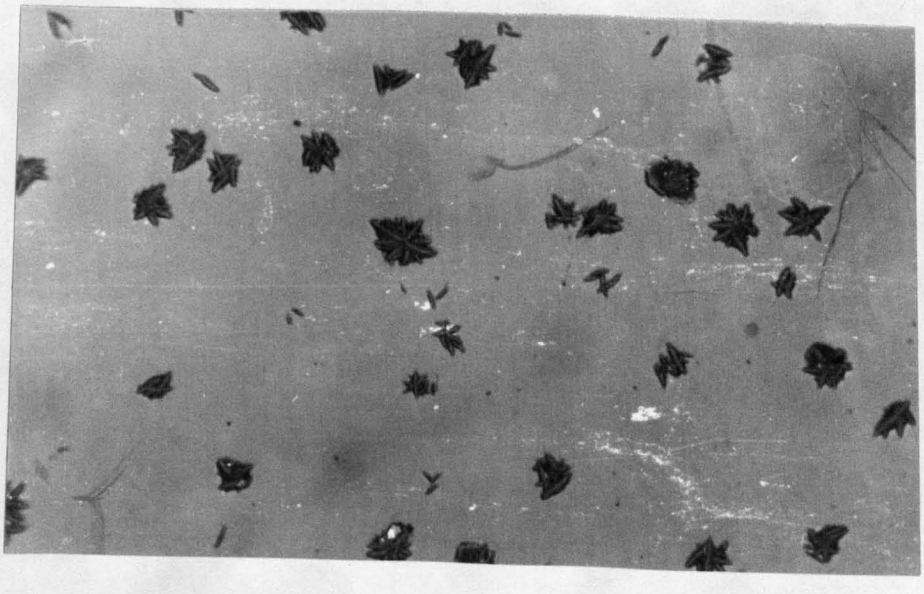

Figure 7.2 Optical micrographs of glass 35 nucleated at 700°C. No growth treatment was given.

Top left: 38 hr 15 min, Mag x600

Top right: 55 hr 05 min, Mag x600

Middle left: 70 hr , Mag x600

Middle right: 87 hr , Mag x600

Bottom left: 96 hr , Mag x600

Bottom right: 116 hr , Mag x600

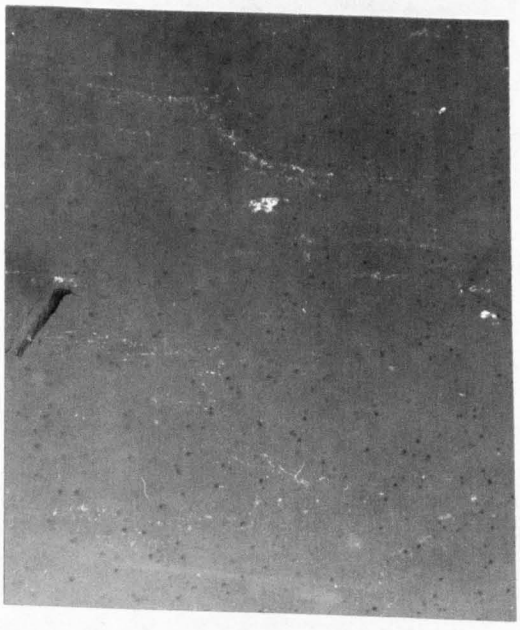

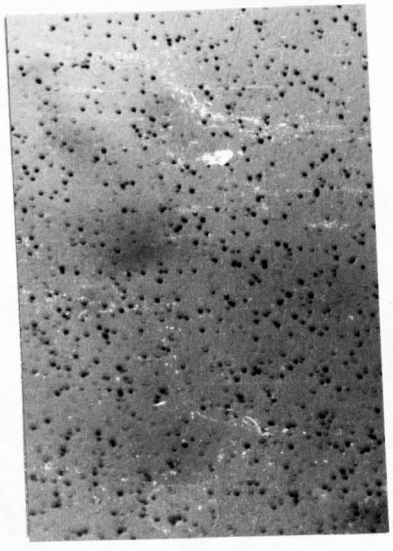

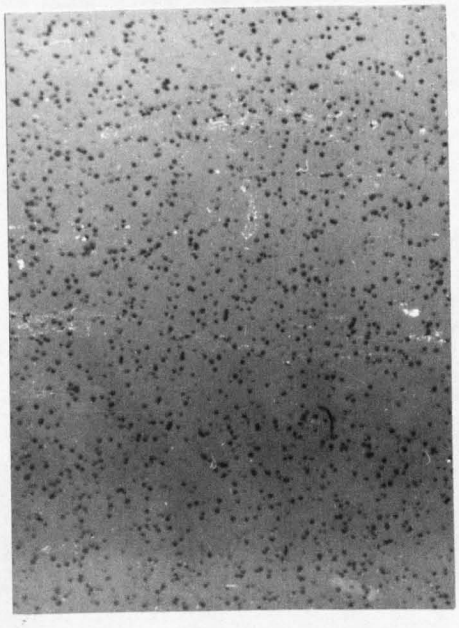

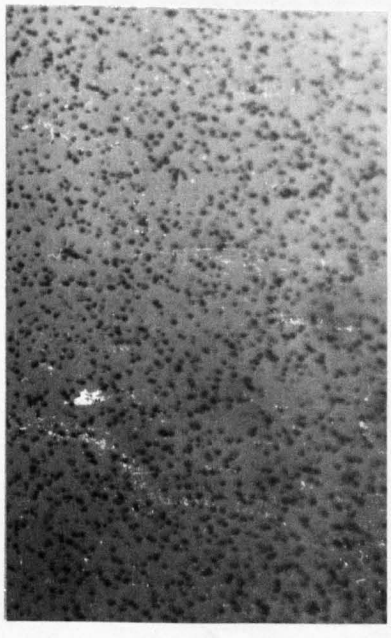

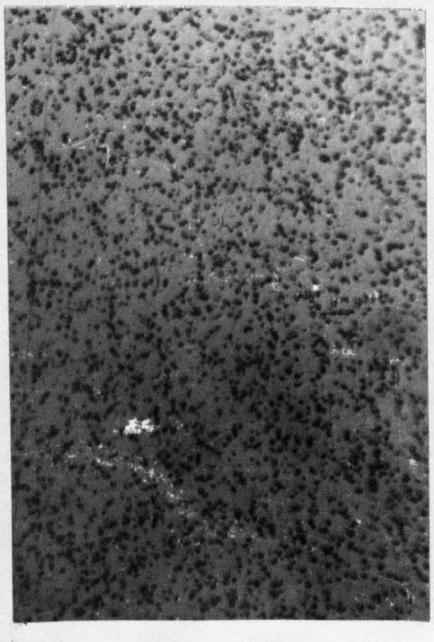

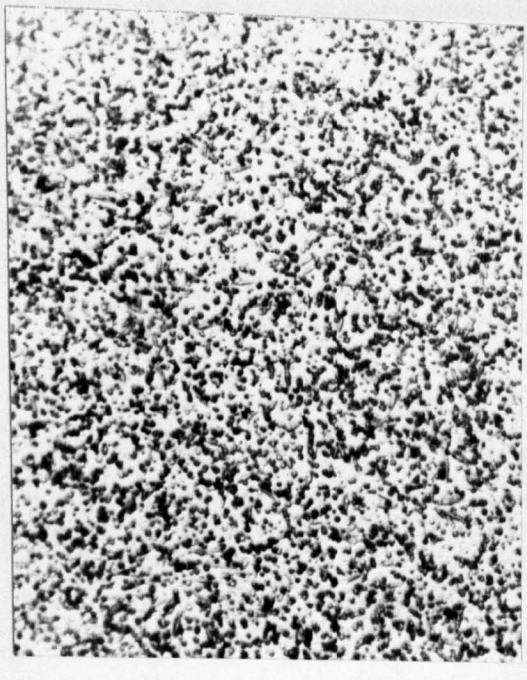

Figure 7.3 Electron micrographs of replicas of glass 35 heated at 700°C. No growth treatment was given.

From the top:

70 hr	Mag	x6400
87 hr	Mag	x6400
96 hr	Mag	x6400
116 hr	Mag	x6400
160 hr	Mag	x6400

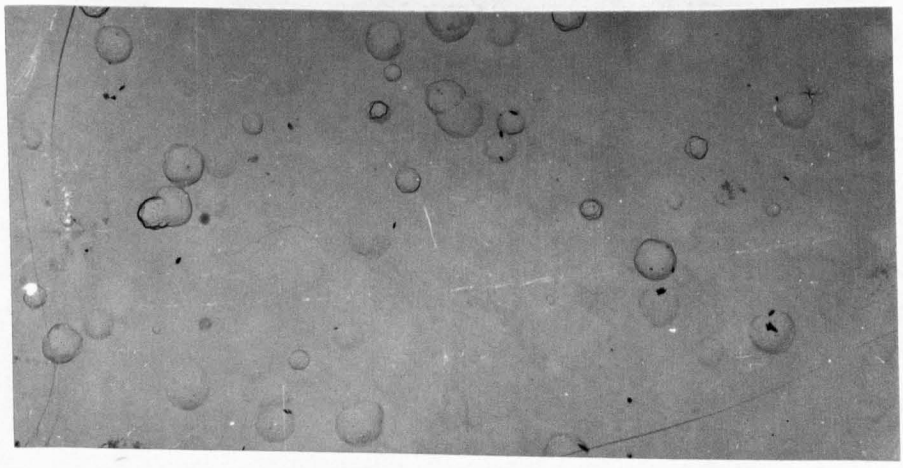

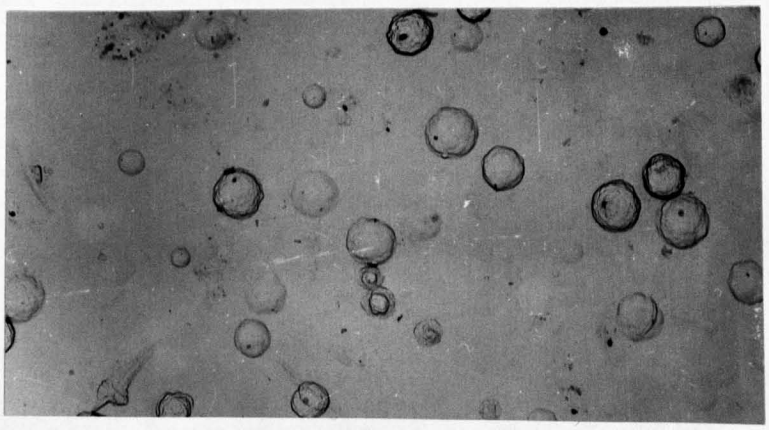

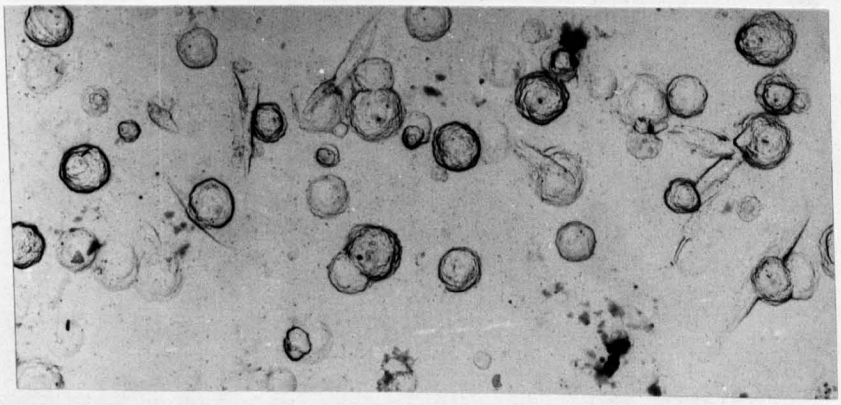

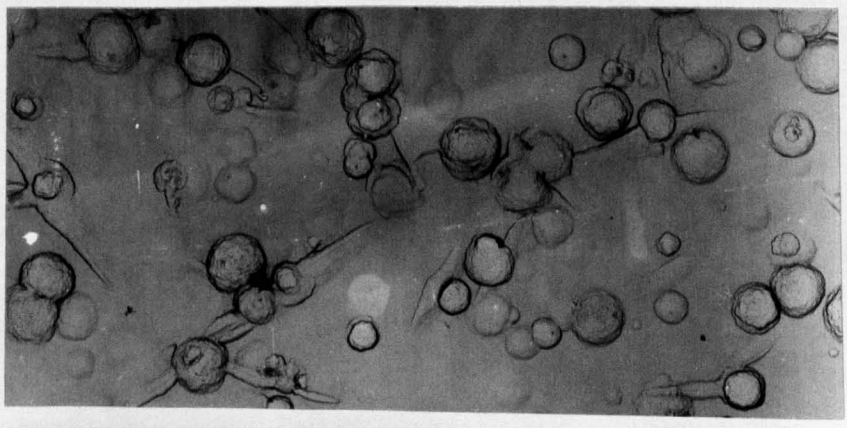

Figure 7.4 Glass 35, heated 700°C, 87 hrs
Mag x38000

Figure 7.5 (two pages)

This page, figure 7.5A, glass 35, heated 116 hrs, 700°C. Mag x29000

Second page, figure 7.5B, glass 35, heated 116 hrs, 700°C. Mag x126000

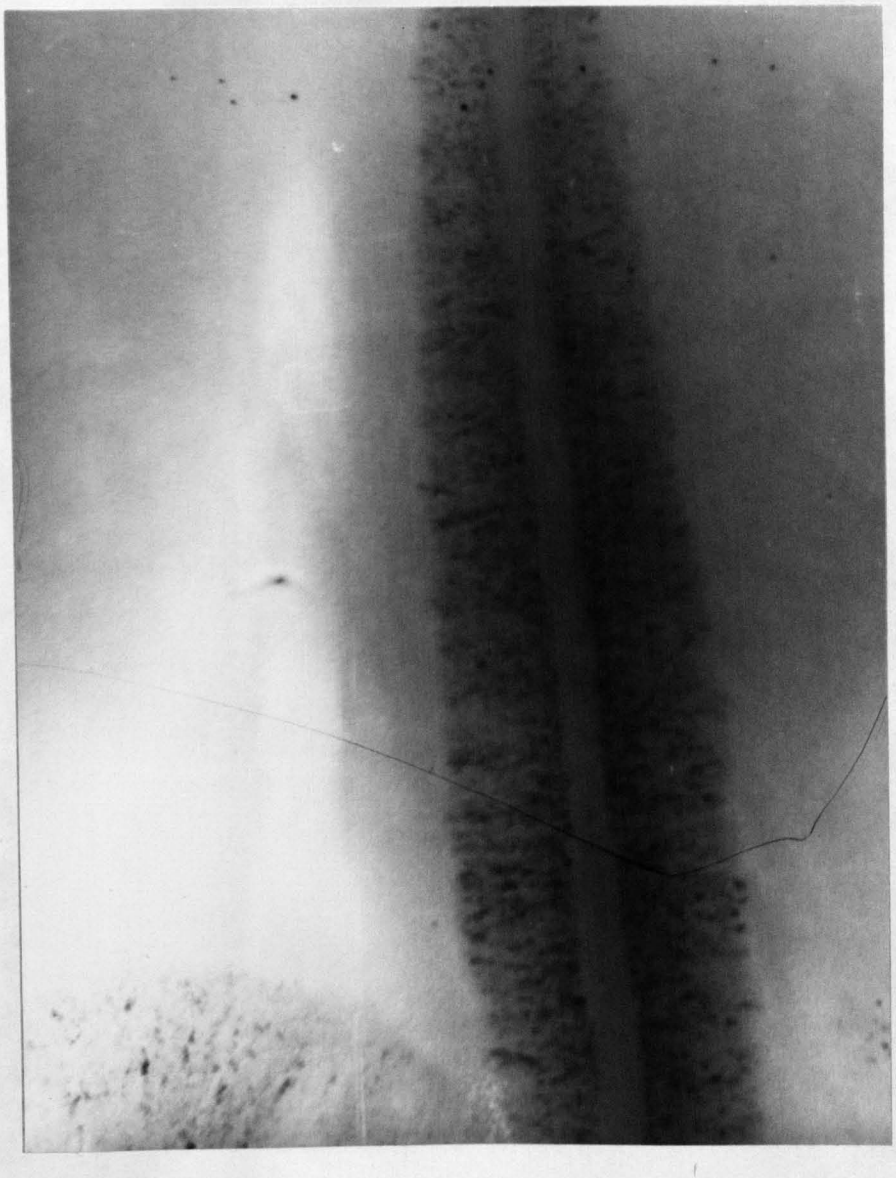

A further stage in crystallization is the nucleation of a second spike on a primary spike. This was observed only rarely because impingement of spheres and spikes occurred after 160 hours (Figure 7.6)).

Optical microscopy[18] showed that spikes continue to nucleate around the central sphere and develop until the resulting radial network constituted a larger spherulite.

The spikes often grow in radial directions from the surface of the initial sphere. However, in some instances spikes grow non-radially (Figure (7.7)). Isolated spikes are infrequently visible, though in these cases it seems likely that the primary sphere was removed during ion beam machining (Figure (7.8)). In a few cases (Figure 7.9) very short spines, containing no crystallites, can be seen protruding from a sphere but in most cases the crystallites grow almost immediately the spine forms. This is evident from the appearance of fibres at the tip. The spines are not as clearly visible near the base due to the greater thickness of the layer of fibres present. The spike is usually sharp at the tip. Most spikes are cone-shaped due to a constant ratio between the growth rates of the fibres and the spine. Blunted tips are probably caused by the intersection of the spike with the surface of the thin film (Figure (7.10)). In some cases spikes are visible with sides that are parallel in regions adjacent to the sphere, and these resemble a lentil in shape (Figures (7.7) and (7.11)). It is possible that the growth of the fibres is depressed in these areas. The rejection of impurities at the junction between the spikes and the spheres might slow down growth in this region.

Preliminary studies on the effect of liquid immiscibility on the crystal morphology were carried out on glass 33. The crystal nucleation and growth heat treatment at 700°C also induced liquid phase separation. As shown in Figure (7.12), the crystal morphology was very similar to that described for glass 35.

Figure 7.6 (two pages) This page, figure 7.6A, glass 35, heated 87 hrs, 700°C. Mag x38000

Second page, figure 7.6B, glass 35, heated 90 hrs, 700°C. Mag x20000

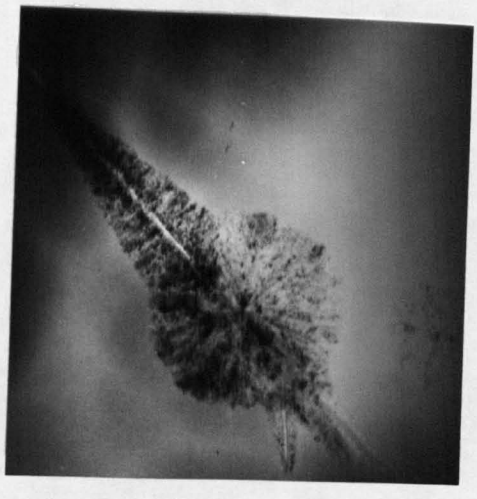

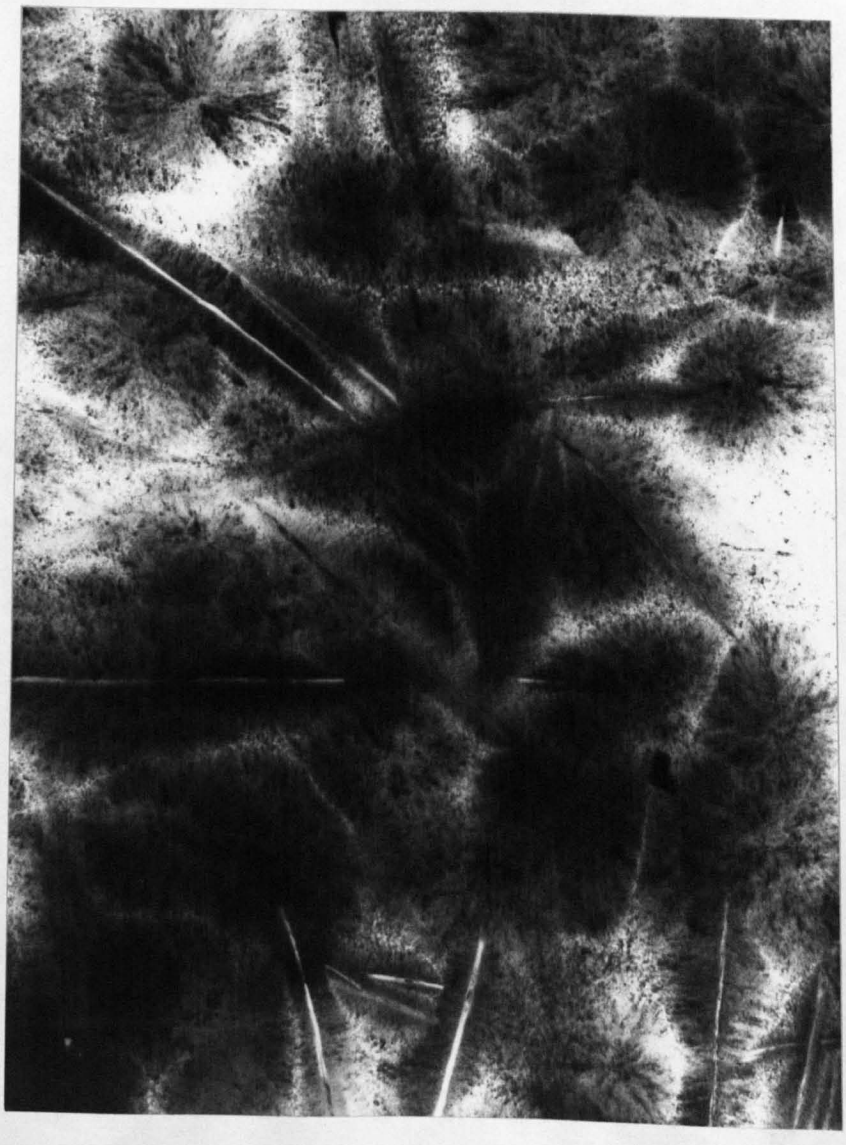

Top left, figure 7.7A, glass 35, heated 96 hrs, 700°C
Mag x38000

Top right, figure 7.7B, glass 35, heated 96 hrs, 700°C
Mag x38000

Bottom left, figure 7.8, glass 35, heated 87 hrs, 700°C
Mag x38000

Bottom right, figure 7.9, glass 35, heated 96 hrs, 700°C
Mag x38000

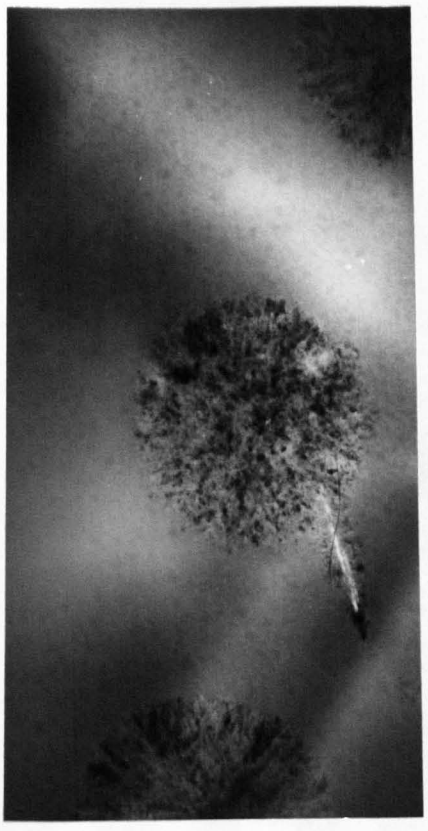

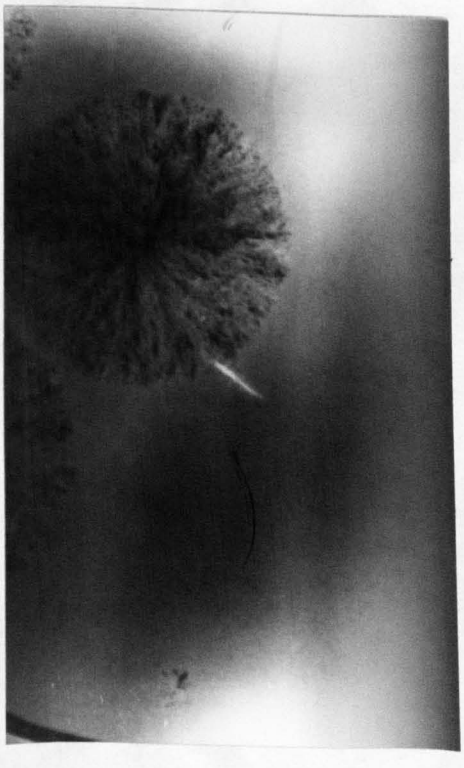

Figure 7.10 Glass 35, heated 116 hrs, 700°C
Mag x303000

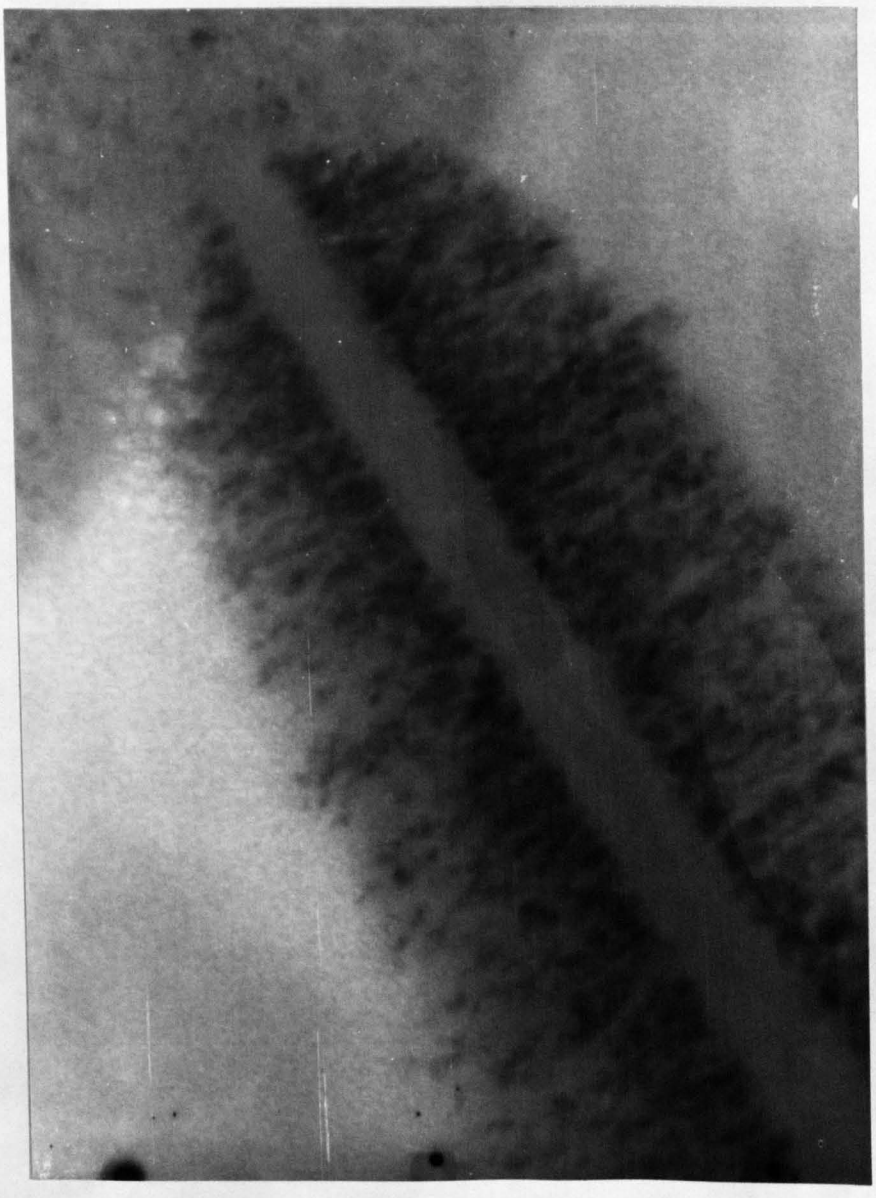

Figure 7.11 Glass 35, heated 87 hrs, 700°C
Mag x38000

Figure 7.12 Electron micrographs of crystals in glass 33, 10^3 kV

Top left heated 80 hrs, 700°C, sphere Mag x64000

Top right: heated 94½ hrs, 700°C, sphere and spike, Mag x41000

Bottom left: heated 80 hrs, 700°C, three spikes, Mag x26000

Bottom right: heated 94½ hrs, 700°C, spikes Mag x24000

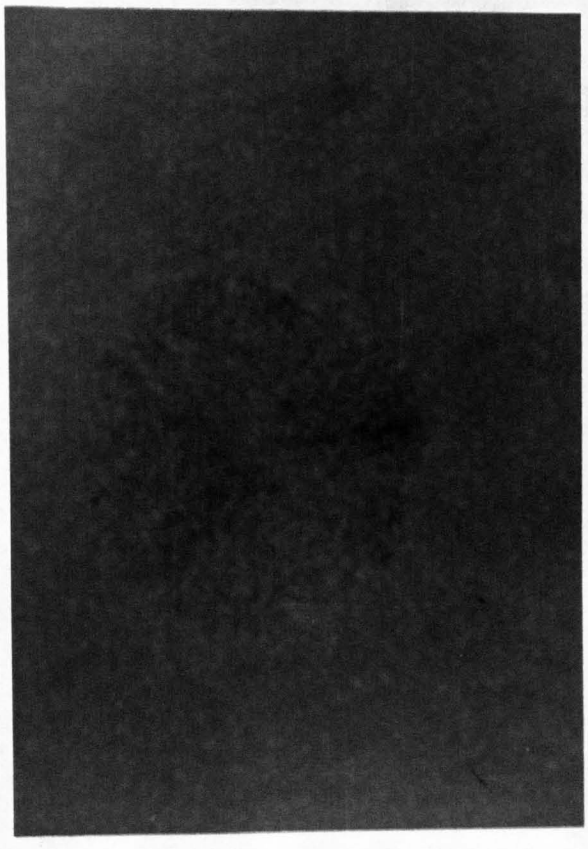

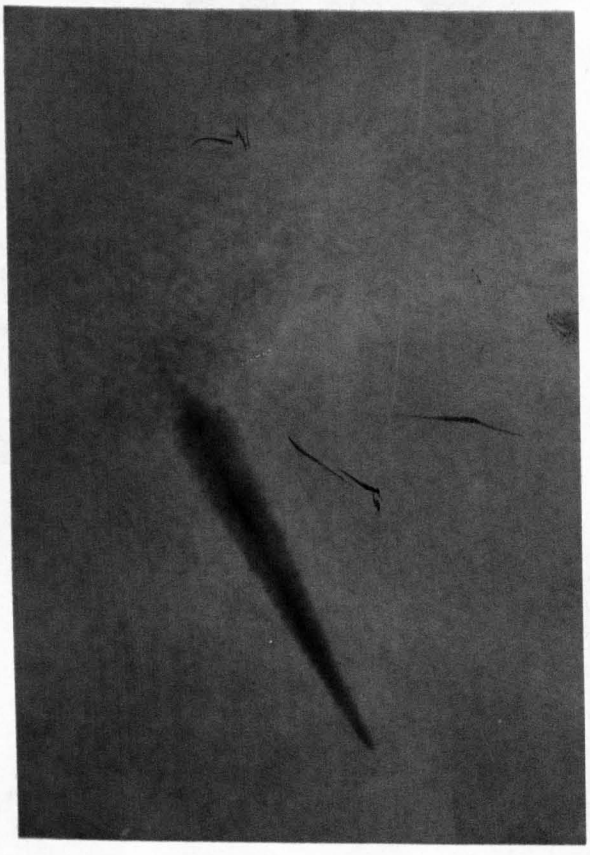

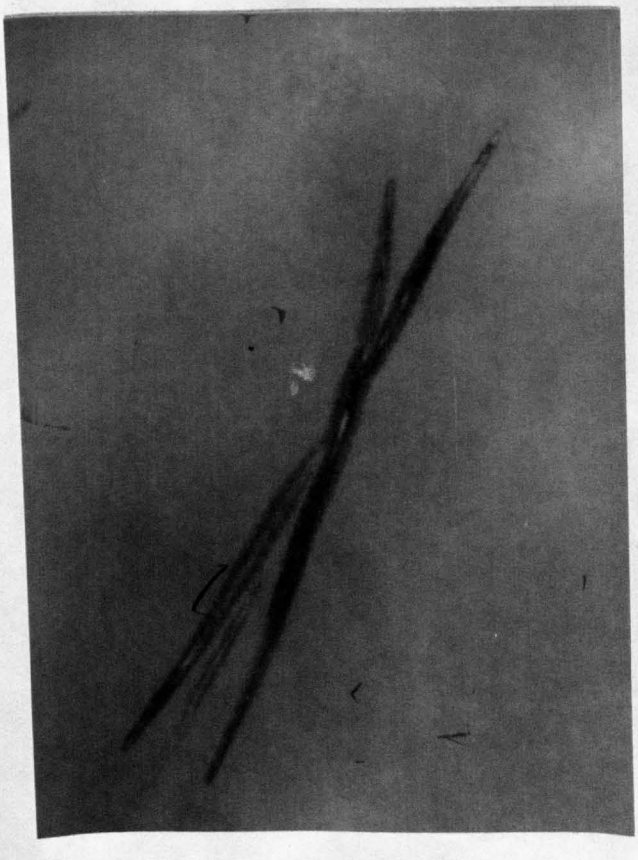

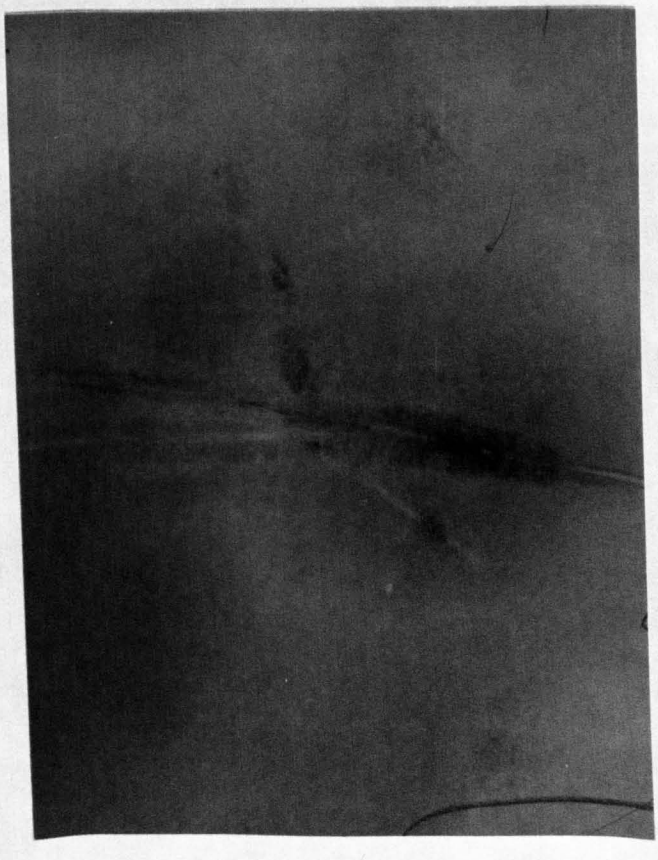

7.1.3 Selected area electron diffraction (S.A.D.) and x-ray diffraction

Several of the glasses were crystallized and examined by x-ray diffraction. The results are summarised in Table (7.1)). There is definite evidence of the presence of 1-BS_2 in glass 33 heat treated at 860°C for 16 hours. Unfortunately the x-ray peaks for heat treatments at 805 and 764°C were broad, diffuse and few in number and so it was difficult

TABLE 7.1

X-RAY DATA

Glass Number	Heat Treatment	Phases identified
37	237 hours at 940°C	1-$BaO2SiO_2$ (Major)
		$5BaO8SiO_2$ (Minor)
35	237 hours at 940°C	1-$BaO2SiO_2$
33	70 hours at 920°C	1-$BaO2SiO_2$ traces cristobalite
	16 hours at 860°C	1-$BaO2SiO_2$ traces cristobalite
TBS_2 (33 mol% BaO, 66% SiO_2 1% TiO_2)	16 hours at 964°C	1-$BaO2SiO_2$ traces cristobalite

to identify the crystal phase at these heat treatments. The diffuse peaks may be due to the glass being only partially crystallized. Although the spherulites have reached the impingement stage glass may still be trapped

between the crystallite in the sphere and may not crystallize until the spherulite to lath transformation occurs. A more likely explanation of the broad peaks is the small dimension of the crystallites. Sharper peaks will be obtained only after recrystallization occurs when the effective crystallite size increases.

The crystallinity of the spheres is shown by the presence of arcs and circles on the selected area electron diffraction pattern (SAD) (see Figure (7.13)). The absence of a single crystal pattern consisting of a regular array of spots showed that the sphere is polycrystalline. The arcing of reflections could be due to some preferred orientation of the crystallites or fibres. In the case of a thin section through one of the spheres, only part of the radiating structure will be included. The fibres in the thin section will not be orientated radially in all possible directions. Thus the diffraction pattern will indicate preferred orientation. It has been mentioned that the apparent morphology of a sphere (i.e. mottled or radiating) may depend on whether the surface of the thin section intersects the sphere. However, no obvious relation between the appearance of the spheres and the SAD pattern could be found.

Selected area diffraction patterns of spikes are composed of both sharp discrete spots (sometimes present as a two dimensional cross-grating pattern) and broader arced spots. This indicates a fairly highly orientated structure (Figure (7.13)).

Two major problems associated with the selected area electron diffraction patterns and their interpretation were: a) the susceptibility of $BaO2SiO_2$ crystals to beam damage at high accelerating voltages, thus limiting the length of time that a crystal could be exposed to the beam, b) the existence of broad spots and arcs preventing accurate estimation of 'd' values in some instances.

All the SAD patterns of the crystals (over 40 were measured) could be assigned to barium disilicate but in most cases the crystal form (h or l) could not be decided. Table (7.2) gives a list of the 'd' spacings for the two forms (reference (40)). Many of the 'd' spacings are very close, which makes distinguishing the two forms difficult. In a few cases positive identification of hBS_2 was made. Two examples are shown in Figure (7.14). Three spot patterns from spikes could be definitely indexed for $h\text{-}BS_2$ (one of the 'd' spacings 5.51, 4.11, 3.53 Å was present). The presence of $h\text{-}BS_2$ in the spikes was definitely established. There was also strong evidence that the spheres were also $h\text{-}BS_2$ since two ring patterns definitely included $h\text{-}BS_2$ reflections.

These observations only partly agree with those of Burnett and Douglas[15], who suggested that the spheres were composed of $h\text{-}BS_2$ and the spikes of the low form. However these authors did not use selected area electron diffraction and relied on comparison of replicas with powder x-ray patterns.

This contradiction leads us to examine again, very carefully all the electron diffraction patterns. In only one case, for a selected area including a spike, were reflections present that could only be indexed for $l\text{-}BS_2$. This would suggest that the spikes contain both forms of BS_2.

In order to reconcile our observations with those of Burnett and Douglas[15] it is tentatively suggested that the spines of the spikes composed of $l\text{-}BS_2$ but the crystallites or fibres growing from the spines are of $h\text{-}BS_2$. Additional support for this interpretation is provided by the similar morphology of the crystallites in the spikes to the crystallites in the spheres, and as we shall see shortly, their closely similar growth rates.

The extent of line broadening on the SAD pattern from the spheres was

Top left, figure 7.13A. Typical SAD of a sphere, glass 35, heated 116 hrs, 700°C, 100 kV

Top right, figure 7.13B. Typical SAD of a spike, glass 35, heated 116 hrs, 700°C, 100 kV

Bottom left, figure 7.14A. SAD pattern of spike from which h-BS_2 was identified, glass 33, 80 hrs 700°C, 10^3 kV

Bottom right, figure 7.14B. SAD pattern of spike and sphere from which both h- and ℓ-BS_2 were identified, glass 35, 116 hrs, 700°C, 100 kV.

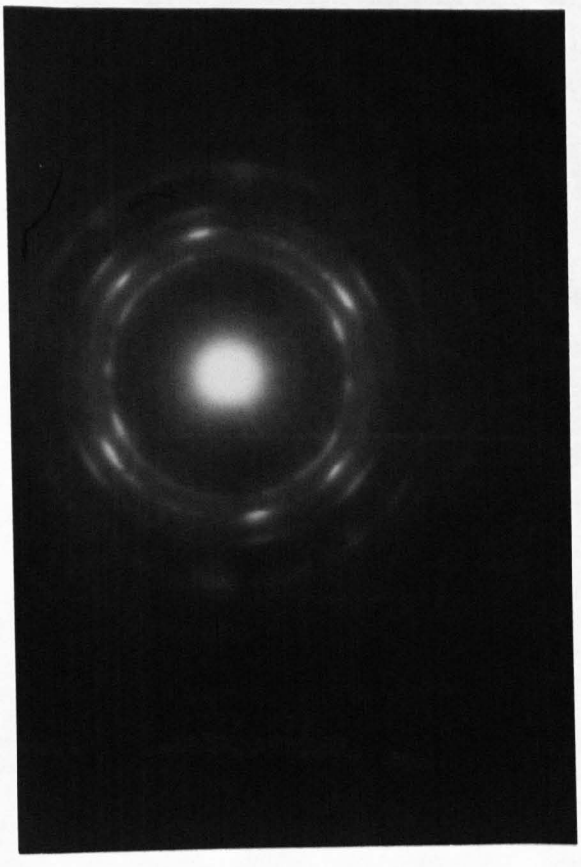

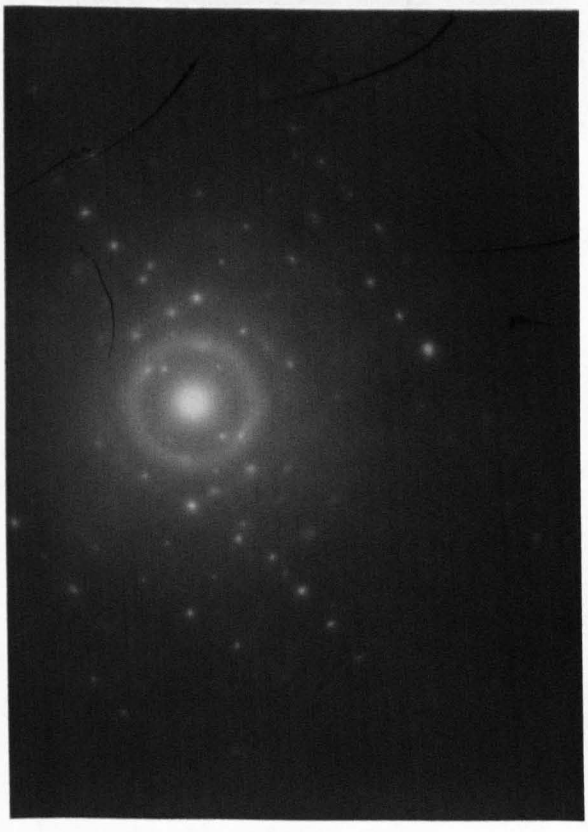

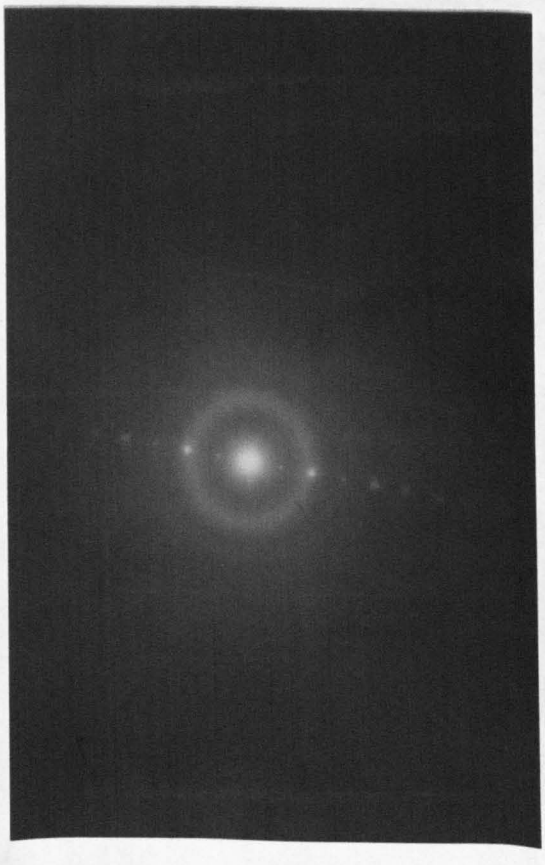

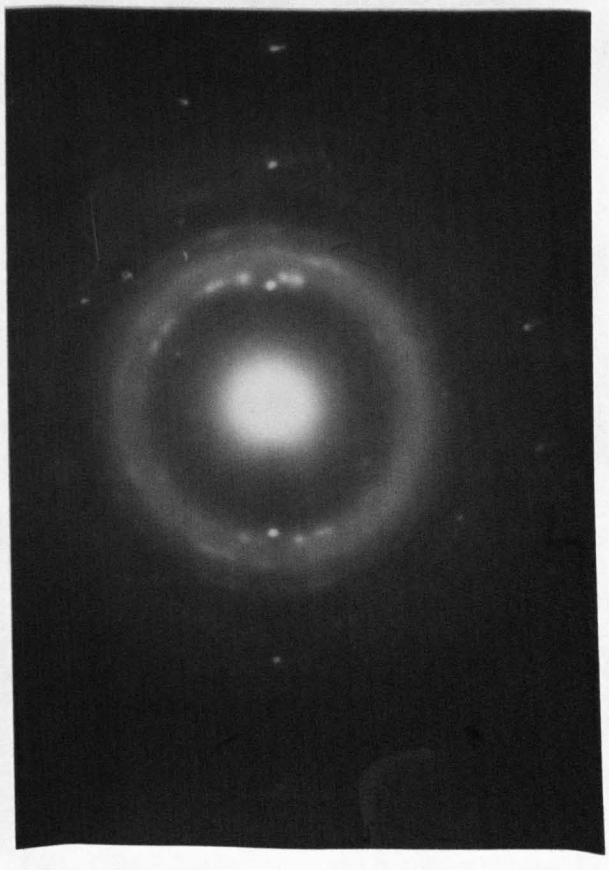

TABLE 7.2

CRYSTALLOGRAPHIC DATA OF h- AND l-BS_2

Low $BaO2SiO_2$

a = 7.689 Å c = 13.522 A w = weak vw = very weak

b = 4.6311 Å orthorhombic m = medium

s = strong vs = very strong

hkl	'd' space Å	strength	hkl	'd' space Å	strength
002	6.76	m			
012	5.07	ms	202	2.191	m
101	4.38	vw	211	2.188	w
110	3.97	vs	016	2.162	mw
020	3.84	vw	132	2.128	s
102	3.82	vw	212	2.108	m
111	3.807	wm	203	2.058	vw
112	3.423	s	034	2.042	mw
004	3.377	w	106	2.026	ms
022	3.341	vs	133	2.008	vw
103	3.229	m	213	1.990	m
014	3.093	s	125	1.997	vw
113	2.975	w			
121	2.891	wm	220	1.983	w
104	2.730	sm	221	1.962	vw
122	2.710	s	116	1.960	vw
114	2.572	m	026	1.945	vw
024	2.537	w	040	1.9225	m
123	2.472	vw	204	1.9107	vw
131	2.42	vw			
032	2.395	w	222	1.9037	m
105	2.334	w	134	1.8680	vw
200	2.316	m	214	1.8543	m
201	2.283	vw	042	1.8493	w
006	2.255	mw	223	1.8151	vw
130	2.243	w	126	1.7915	ms
115	2.235	sm	117	1.7354	w
124	2.226	m	224	1.7093	wm
231	1.7042	wm	008	1.6916	m
232	1.6660	w	143/ 018	1.6513	w
225	1.5997	wm	108	1.5878	w
216	1.5806	m	144	1.5718	m

High $BaO2SiO_2$

a = 23.202 Å, b = 4.661 Å, c = 13.613 Å, monoclinic β = 97.54°

hkl	'd' space Å	strength	hkl	'd' space Å	strength
002	6.77	m	314	2.493	vw
202	6.20	w	514	2.466	vw
400	5.76	vw	712	2.408	w
202	5.51	s	115	2.354	w
402	4.69	m	020	2.329	m
402	4.11	ms	115/ 021	2.296	w
310	3.980	vs	514	2.247	m
311	3.890	vw	714	2.220	m
600/ 112	3.832	w	022	2.202	s
311	3.751	vw	515	2.186	w
112	3.739	vw	206	2.154	vw
312	3.534	s	222	2.145	w
312	3.344	m	422	2.096	w
113	3.245	m	023	2.069	vw
113	3.165	vw	804/ 223	2.059	vw
602	3.159	m	912	2.056	m
204	3.127	m	116	2.039	w
511	3.117	vw	422	2.028	vw
404	3.091	m	223/ 715	2.015	w
512	3.058	w	515	1.9943	w
313	2.887	vw	423	1.9881	w
512	2.841	s	622	1.9454	m
802	2.782	w	224	1.9155	m
513	2.775	w	423/ 11.1.0	1.9099	vw
114	2.745	s	11.1.2/ 806	1.8949	vw
604	2.715	vw	622	1.8764	m
114	2.683	vw	623/ 224	1.8682	m
314	2.665	w	424/ 11.1.1	1.8599	m
712	2.591	s	716	1.8219	w
802	2.529	w	821	1.8153	m
516/ 623	1.7775	m	624	1.7685	vw
10.0.6	1.7251	w	822	1.7134	w
208	1.7001	w	11.1.3/ 008	1.6854	vw
806/ 13.1.1	1.6680	w	10.2.1/ 14.0.0	1.6447	vw
10.2.2	1.6266	vw	026	1.6184	vw
10.2.1	1.6093	w	426/ 517	1.5976	m
226/ 11.1.4	1.5818	w	131	1.5419	m
10.2.5/ 133	1.4621	vw	12.2.1	1.4570	m

used to determine the crystallite size. The following equation[145] was employed for this purpose:

$$t = \frac{0.9\ \lambda}{B\ \cos\theta}$$

where λ is the wavelength of the electron beam (.039 Å at 100 kV accelerating voltage), B is the half width of the spot (in radians) and 2θ is the diffraction angle (in degrees). The average crystallite size was calculated approximately as 100 Å. This agreed with the crystal size obtained from the broadening of the x-ray peaks diffracted from glass 33 heat treated at 805°C for 17 hours. However, when glass 33 was heat treated at high temperatures the apparent crystallinity increased and the peaks narrowed. On heat treatment at 940°C for 23 hours a crystal size of approximately 750 Å was calculated.

7.1.4 Early stage growth kinetics of $BaO2SiO_2$ in glass 35 at 700°C

The sizes of the longest spikes and the largest 'primary spheres' were measured from the electron micrographs for a series of heat treatment times at 700°C. These values are plotted in Figure (7.15). Approximately straight line relations were observed. The growth rates in Table (7.3) are compared with the overall crystal growth rate at 700°C extrapolated from Rowlands' data[18] on glass 35G (Figure 7.16)).

The growth rate of the sphere radius and the lateral growth rate of the spikes are very similar, and both are small compared with the longitudinal growth of the spikes. This supports our suggestion above that both the spheres and the lateral crystallites on the spikes are composed of h-BS_2.

The growth line for the spheres shows a very small (or zero) intercept

Figure 7.15 Plot of dimensions of $BaO2SiO_2$ crystals in glass 35 at 700°C versus time

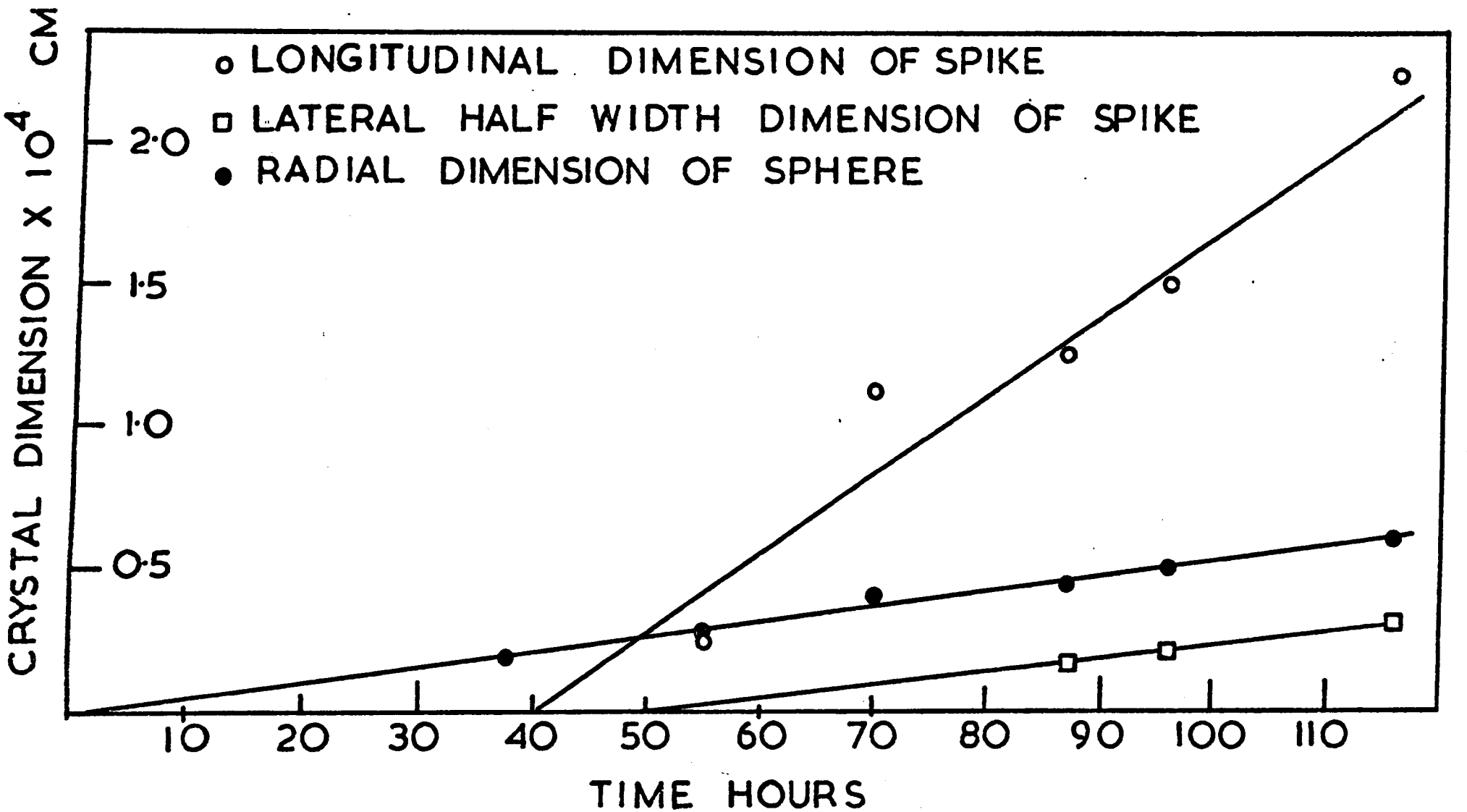
o LONGITUDINAL DIMENSION OF SPIKE
□ LATERAL HALF WIDTH DIMENSION OF SPIKE
● RADIAL DIMENSION OF SPHERE
CRYSTAL DIMENSION X 10^4 CM
2·0
1·5
1·0
0·5
10
20
30
40
50
60
70
80
90
100
110
TIME HOURS

Figure 7.16 Plot of $\log_{10} u$ (cm sec^{-1}) versus $\frac{10^3}{T}$ ($°K^{-1}$) for glass 35G (taken from reference 18).

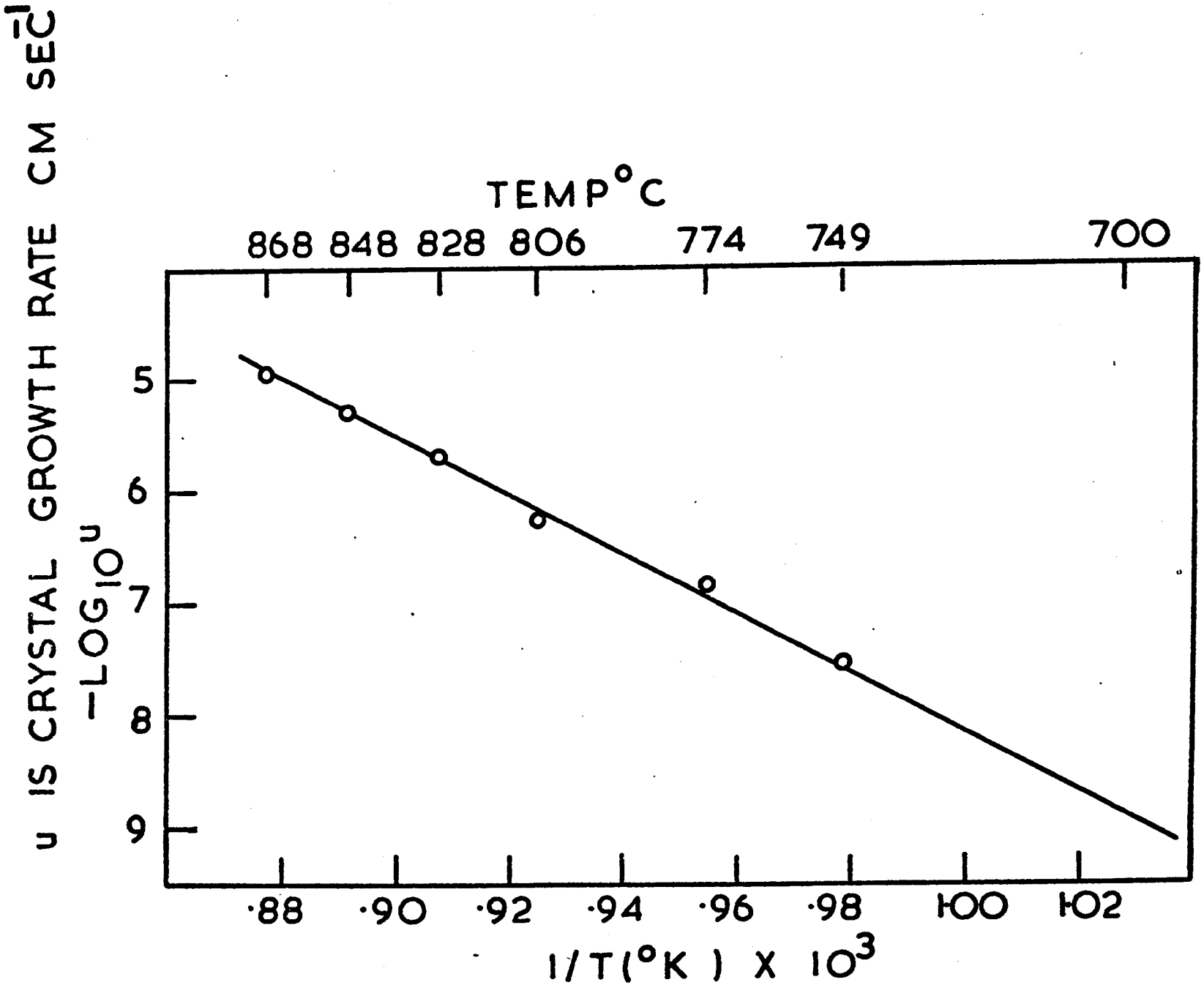
u IS CRYSTAL GROWTH RATE CM SEC⁻¹
TEMP °C
868 848 828 806 774 749 700
5
6
7
8
9
−LOG10 u
·88 ·90 ·92 ·94 ·96 ·98 100 102
1/T(°K) X 10³

TABLE 7.3

GROWTH RATES OF $BaO2SiO_2$ (35) at 700°C

	Rowlands data for 35G (extrapolated by author)	longitudinal growth of spike	radial growth of sphere	half width growth of spike (lateral growth)
	1.3×10^{-9} cms sec^{-1}	8.9×10^{-10} cms sec^{-1}	1.4×10^{-10} cms sec^{-1}	1.5×10^{-10} cms sec^{-1}
Intercept time	11 hours	35 hours	3 hours	56 hours

with the time axis. This is consistent with the very small nucleation induction time at 700°C observed earlier for glass 32 (less than ½ hour) since the spheres are the first particles to be nucleated. The spikes, however, show an intercept time of 20-35 hours (Figure (7.15)), indicating that there is an induction time before the spikes (spines) can nucleate on or near the surfaces of the growing spheres. The lateral growth of the spikes also indicates a similar intercept time showing that the lateral fibres or crystallites begin to grow immediately the spike forms. This is supported by the micrographs (Figure 7.6).

Since isolated spikes are rarely observed it is probably easier for the spikes to nucleate on sphere surfaces rather than directly from the glass.

The comparison between the longitudinal growth of the spikes and the radial growth of the large spherulites, calculated from Rowlands data[18], is close considering that the measurements were taken on two different but

nominally stoichiometric $BaO2SiO_2$ glasses. This indicates that the radial growth measured by Rowlands can be identified with the longitudinal growth of the spikes. The intercept time reported by Rowlands[18] in the growth rate of $BaO2SiO_2$ glasses at temperatures below 828°C is a reflection of the delay time in the appearance of the spikes (spines). This can be demonstrated by constructing a graph of $\log 1/\tau_1$ versus 1/T, where τ_1 is the growth intercept time at an absolute temperature T taken from Rowlands data (Figure (7.17)). A straight line is obtained which implies that the process involved in the formation of the spikes is thermally activated. Extrapolating to 700°C, the induction time is 11 hours. This is in reasonable agreement with the above approximate estimate of the spike induction time (20-40 hours) in view of the different techniques and glasses used.

The results of a recent study by Lewis and Smith[171] on the morphological and crystallographic development of $BaO2SiO_2$ crystals were published shortly after the completion of the work described here. It confirms many of the observations reported or inferred in this subsection. For example, it definitely establishes a) the presence of h-BS_2 in both spheres and spikes; b) the spine is a single crystal of l-BS_2.

7.2 THE KINETICS OF CRYSTAL GROWTH IN BARIA-SILICA GLASSES

7.2.1 General description of growth results

The radii of the large spherulites were plotted against time (Figures (7.18-7.21)) and the slope was determined using the method of least squares (for details refer to Appendix (5.5)). An Arrhenius plot of $\log_{10} u$ versus 1/T was constructed for each of the glasses (26, 28, 30, 32) (Figures (7.22-7.25)). The slope, according to growth theory is equal to $\Delta H_D/R$ for growth temperatures far below the liquidus.

Figure 7.17 Plot of $\log_{10} 1/\tau_1$ ($mins^{-1}$) versus $\frac{10^3}{T}$ ($°K^{-1}$) for glass 35G (extrapolated from reference 18)

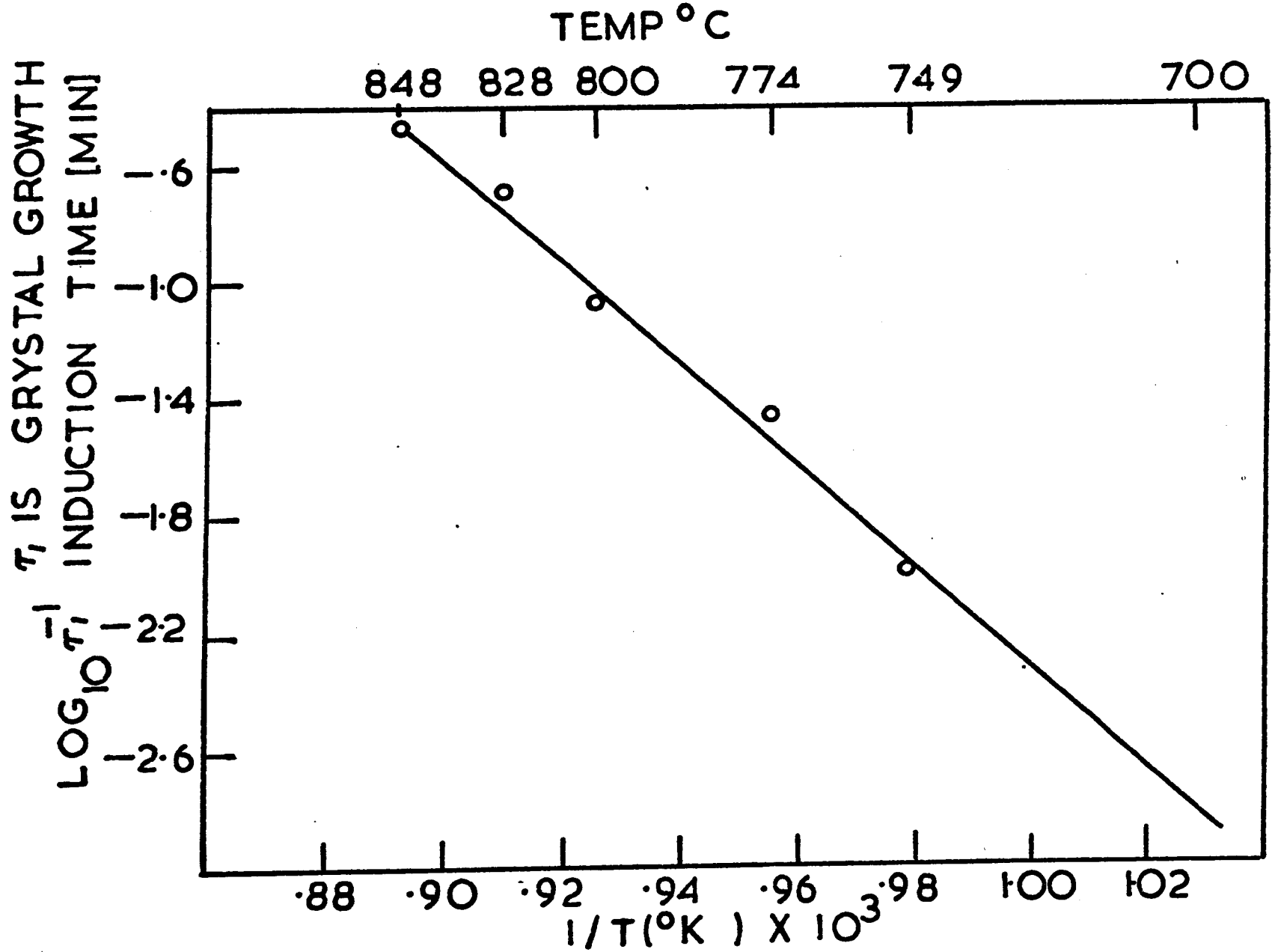
TEMP °C
848
828
800
774
749
700
τ_i IS GRYSTAL GROWTH INDUCTION TIME [MIN]
$\log_{10}\tau_i^{-1}$
-·6
-1·0
-1·4
-1·8
-2·2
-2·6
·88
·90
·92
·94
·96
·98
1·00
1·02
1/T(°K) X 10^3

Figure 7.18 (two pages) Plot of crystal size (radii of largest spherulites t′ cm) versus time for glass 32.

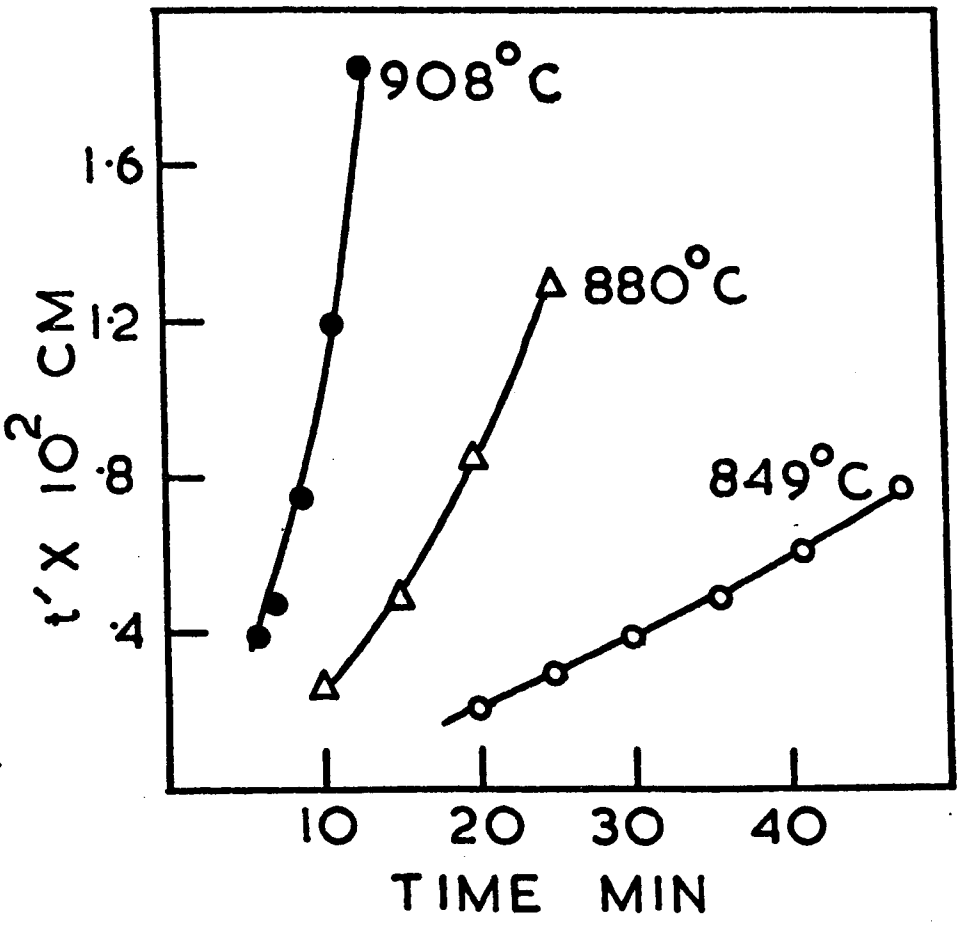
908°C
880°C
849°C
1·6
1·2
·8
·4
t' X 10² CM
10
20
30
40
TIME MIN

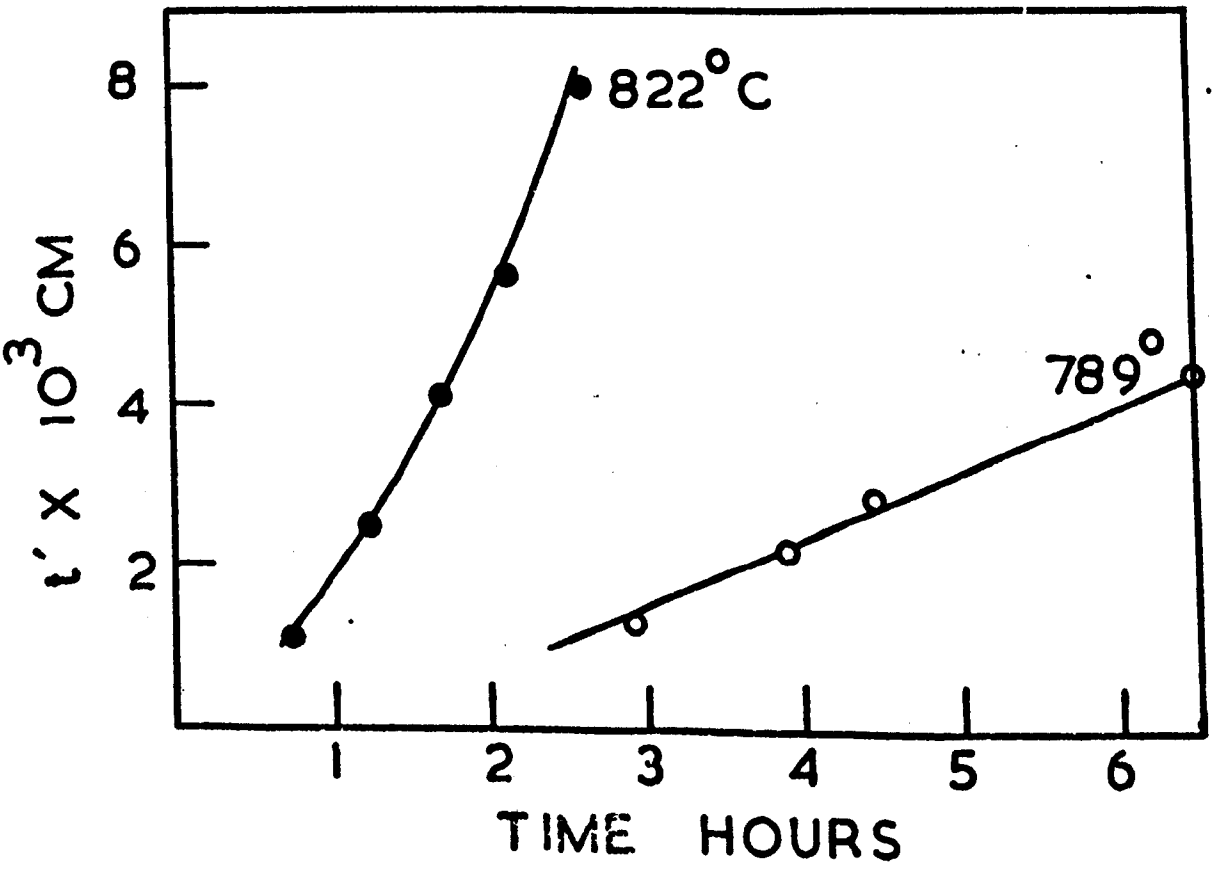
822°C
789°
8
6
4
2
t' X 10³ CM
1
2
3
4
5
6
TIME HOURS

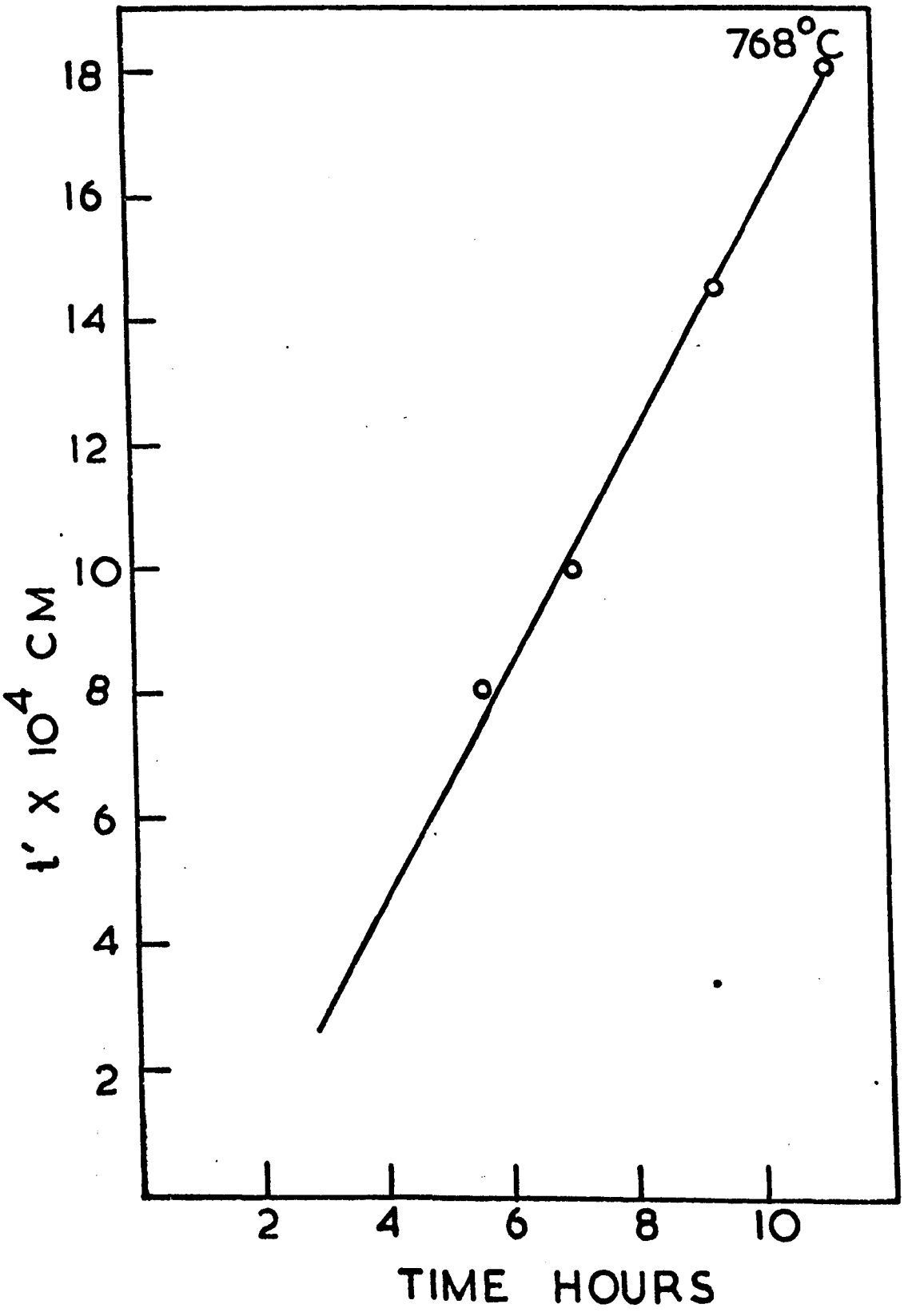
768°C
18
16
14
12
10
8
6
4
2
t' X 10^4 CM
2
4
6
8
10
TIME HOURS

Figure 7.19 (three pages) Plot of crystal size (radii of largest spherulites t′ cm) versus time for glass 30

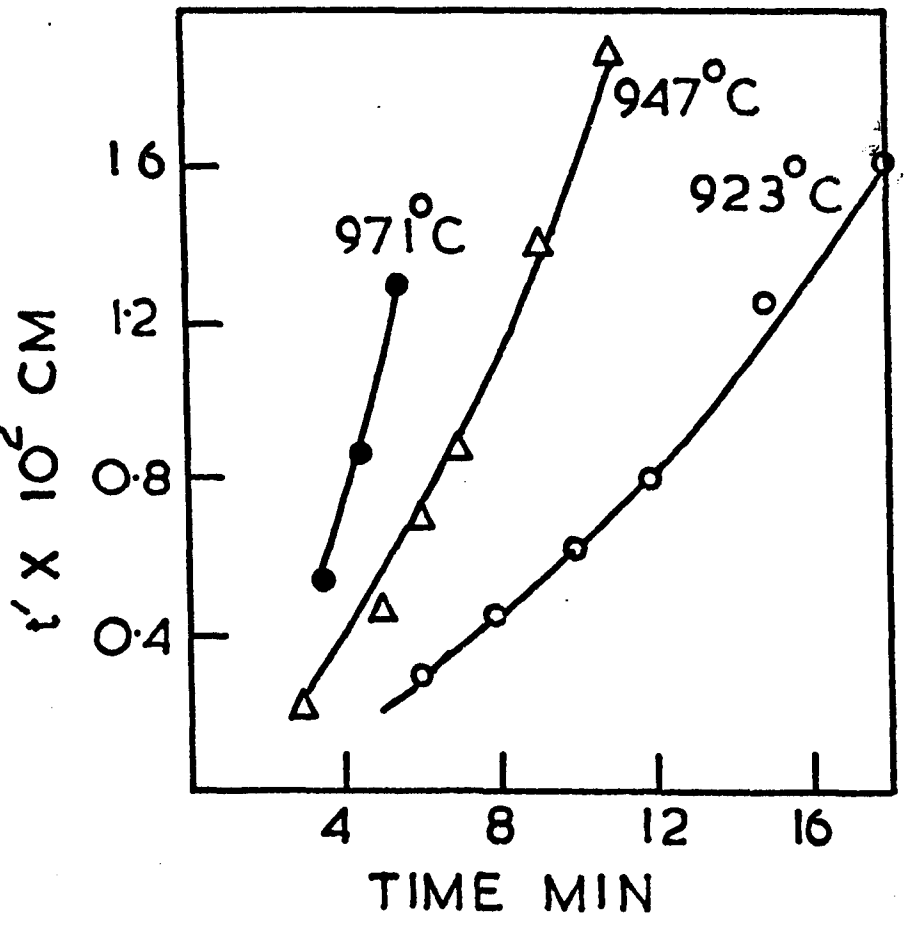
947°C
971°C
923°C
1·6
1·2
0·8
0·4
t' X 10² CM
4
8
12
16
TIME MIN

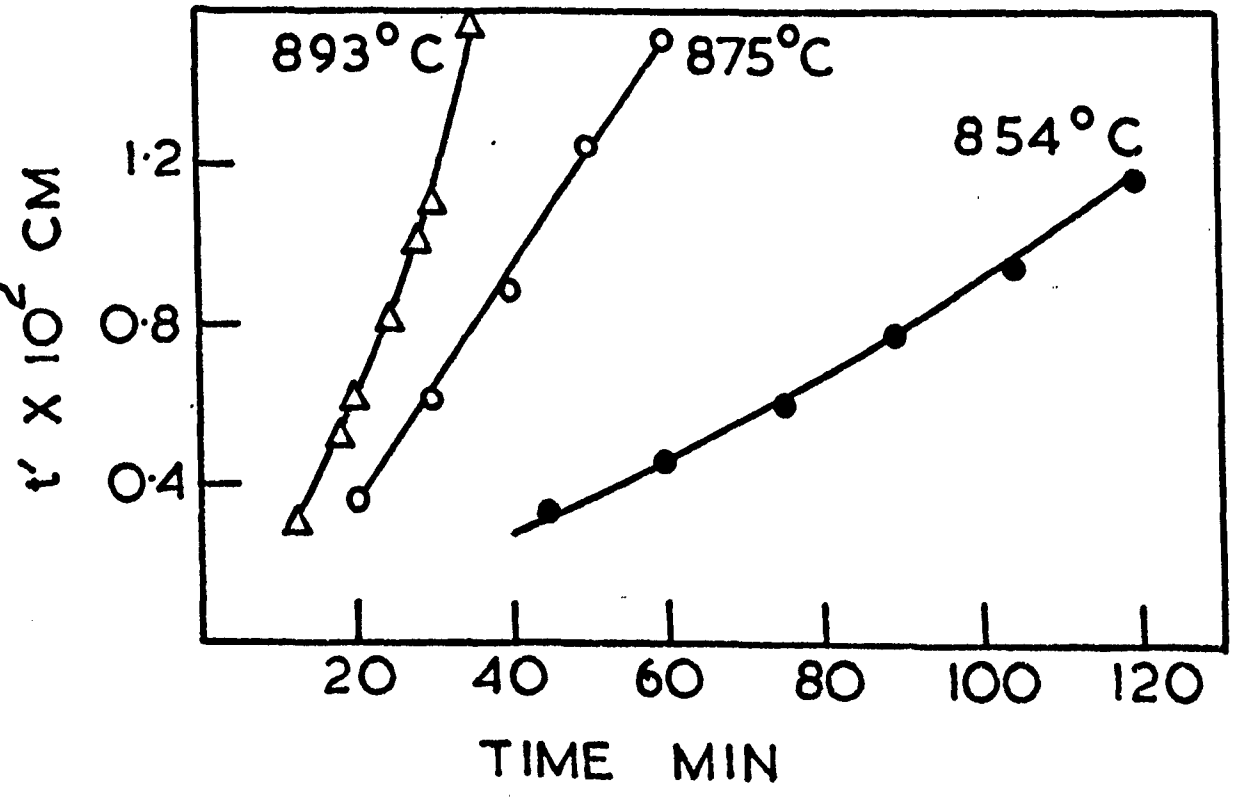
893°C
875°C
854°C
1·2
0·8
0·4
t' X 10² CM
20
40
60
80
100
120
TIME MIN

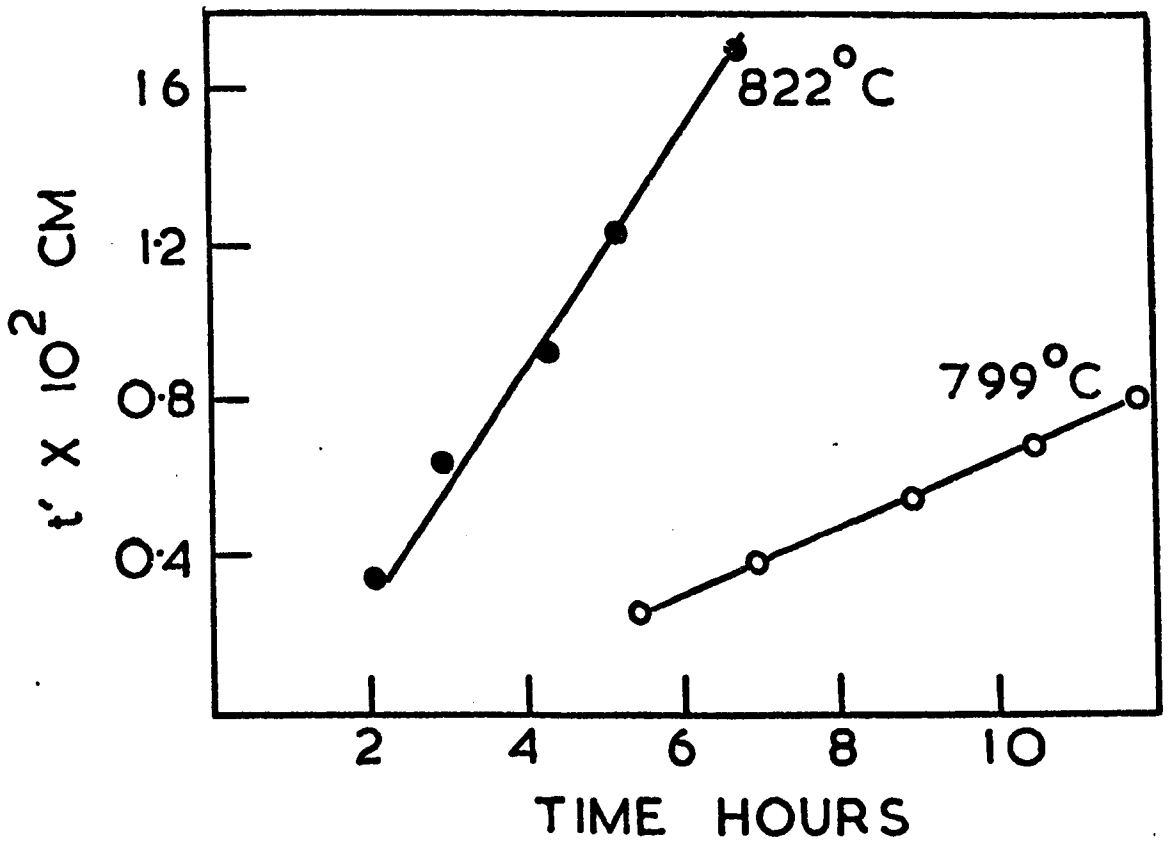
822°C
799°C
1·6
1·2
0·8
0·4
t' X 10² CM
2
4
6
8
10
TIME HOURS

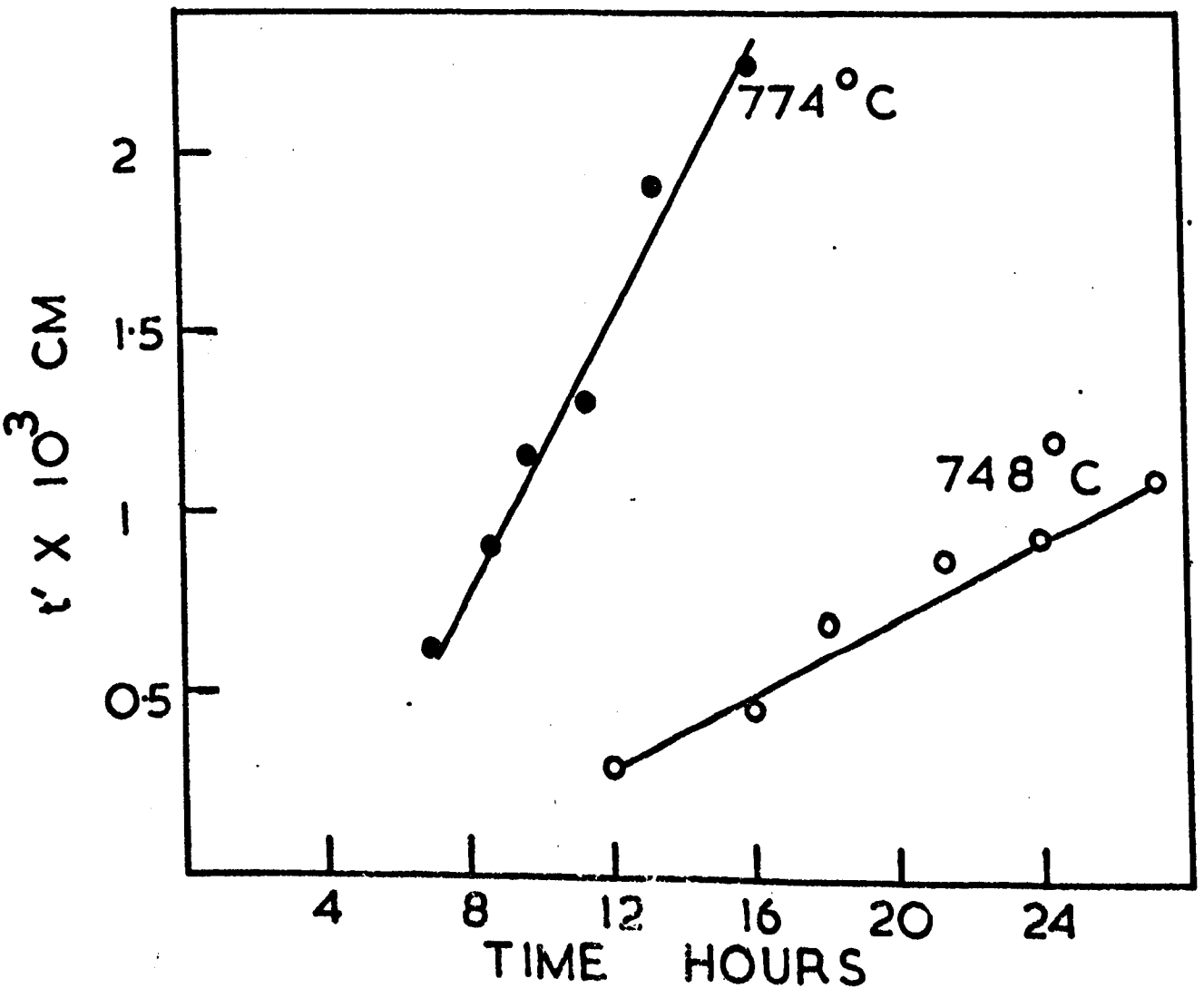
774°C
748°C
2
1·5
1
0·5
t' X 10³ CM
4
8
12
16
20
24
TIME HOURS

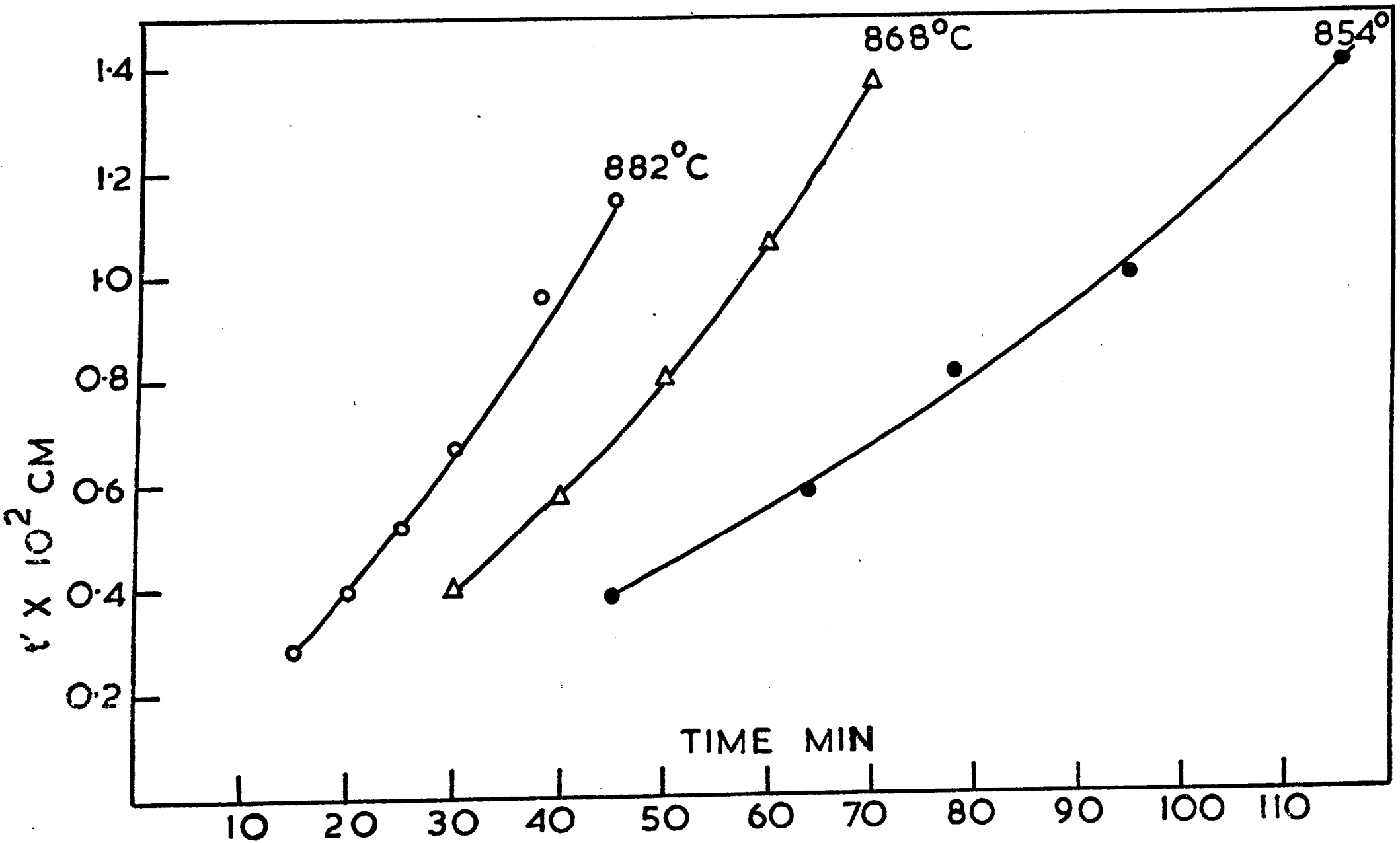
868°C
854°
882°C
1·4
1·2
1·0
0·8
0·6
0·4
0·2
t' X 10² CM
TIME MIN
10
20
30
40
50
60
70
80
90
100
110

Figure 7.20 (two pages)

Plot of crystal size (radii of largest spherulite t′ cm) versus time for glass 28

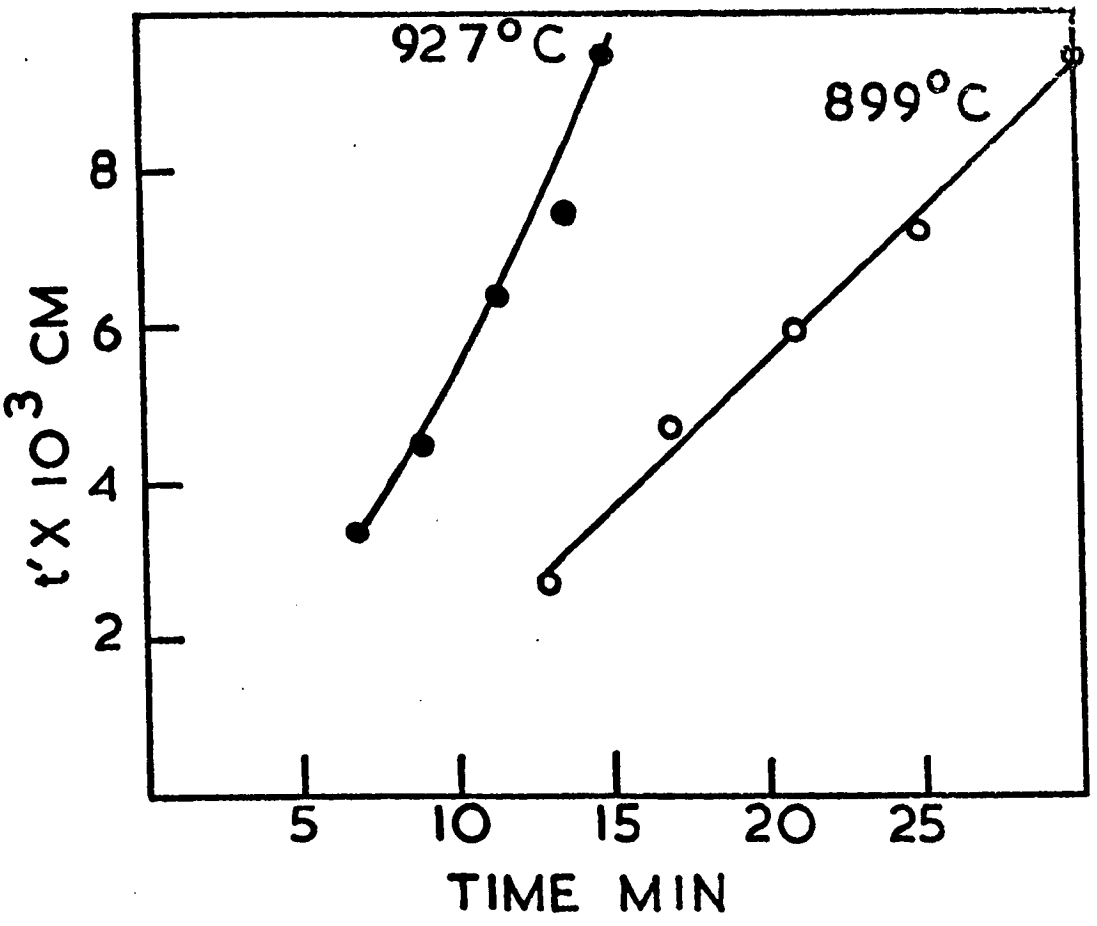
927°C
899°C
t' X 10³ CM
8
6
4
2
5
10
15
20
25
TIME MIN

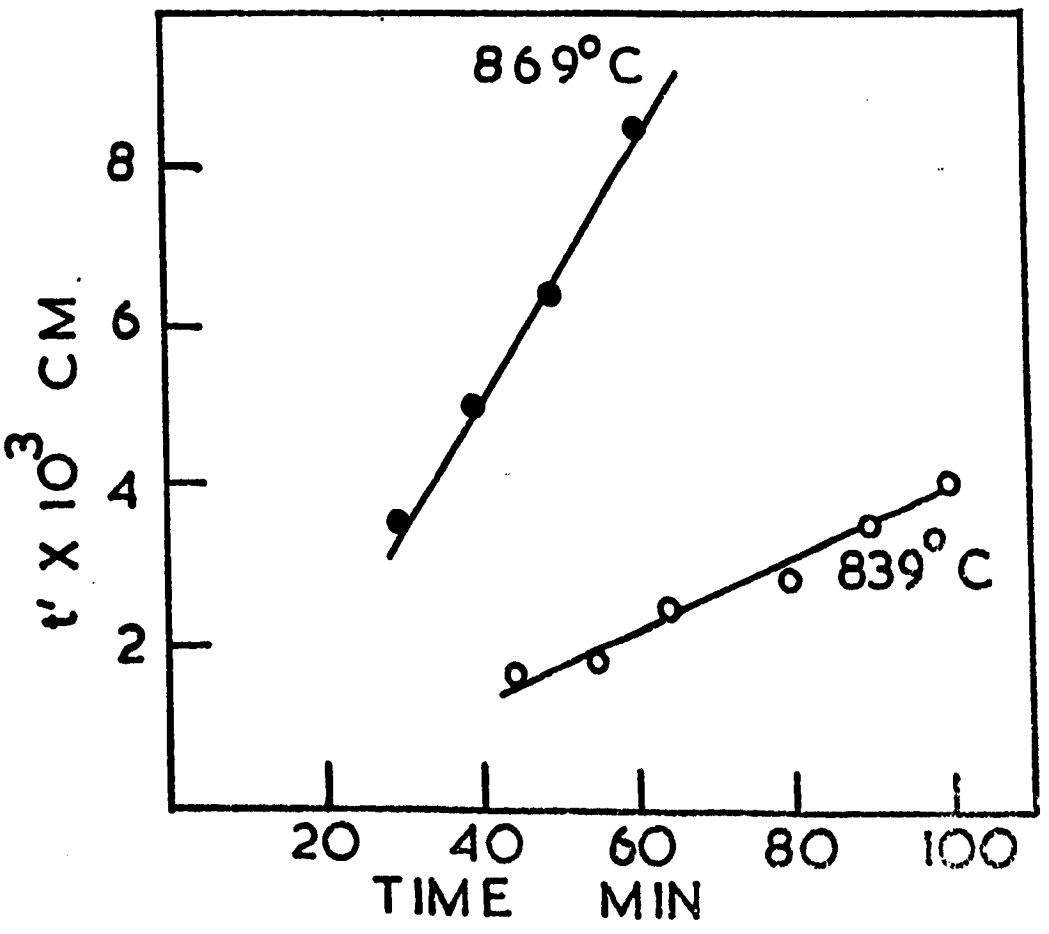
869°C
839°C
t' X 10³ CM.
8
6
4
2
20
40
60
80
100
TIME MIN

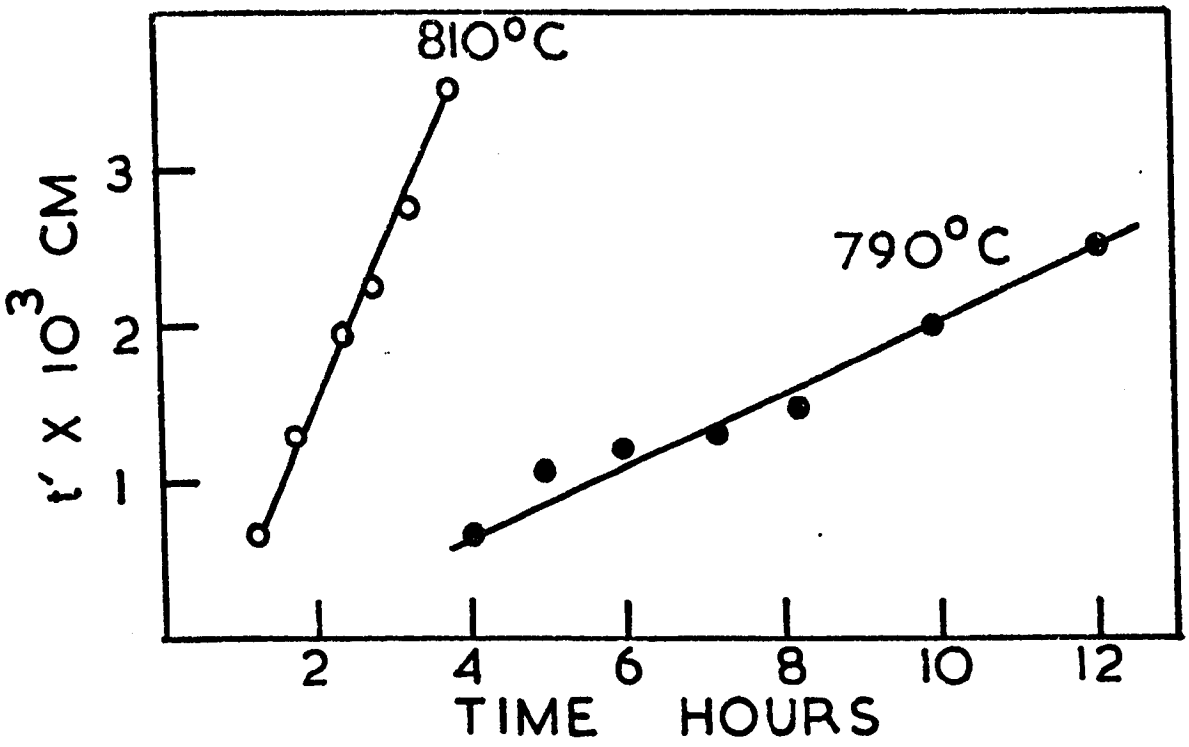
810°C
790°C
t' X 10^3 CM
3
2
1
2
4
6
8
10
12
TIME HOURS

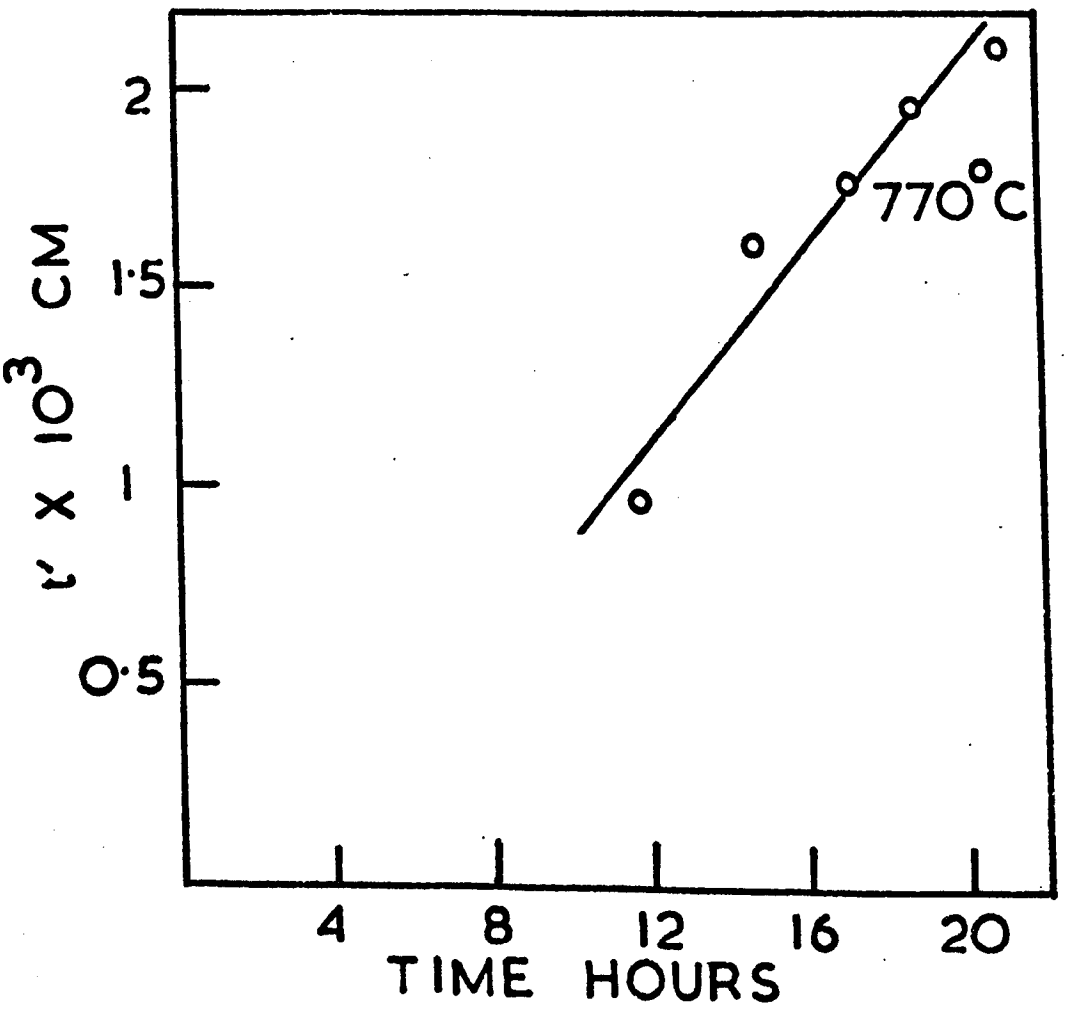
770°C
t' X 10^3 CM
2
1·5
1
0·5
4
8
12
16
20
TIME HOURS

Figure 7.21 (two pages) Plot of crystal size (radii of largest spherulite t´ cm) versus time for glass 26

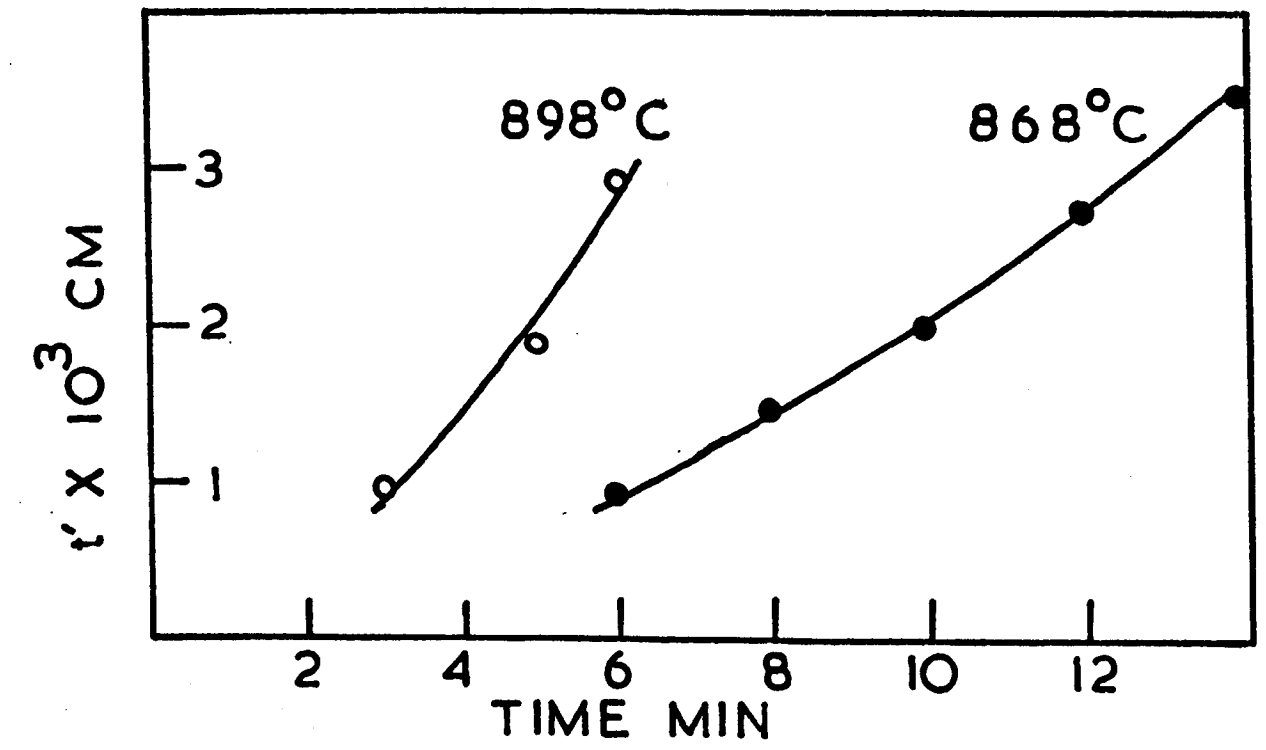
898°C
868°C
t' X 10^3 CM
3
2
1
2
4
6
8
10
12
TIME MIN

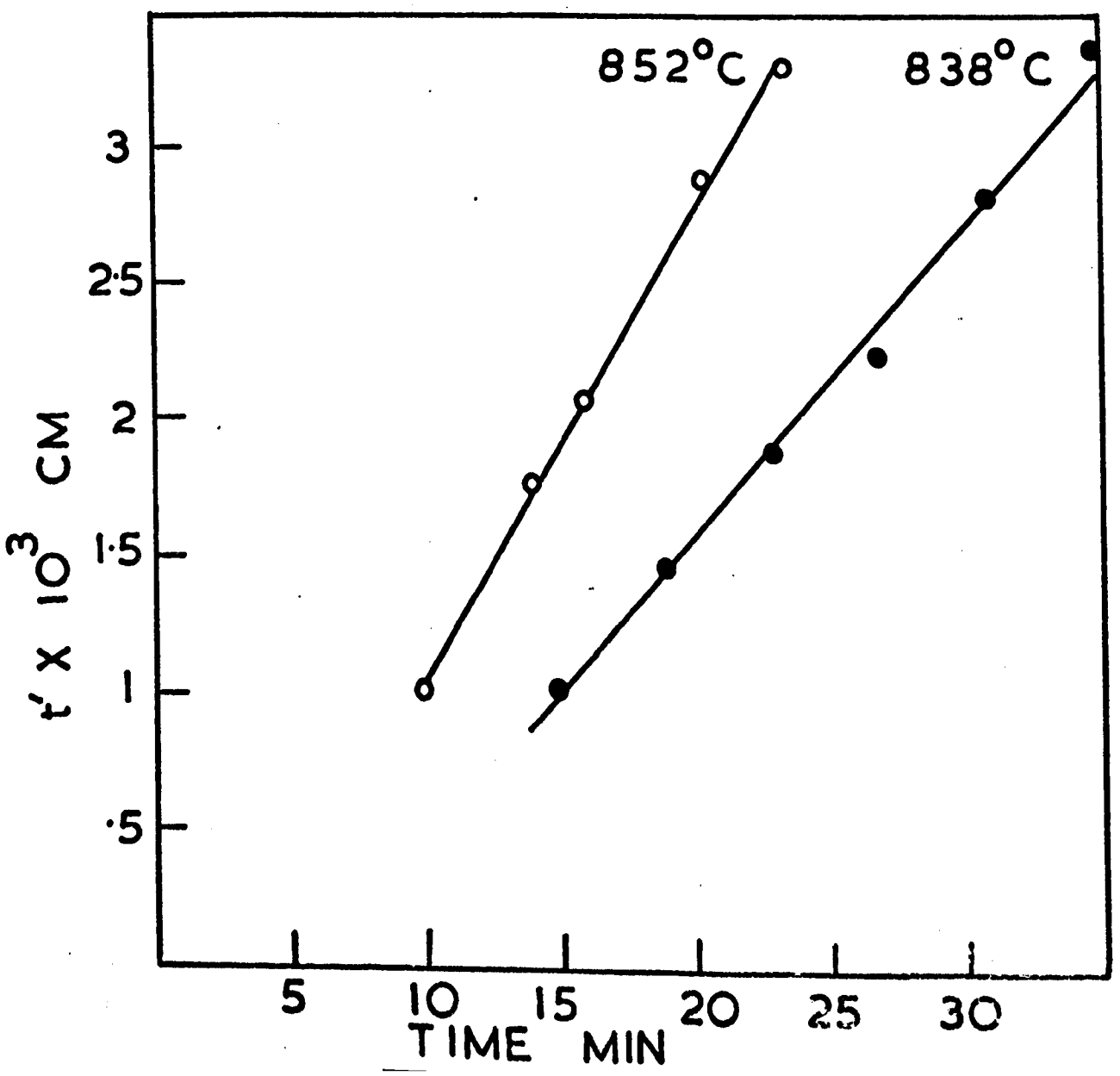
852°C
838°C
t' X 10^3 CM
3
2·5
2
1·5
1
·5
5
10
15
20
25
30
TIME MIN

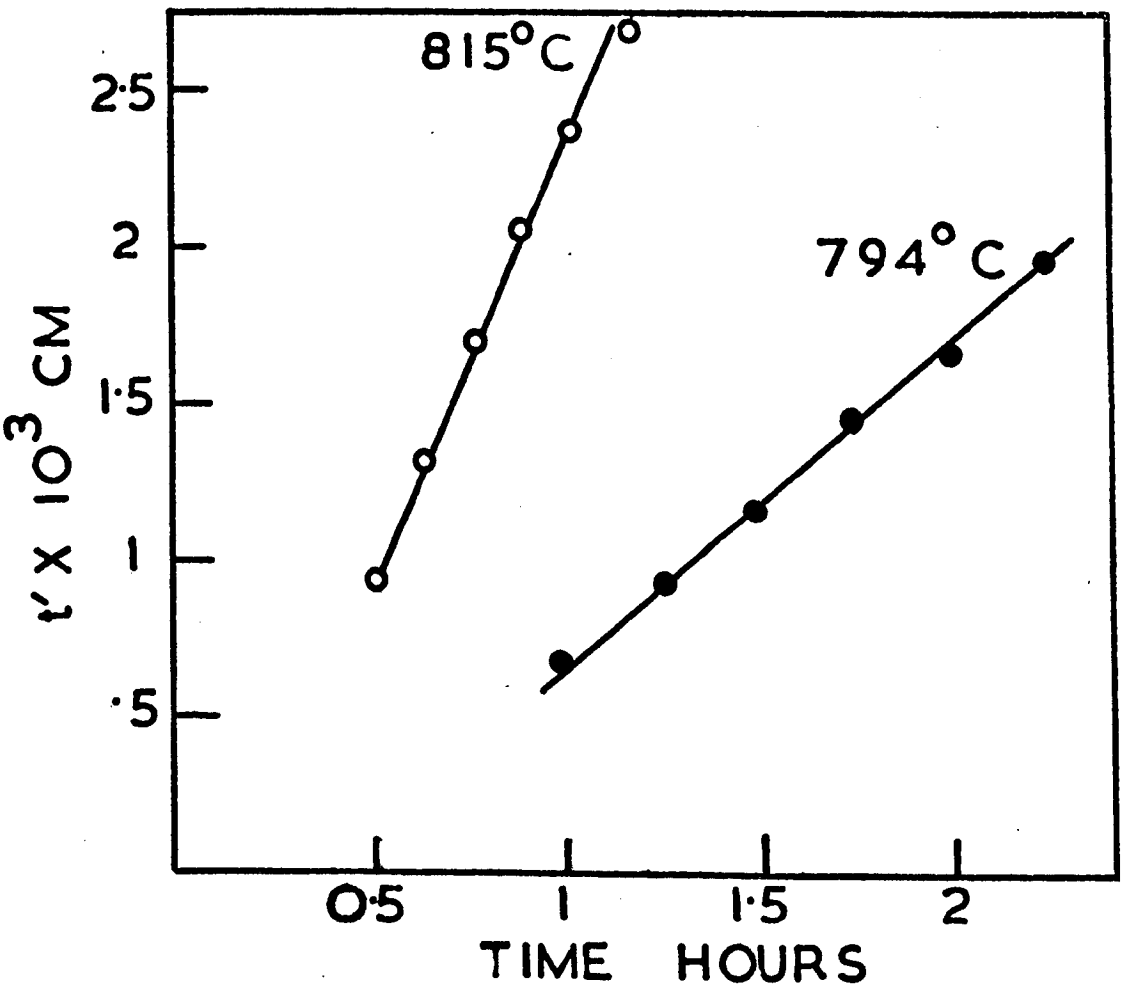
815°C
794°C
2·5
2
1·5
1
·5
t' X 10³ CM
0·5
1
1·5
2
TIME HOURS

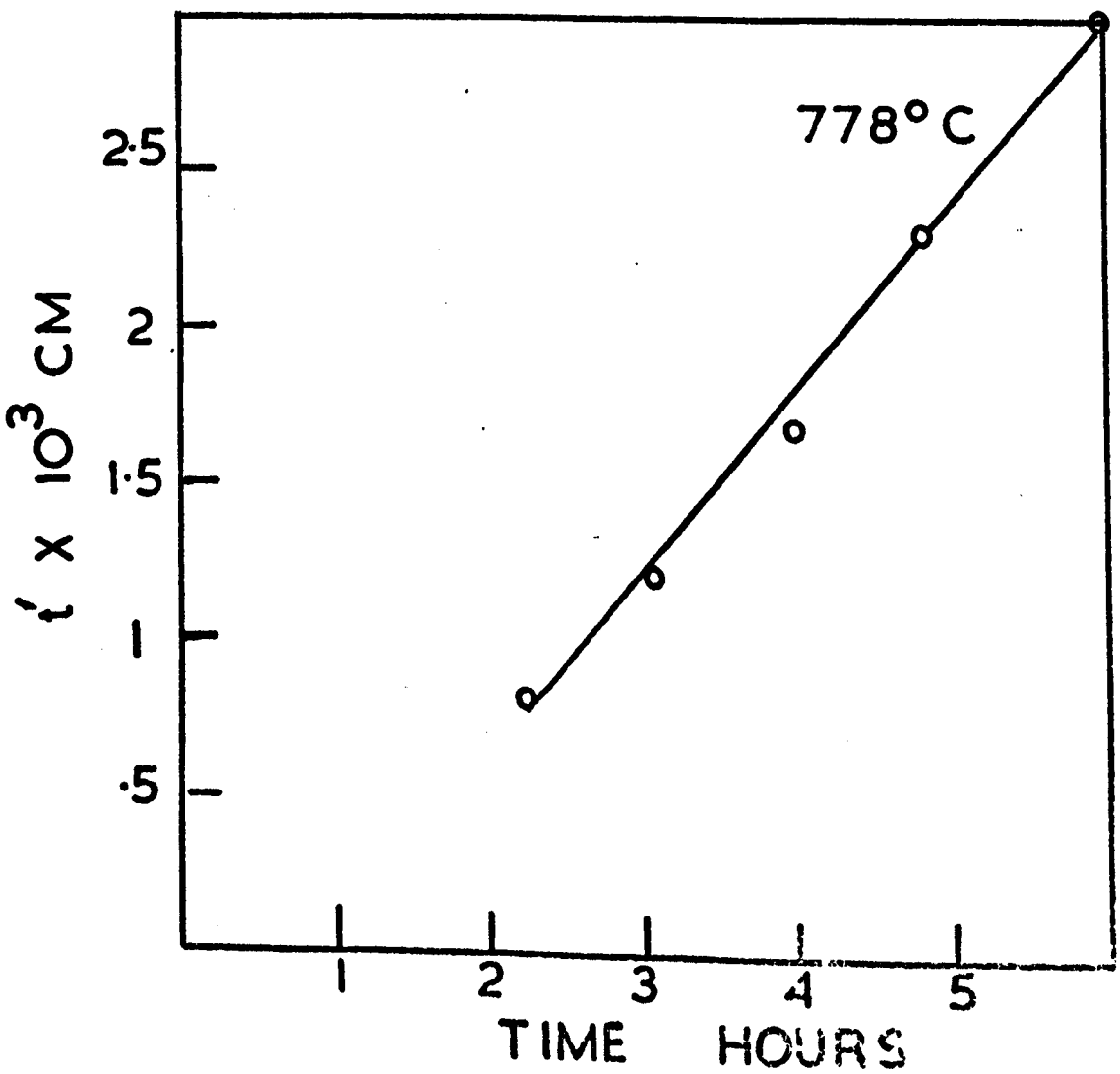
778°C
2·5
2
1·5
1
·5
t' X 10³ CM
1
2
3
4
5
TIME HOURS

Figure 7.22 Plot of $\log_{10} u$ (cm sec^{-1}) versus $\frac{10^3}{T}$ ($°K^{-1}$) for glass 32

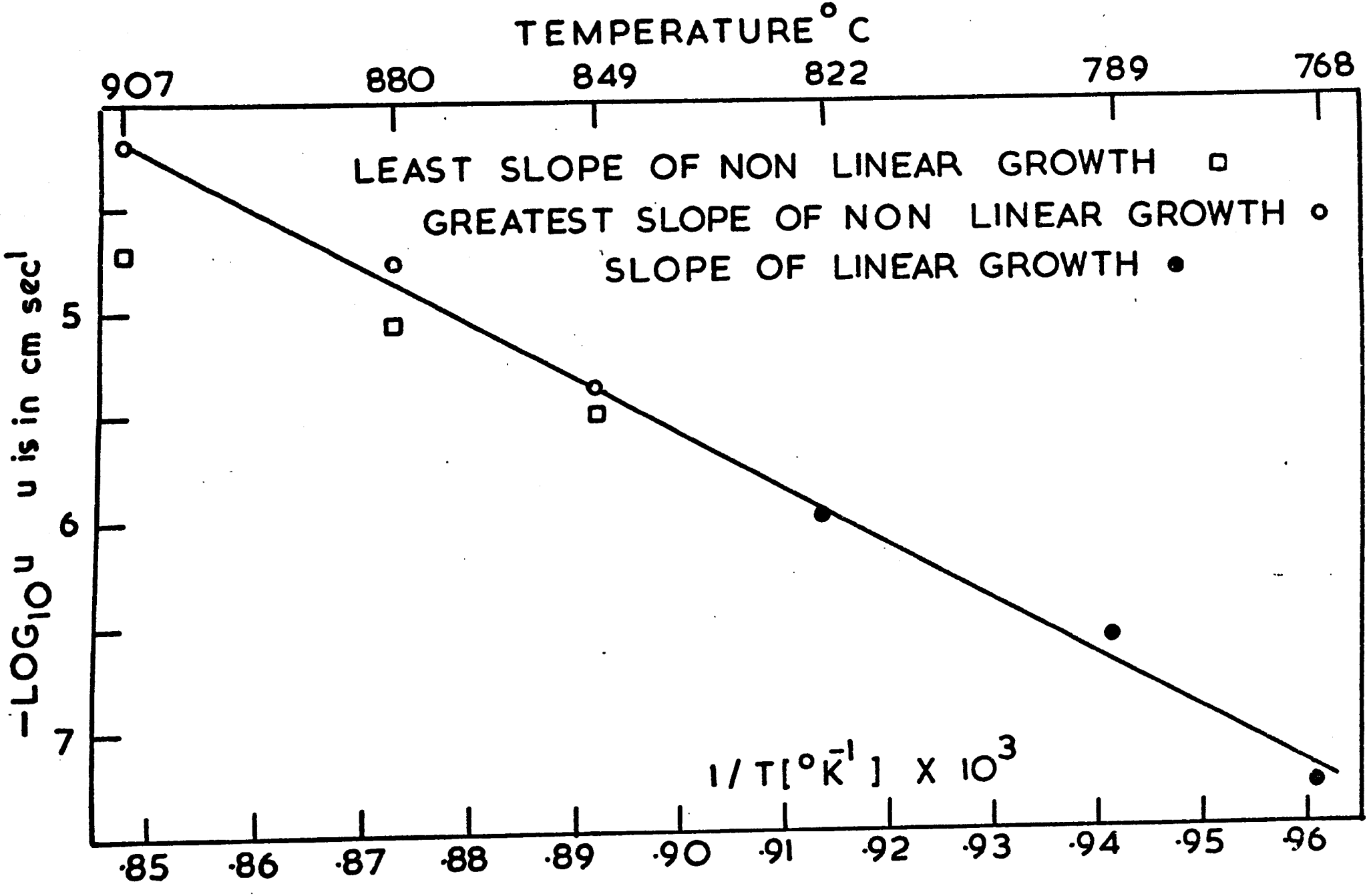
TEMPERATURE °C
907
880
849
822
789
768
LEAST SLOPE OF NON LINEAR GROWTH
GREATEST SLOPE OF NON LINEAR GROWTH
SLOPE OF LINEAR GROWTH
$-\log_{10} u$ u is in cm sec^{-1}
5
6
7
1/T[°K^{-1}] X 10^3
·85
·86
·87
·88
·89
·90
·91
·92
·93
·94
·95
·96

Figure 7.23 Plot of $\log_{10}$ u (cm sec^{-1}) versus ($\frac{10^3}{T}$ $°K^{-1}$) for glass 30

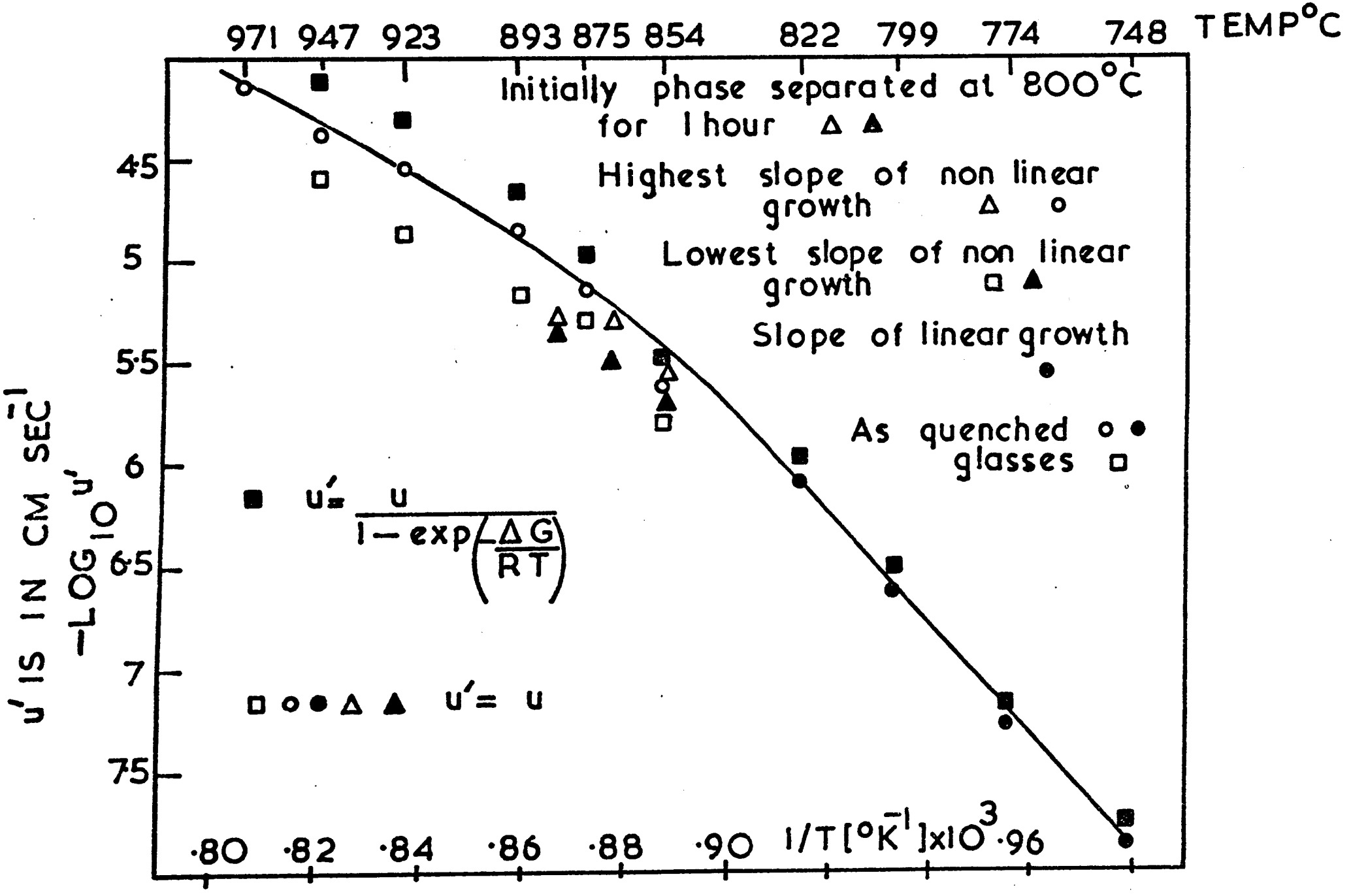
971 947 923 893 875 854 822 799 774 748 TEMP°C
Initially phase separated at 800°C for 1 hour
Highest slope of non linear growth
Lowest slope of non linear growth
Slope of linear growth
As quenched glasses
u' = u / (1 − exp(−ΔG/RT))
u' = u
u' IS IN CM SEC⁻¹
−LOG10 u'
4·5
5
5·5
6
6·5
7
7·5
·80 ·82 ·84 ·86 ·88 ·90 ·96
1/T [°K⁻¹] x10³

Figure 7.24 Plot of $\log_{10} u$ (cm sec^{-1}) versus $(\frac{10^3}{T}\,^{\circ}K^{-1})$ for glass 28

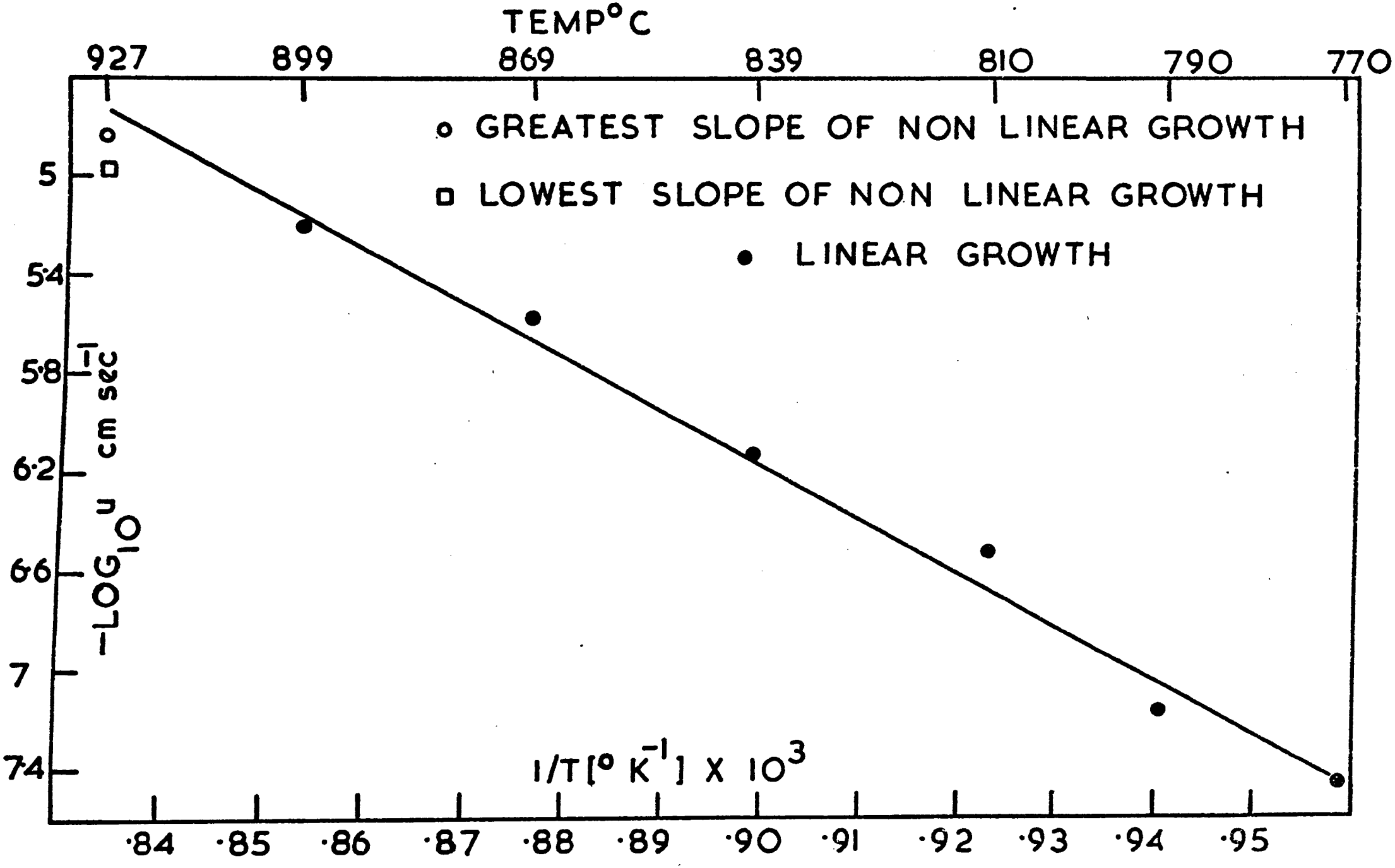
TEMP°C
927
899
869
839
810
790
770
o GREATEST SLOPE OF NON LINEAR GROWTH
□ LOWEST SLOPE OF NON LINEAR GROWTH
● LINEAR GROWTH
5
5·4
5·8
6·2
6·6
7
7·4
$-\log_{10} u$ cm sec^{-1}
1/T[° K^{-1}] X 10^3
·84
·85
·86
·87
·88
·89
·90
·91
·92
·93
·94
·95

Figure 7.25 Plot of $\log_{10}$ u (cm sec^{-1}) versus ($\frac{10^3}{T}$ $^\circ K^{-1}$) for glass 26

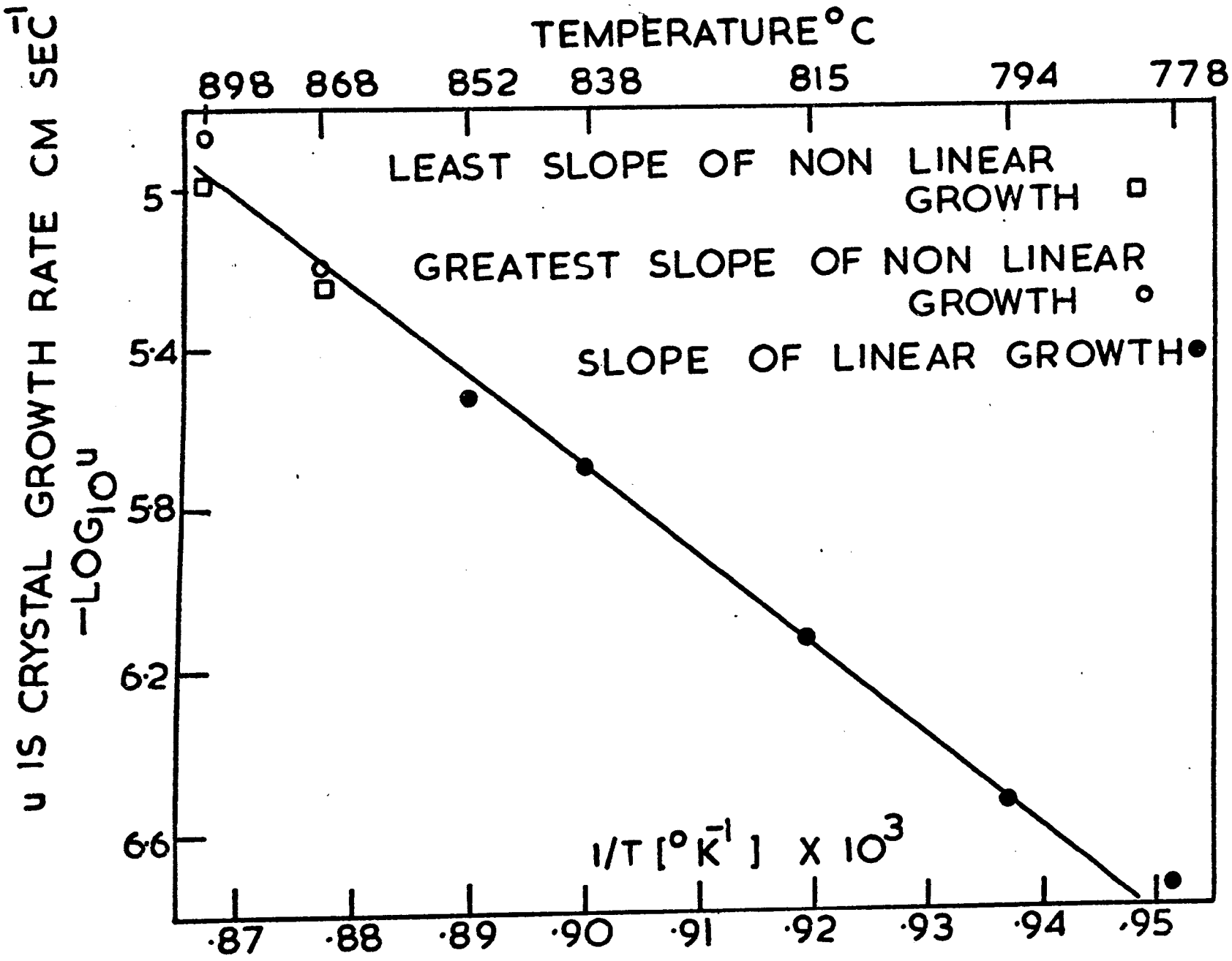
TEMPERATURE °C
898
868
852
838
815
794
778
LEAST SLOPE OF NON LINEAR GROWTH
GREATEST SLOPE OF NON LINEAR GROWTH
SLOPE OF LINEAR GROWTH
u IS CRYSTAL GROWTH RATE CM SEC⁻¹
−LOG10 u
5
5·4
5·8
6·2
6·6
1/T [°K⁻¹] X 10³
·87
·88
·89
·90
·91
·92
·93
·94
·95

The plots of the crystal dimension of the spherulites versus the growth time have certain features that are common to all four glasses:

1) A pronounced curvature at higher temperatures, (e.g. 854°C glass 30) with a tendency for the growth rates to increase slightly with time.
2) At lower temperatures the more usual linear growth relation is obtained. When extrapolated back to the time axis a sizeable intercept is generally noted (e.g. glass 30 799°C, τ_1 is 2.5 hours).

In the case of glass 35G only straight line relations were observed[18]. However, it should be noted that Rowlands employed shorter times and smaller temperature ranges compared with those used in this study. For glasses 32, 30 and 26, the linear growth transformed to non-linear behaviour at about 850°C and for 28 at about 900°C.

In the case of the curved plots the growth rates were calculated from both the steepest and shallowest parts of the curve. Although this is a somewhat arbitrary procedure, since even higher growth rates might be observed for longer growth times, these highest and lowest values observed at each temperature were used as a basis of comparison between the different glasses. On the Arrhenius plots these are labelled for clarity.

7.2.2 Discussion of the Arrhenius plots

The results of Tomozawa[143] in the Li_2O-SiC_2 system showed that as the Li_2O2SiO_2 composition was approached the activation enthalpy (ΔH_D) increased. He found that phase separated glasses had a lower ΔH_D than homogeneous glasses outside the liquid immiscibility dome. As the growth temperature of the phase separated glass was lowered the composition of the matrix phase approached Li_2O2SiO_2 and thus the crystal growth rate became

relatively greater. Thus the slope of the Arrhenius plots for phase separated glasses was less than for homogeneous glasses outside the immiscibility dome.

Ogura et al[144] determined the growth rates and the activation enthalpies of a series of $Li_2O.xSiO_2$ (x=1.5-3.5) glasses. Within the liquid immiscibility dome the activation enthalpies were constant but increased with Li_2O content outside the immiscibility dome. Again the activation enthalpies were less for phase separated glasses than for glasses outside the liquid immiscibility dome. Furthermore, the Arrhenius plots were nearly coincidental for glasses within the liquid immiscibility dome, indicating that the liquid immiscibility effect was mainly compositional rather than morphological.

The present results for the $BaO-SiO_2$ system are shown in Figures (7.22-7.25). In the case of non-linear growth both the lowest and highest growth rates measured were plotted, as explained above. The low alumina impurity glasses (26, 32, 35G) are plotted together for comparison in Figure (7.26) and the higher alumina glasses (28, 30, ABS_2) are shown in Figure (7.27). The Arrhenius plots for most of the glasses are approximate straight lines, with the exception of glass 30 which exhibits a definite 'break' or change in slope (Figure (7.23)). There was some evidence, particularly for glass 32, (Figure (7.22)) that a more linear Arrhenius plot could be drawn by using the highest measured growth rates at the higher temperatures.

Straight lines were fitted to the lower temperature data on each Arrhenius plot using only those points that corresponded to linear growth. The activation enthalpies obtained from the slopes and the 95% confidence limits are given in Table (7.4).

Figure 7.26 Plots of $\log_{10}$ u (cm sec^{-1}) versus ($\frac{10^3}{T}$ $°K^{-1}$) for glasses 32, 26 and 35G

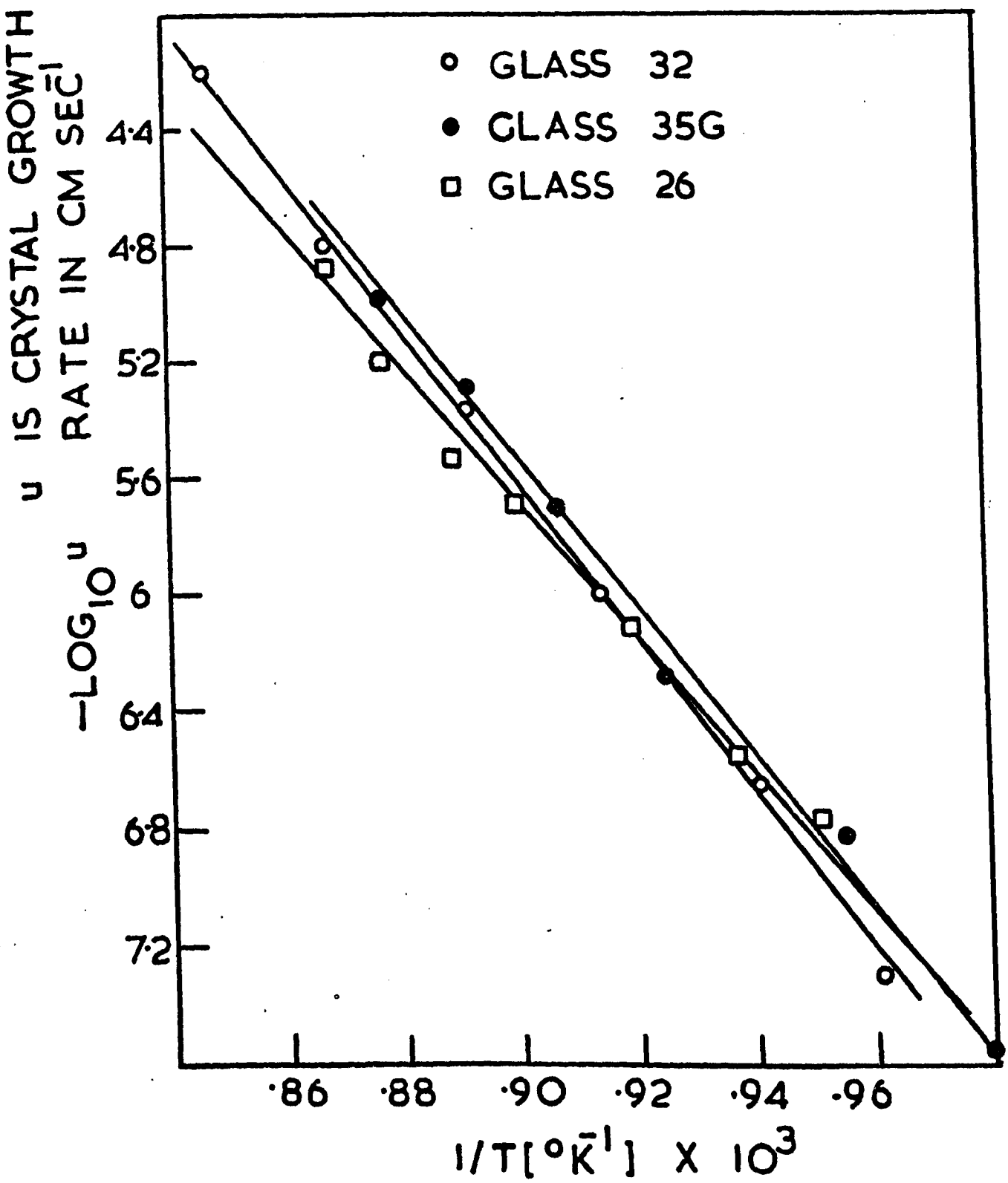
u IS CRYSTAL GROWTH RATE IN CM SEC⁻¹
−LOG10 u
4·4
4·8
5·2
5·6
6
6·4
6·8
7·2
·86
·88
·90
·92
·94
·96
1/T[°K⁻¹] X 10³
GLASS 32
GLASS 35G
GLASS 26

Figure 7.27 Plots of $\log_{10}$ u versus $(\frac{10^3}{T}{}^{\circ}K^{-1})$ for glasses 30, 28 and ABS_2

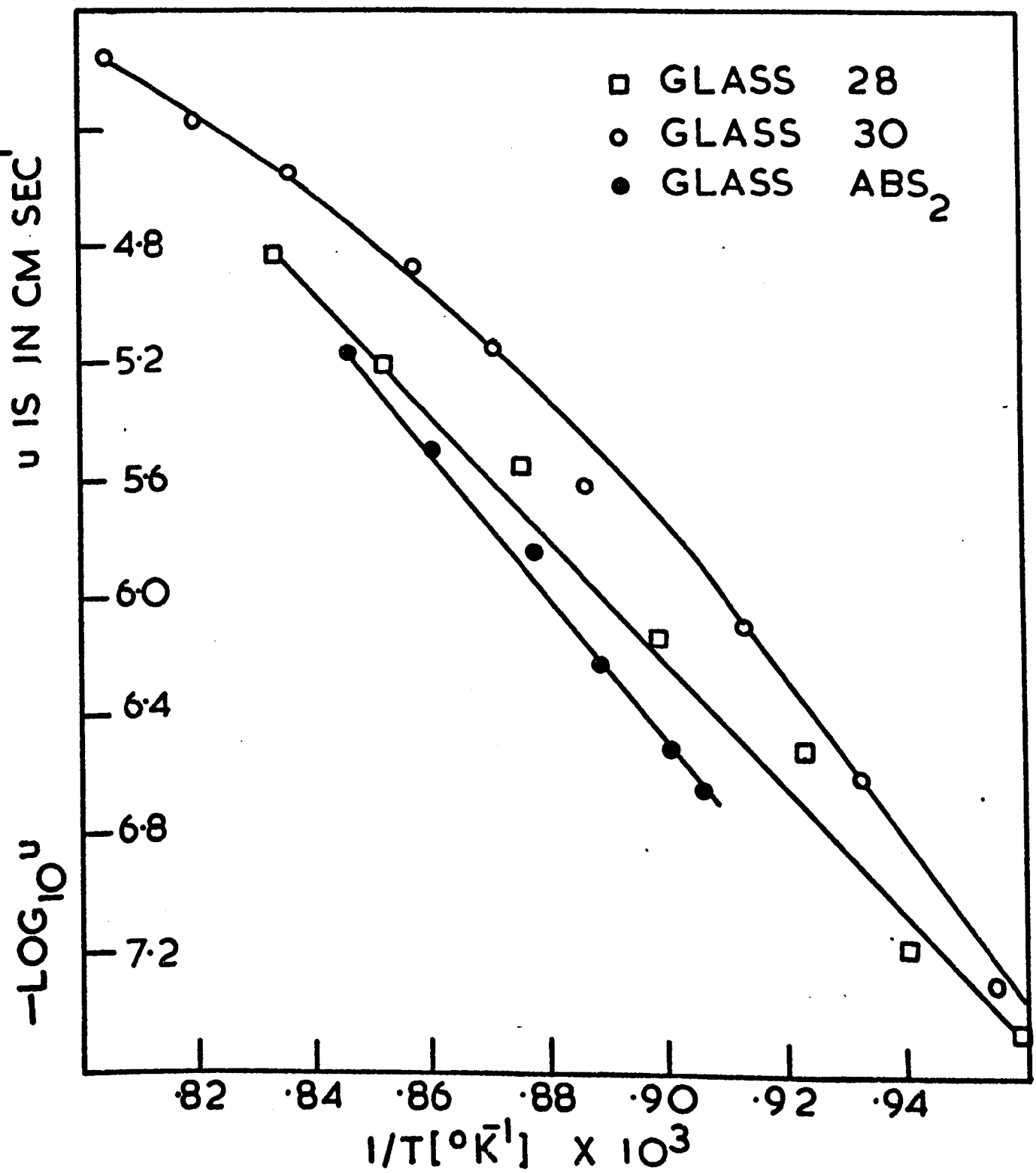
GLASS 28
GLASS 30
GLASS ABS2
4·8
5·2
5·6
6·0
6·4
6·8
7·2
-LOG10 u
u IS IN CM SEC-1
·82
·84
·86
·88
·90
·92
·94
1/T[°K-1] X 10³

TABLE 7.4

ACTIVATION ENTHALPIES ΔH_D

Glass	ΔH_D kcals mol^{-1} *	Temp. range of calculation	Description of immiscibility
35G	119 ±9	749-868°C (6 points)	No phase separation
ABS_2	114 ±17	830-903°C (6 points)	No phase separation
32	122 ±10	768-849°C	No phase separation
30	122 ±23	748-822°C (4 points)	Phase separates below 850°C
28	99 ±16	770-899°C (6 points)	Phase separates
26	94 ±10	778-852°C (5 points)	Phase separates

* 95% confidence limits quoted

Comparing the Arrhenius plots for the two non-phase separating glasses in the low alumina group (32 and 35G), the growth rates are consistently slightly lower for 32 - the plots are nearly parallel and the ΔH_D values are similar (Table 7.4). The higher growth rates for 35G are not surprising since 35G is closer to the disilicate composition than 32.

For glass 26, also in the low alumina group, the growth rates are close to glasses 32 and 35G at lower temperatures but the growth rates are lower at high temperatures. The overall slope of the Arrhenius plot is smaller (ΔH_D = 94 kcals $mole^{-1}$ compared with 122 kcals $mole^{-1}$ for glass 32.).This behaviour is probably due to the phase separation of glass 26. Generally,a glass inside the immiscibility dome will separate rapidly at

the growth temperature into a silica-rich phase and a phase increasingly rich in baria for a decrease in temperature. Hence the Arrhenius plot for the phase separated glass will approach that for a glass just outside the dome (e.g. 32 or 35G) at lower temperatures. Strictly the plot should now exhibit curvature but the accuracy of growth measurements generally will not be sufficient to detect it, and the main effect observed will be a decrease in the apparent slope of the plot. Hence the apparent activation enthalpy of the phase separated glass will appear less than the glasses that do not phase separate, as in fact observed for glass 26. Thus the present results agree with the conclusions of Tomozawa[143] in the Li_2O-SiO_2 system.

Consider now the results for glasses 28 and 30 which contain higher levels of alumina impurity. Glass 30, as already pointed out, phase separates at lower temperatures but not at higher temperatures (greater than 850°C). In this case the Arrhenius plot should show a change in slope somewhere below the immiscibility temperature T_m (below 905°C remembering that a metastable zone of no separation exists below T_m). This possible behaviour is illustrated schematically in Figure (7.28). A change in slope (in fact a curvature) does occur for glass 30 (figure (7.23)) but in the opposite sense to that shown in Figure (7.28). Hence the observed curvature is unlikely to be caused by composition changes produced by phase separation. However, the curved part of the plot coincides with the region of non-linear growth at higher temperatures. We are unable to explain this effect although it is presumably related to the non-linear growth in some way. The growth rates for glass 28 are lower than for glass 30. This is probably due mainly to the higher level of alumina in glass 28.

The effect of a deliberately added quantity of alumina (1 mol%) to

Figure 7.28 a) Schematic representation of log u versus 1/T plots for non-phase separated glasses assuming similar activation enthalpies. A > B > C in baria content.

Figure 7.28 b) Schematic representation of $\log_{10}$ u versus 1/T for a phase separated glass F and a non-phase separated glass D. E represents a glass that phase separated at low temperatures but not at high temperatures

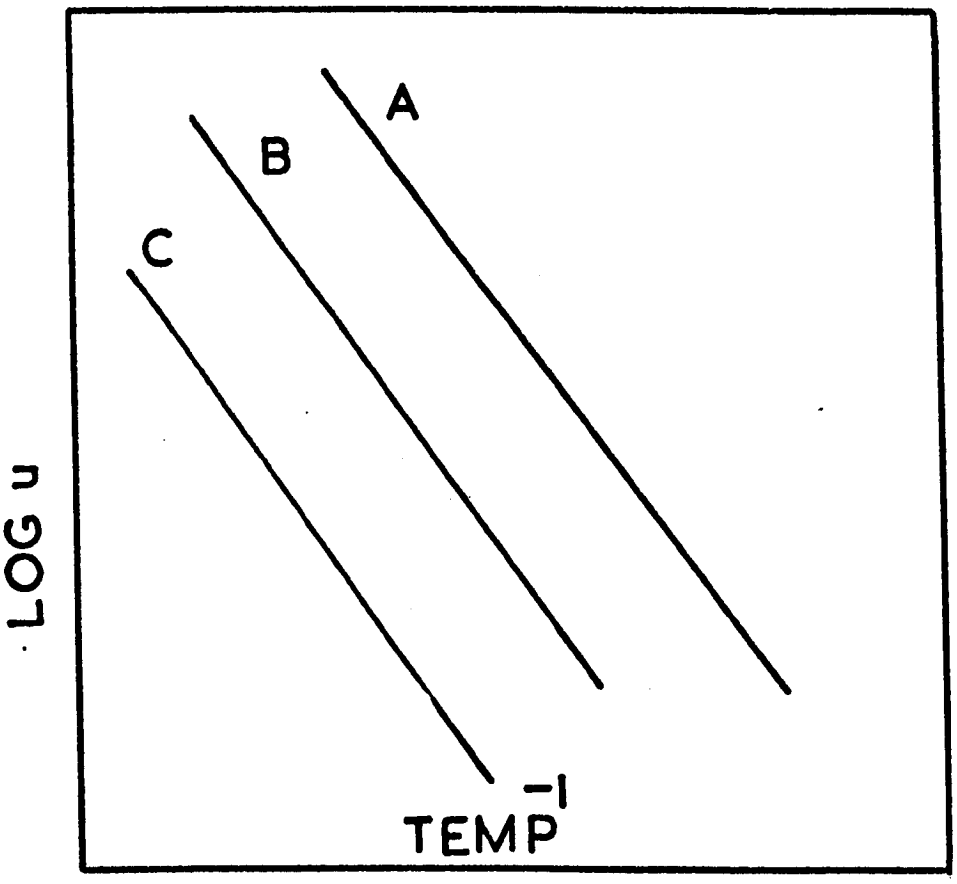

a)

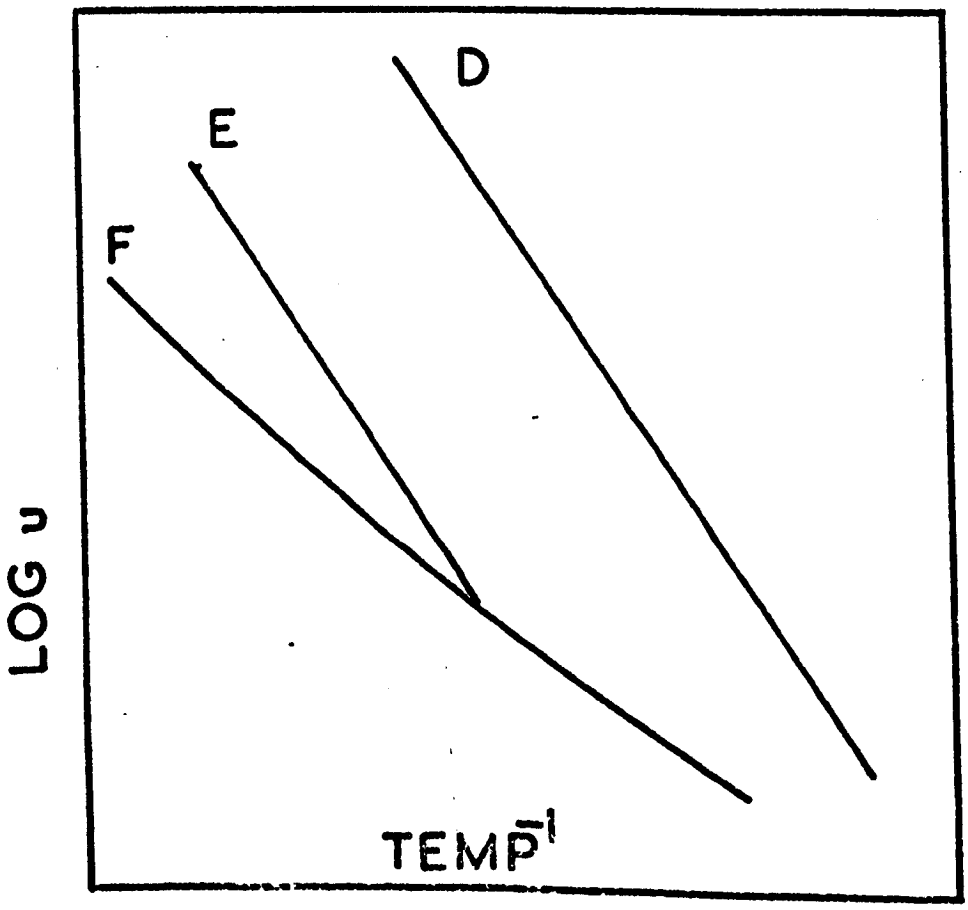

b)

the $BaO2SiO_2$ composition is to reduce the growth rates by two orders of magnitude over the entire temperature range under investigation (Figure (7.27)). The effect on the activation enthalpy is minimal, the plots being almost parallel. Thus alumina affects the overall growth rate rather than the activation enthalpy.

It is also interesting to compare glasses 26 and 28 which have nearly the same BaO content but differing alumina impurity levels. Both glasses phase separate. As expected the Arrhenius plots are almost parallel and give similar activation enthalpies (Table 7.4). The alumina impurity is seen to inhibit growth in glass 28 compared with 26.

Although the above discussion is not dependent on any particular model for the growth kinetics, it is implied that the slopes of the plots give the value ΔH_D. This is only true if, assuming the normal growth model, the factor $\left[1 - \exp(-\frac{\Delta G}{RT})\right]$ can be taken as unity, i.e. $\Delta G >> RT$ (see equation (3.19)). It is possible that this assumption might not be valid, particularly for glass 30 where measurements are extended over a wide temperature range. This is tested by calculating the above factor assuming that ΔG for glass 30, as a first approximation, is the same as $BaO2SiO_2$, i.e. $\Delta G = \frac{\Delta H \Delta T}{T_m}$ where $\Delta H = 8.6$ kcals mole^{-1}. In fact $\left[1 - \exp(-\frac{\Delta G}{RT})\right]$ varies from 0.61 at 971°C t.. 0.82 at 748°C. By comparing a graph of

$\log_{10} \frac{u}{\left[1 - \exp(-\frac{\Delta G}{RT})\right]}$ vs 1/T with $\log_{10}$ u vs 1/T the effect of ignoring ΔG was assessed. The new curve is raised slightly, this effect being greater at higher temperatures (see Figure (7.23)). Thus when ΔG considerations are included, the plot is straighter but only slightly. This is because changes in growth rate as a function of temperature heavily outweigh changes in $\left[1 - \exp(-\frac{\Delta G}{RT})\right]$. The effect of neglecting ΔG on the other plots is similar, i.e. the slopes are altered only slightly.

DTA was used to investigate further the effect of phase separation on crystallization in glasses 26 and 30. Comparison was made between the thermograms of untreated glasses and glasses given an initial heat treatment to phase separate them. No significant difference was detected (Table 6.3). This was probably because, once the growth temperature had been attained, liquid immiscibility had occurred in the initially homogeneous glass to the same extent as the initially phase separated glass.

Only slight variations in the temperatures of crystallization Tx between the glasses were observed. This implied similar growth rates for the glasses. Also surface crystallization predominated over internal crystallization due to the fine particle size used in the powdered DTA glass samples, so that differences in internal nucleation between the glasses were not reflected in the crystallization peaks. However, the slightly lower crystallization peak temperature in glass 35 was probably due to the very high nucleation rate in this glass.

7.3 DISCUSSION OF THE INTERCEPTS WITH THE TIME AXIS

The intercept time (τ_1) results displayed in Figures (7.29-7.32) are plots of $\log_{10} 1/\tau_1$ vs 1/T. The value of τ_1 was calculated from the linear growth plots using the method of least squares. In the case of slightly curved growth plots, τ_1 was obtained by extrapolating the growth data at shorter times to the time axis. The low alumina impurity glasses (26, 32, 35G) are plotted together for comparison in Figure (7.33) and the higher alumina glasses (28, 30) are shown in Figure (7.34).

The Arrhenius plots of $\log_{10} 1/\tau_1$ versus 1/T are approximate straight lines. However, there is considerably more scatter than for the $\log_{10}$ u versus 1/T plots. It is thus not possible to distinguish if glass 30, for example, displayed a curved Arrhenius plot corresponding to that observed in the $\log_{10}$ u versus 1/T plots.

Figure 7.29 Plot of $\log_{10} 1/\tau_1$ ($mins^{-1}$) versus $\frac{10^3}{T}$ $(°K)^{-1}$ for glass 32

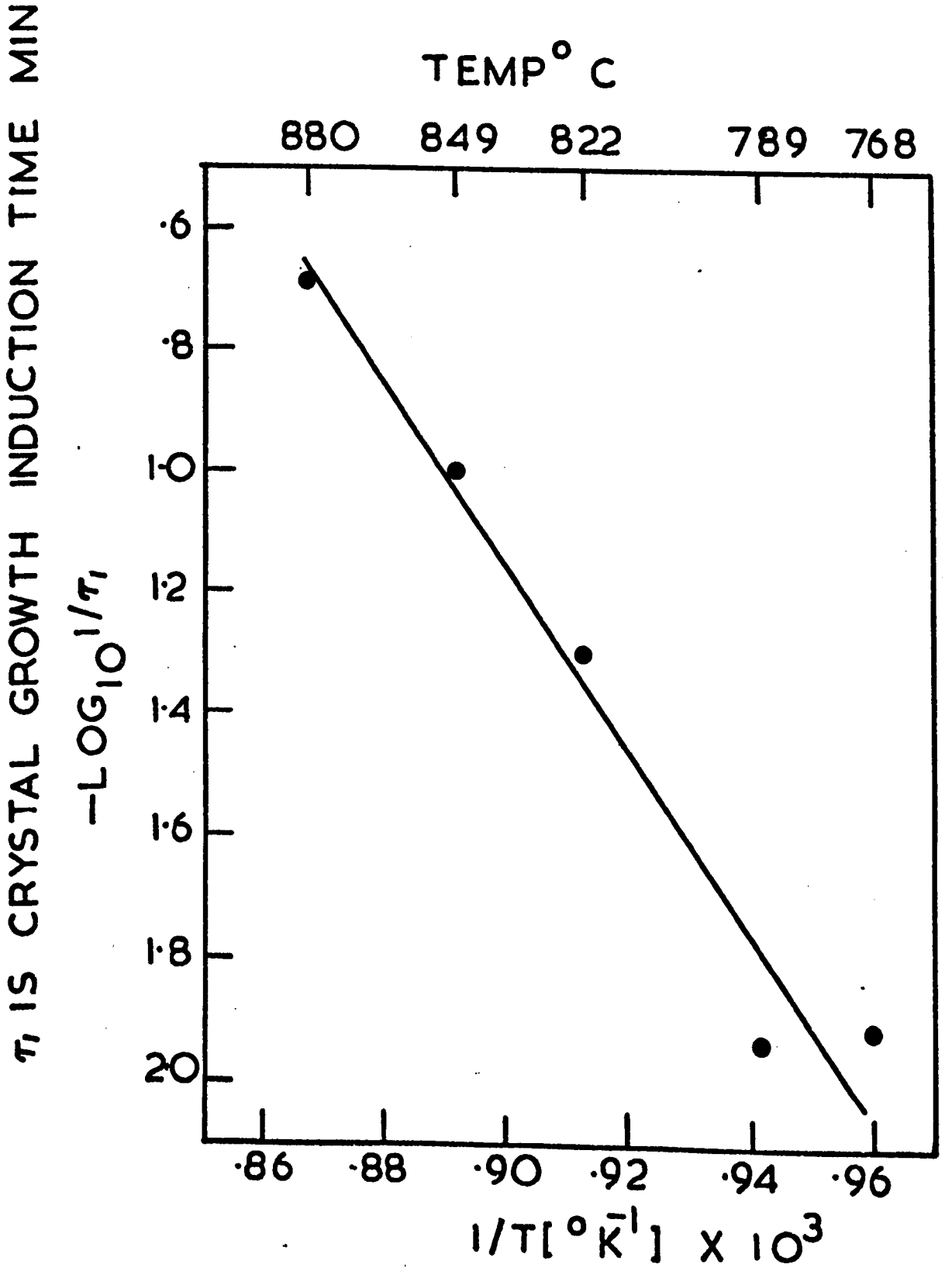
TEMP° C
880
849
822
789
768
·6
·8
1·0
1·2
1·4
1·6
1·8
2·0
$-LOG_{10}1/\tau_1$
·86
·88
·90
·92
·94
·96
$1/T[°K^{-1}] \times 10^3$
τ_1 IS CRYSTAL GROWTH INDUCTION TIME MIN

Figure 7.30 Plot of $\log_{10} 1/\tau_1$ ($mins^{-1}$) versus $\frac{10^3}{T}$ ($°K^{-1}$) for glass 30

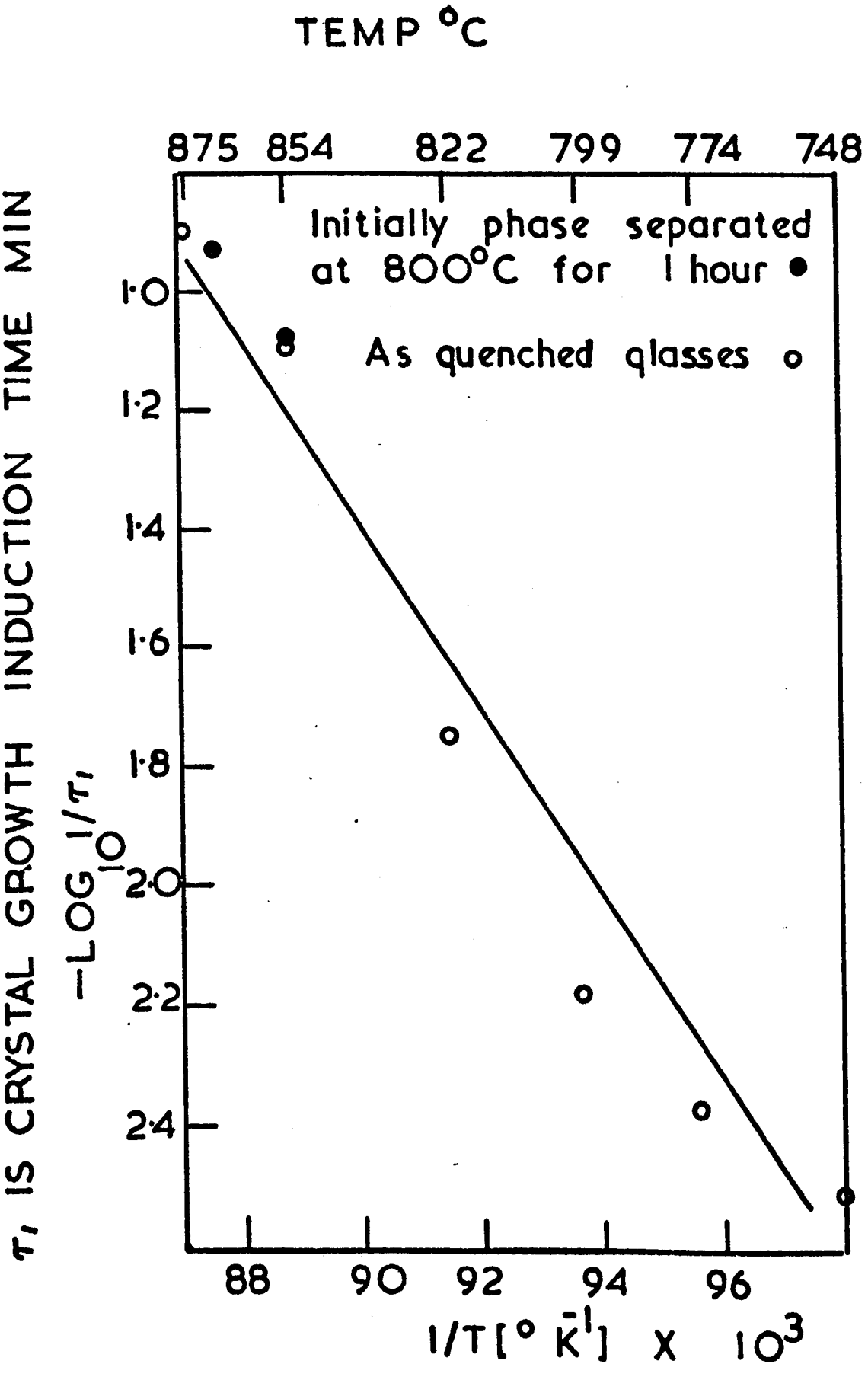
TEMP °C
875 854 822 799 774 748
Initially phase separated at 800°C for 1 hour ●
As quenched qlasses o
1·0
1·2
1·4
1·6
1·8
2·0
2·2
2·4
$-\log_{10} 1/\tau_1$
τ_1 IS CRYSTAL GROWTH INDUCTION TIME MIN
88 90 92 94 96
$1/T[^\circ \bar{K}^1] \times 10^3$

Figure 7.31 Plot of $\log_{10} 1/\tau_1$ ($mins^{-1}$) versus $\frac{10^3}{T}$ ($°K^{-1}$) for glass 28

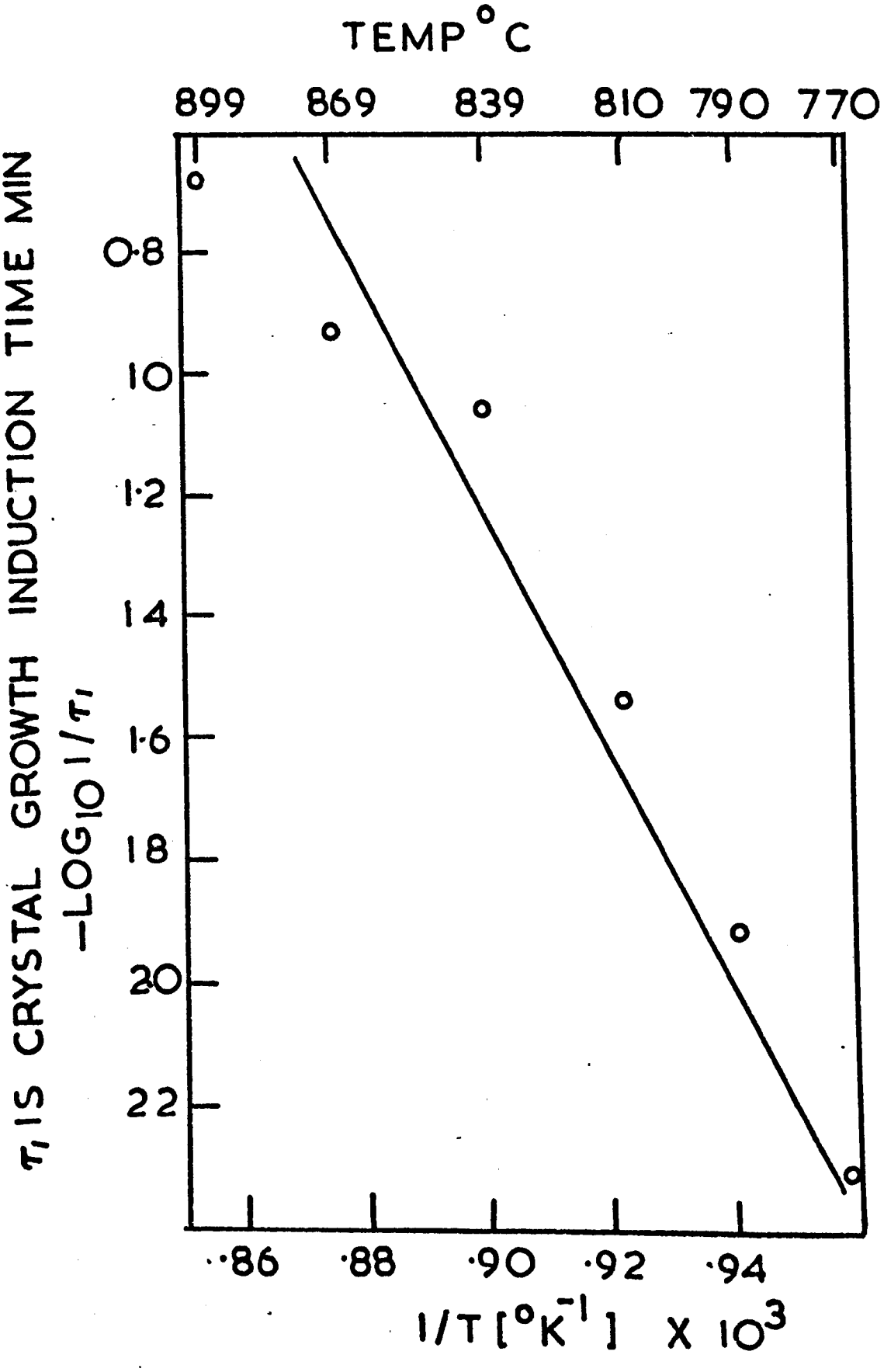
TEMP °C
899
869
839
810
790
770
0·8
1·0
1·2
1·4
1·6
1·8
2·0
2·2
τ_1 IS CRYSTAL GROWTH INDUCTION TIME MIN
$-\log_{10} 1/\tau_1$
·86
·88
·90
·92
·94
$1/T\,[°K^{-1}] \times 10^3$

Figure 7.32 Plot of $\log_{10} 1/\tau_1$ (mins^{-1}) versus $\frac{10^3}{T}$ ($^\circ K^{-1}$) for glass 26

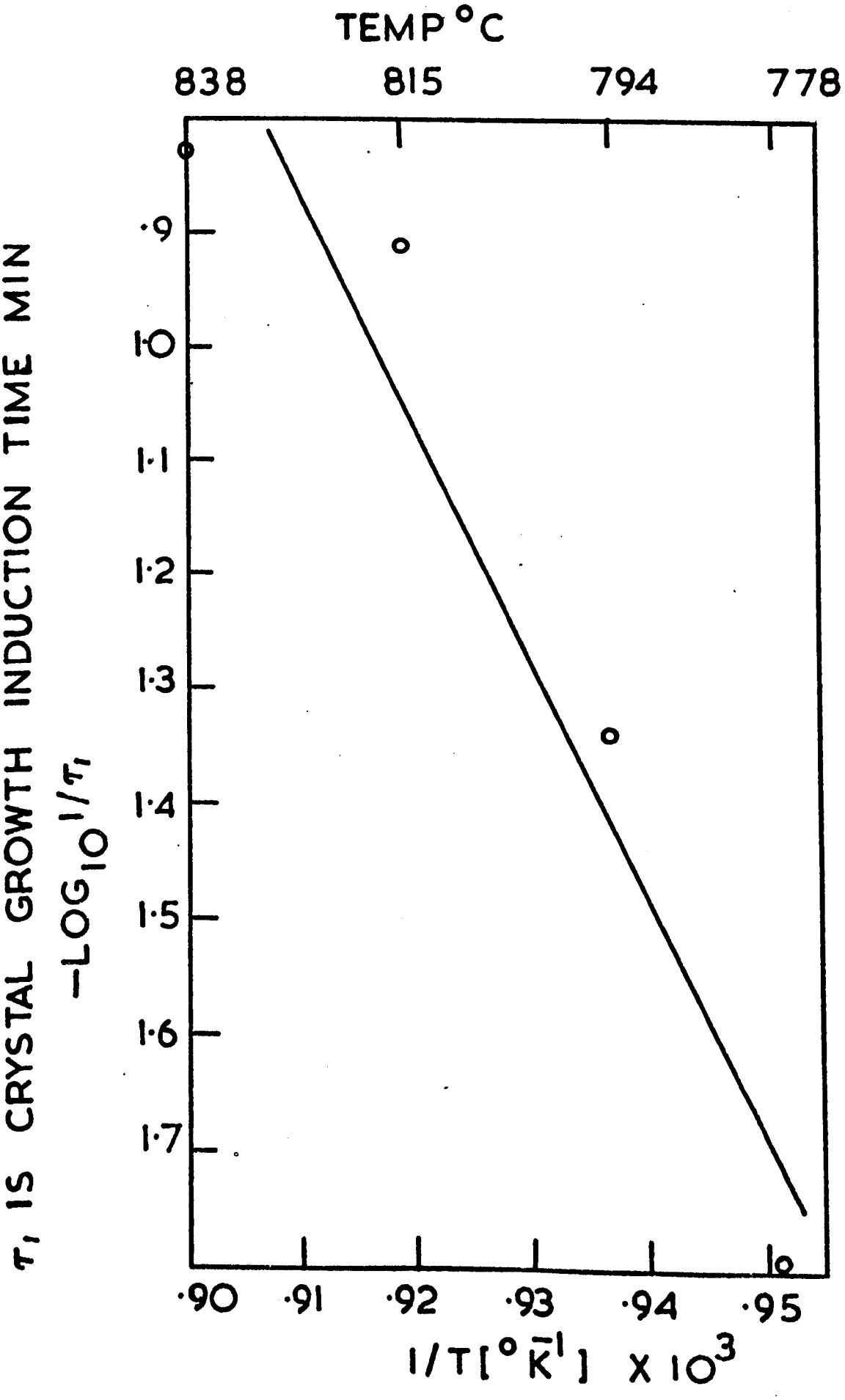
TEMP °C
838
815
794
778
·9
1·0
1·1
1·2
1·3
1·4
1·5
1·6
1·7
·90
·91
·92
·93
·94
·95
1/T[°K⁻¹] X 10³
τ, IS CRYSTAL GROWTH INDUCTION TIME MIN
−LOG₁₀ 1/τ₁

Figure 7.33 Plots of $\log_{10} 1/\tau_1$ ($mins^{-1}$) versus $\frac{10^3}{T}$ ($°K^{-1}$) for glasses 32, 26 and 35G

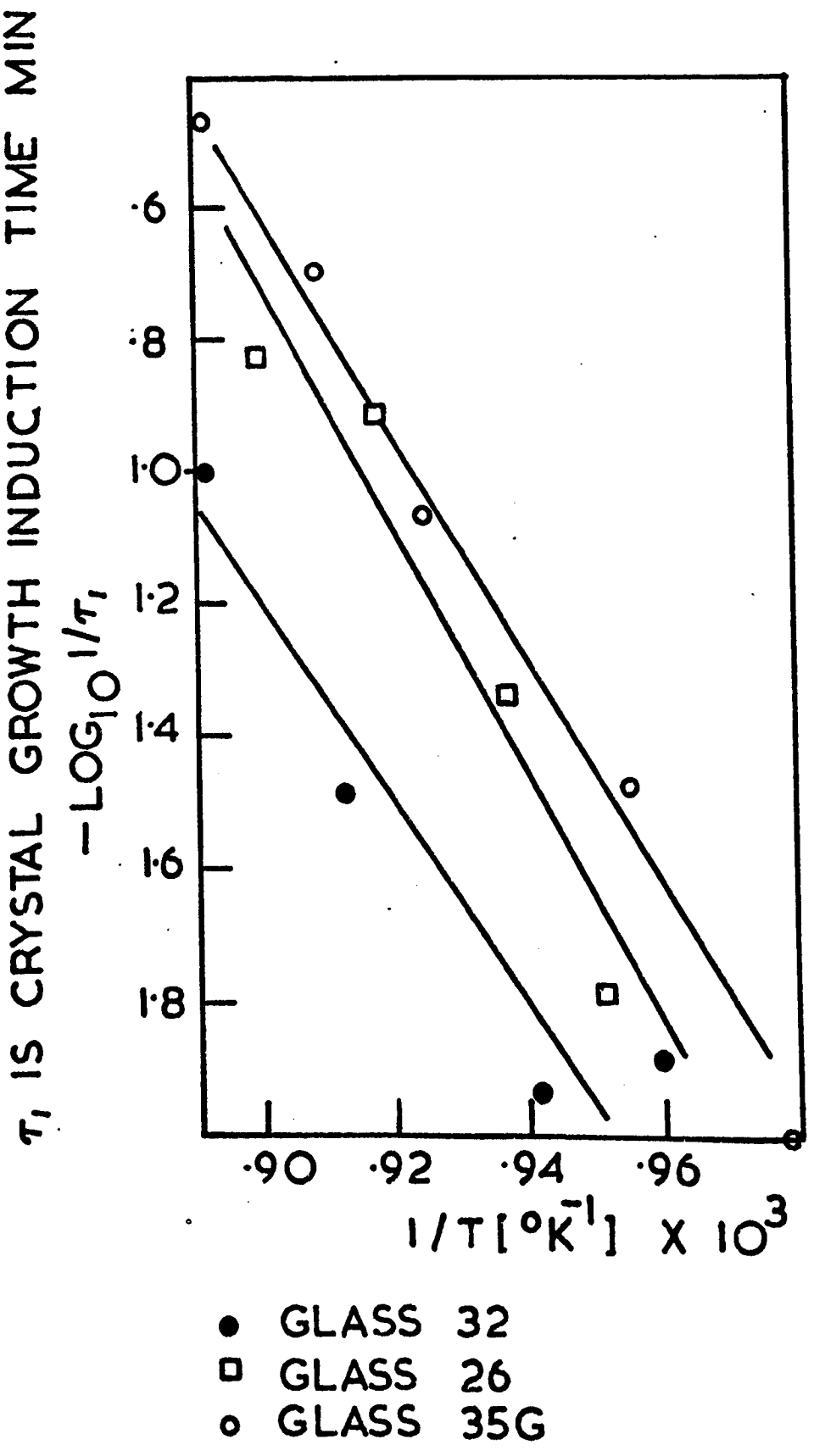
τ_1 IS CRYSTAL GROWTH INDUCTION TIME MIN
$-\log_{10} 1/\tau_1$
·6
·8
1·0
1·2
1·4
1·6
1·8
·90
·92
·94
·96
$1/T[^{\circ}K^{-1}] \times 10^3$
GLASS 32
GLASS 26
GLASS 35G

Figure 7.34 Plots of $\log_{10} 1/\tau_1$ ($mins^{-1}$) versus $\frac{10^3}{T}$ ($°K^{-1}$) for glasses 28 and 30

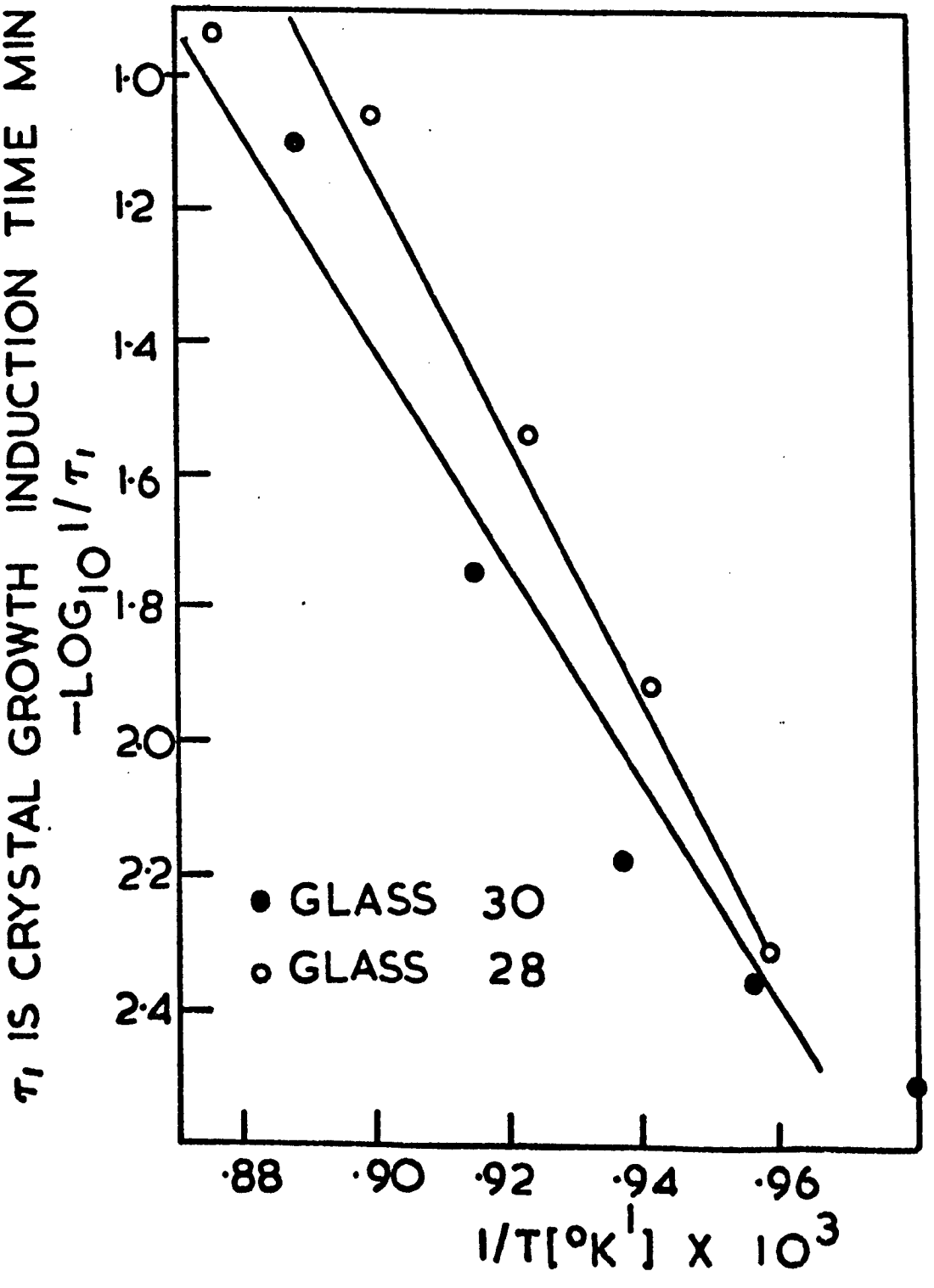
τ_1 IS CRYSTAL GROWTH INDUCTION TIME MIN
$-\log_{10} 1/\tau_1$
1·0
1·2
1·4
1·6
1·8
2·0
2·2
2·4
● GLASS 30
○ GLASS 28
·88
·90
·92
·94
·96
$1/T[^{\circ}K^{-1}] \times 10^3$

Straight lines were fitted to the lower temperature data on each Arrhenius plot using only those points that a) exceeded five minutes, b) corresponded to linear growth. The activation energies obtained from the slopes are given in Table (7.5). These values are useful as a rough guide only since they are subject to a much larger uncertainty than the activation energies for crystal growth.

TABLE 7.5

INDUCTION TIME ACTIVATION ENTHALPIES ΔH_τ

Glass	ΔH_τ kcals mole^{-1}	Temperature range of calculation °C
35C	83	749-828 (4 points)
32	62	768-849 (4 points)
30	51	748-822 (4 points)
28	79	770-869 (5 points)
26	86	778-838 (4 points)

A possible explanation for the presence of an induction time might be the time necessary for the small samples to reach the growth temperatures when inserted in the hot furnace. However, this time was no more than three minutes so it is impossible to explain the very large intercept times observed particularly at lower temperatures. For this reason τ_1 values less than five minutes were considered to be inaccurate.

The most likely explanation of the intercept times was given in an earlier section (7.1) where the intercept for glass 35 was found to be due to the induction time required to nucleate a spike (spine) on the initially formed sphere. The rapid longitudinal growth of the spike (spine) was identified as the radial growth of the spherulites on optical micrographs. Also, it was suggested that the spines were composed of low BS_2 and grew much more rapidly than the spheres composed of high BS_2.

For compositions other than 35 the same mechanism (i.e. nucleation of a spike) may give different induction times. The nucleation induction time of the spike (spine) will probably be dependent on ΔG_v (the free energy driving force per unit volume for nucleation of spikes), the effective surface energy σ, and the viscosity of the glass η according to the following equation[65]:

$$\tau_1 \propto \frac{\sigma\eta}{(\Delta G_v)^2}$$

Thus τ_1 is affected by a) the overall composition (BaO content), b) the occurrence of liquid immiscibility, c) the presence of impurities, such as Al_2O_3.

The occurrence of phase separation may affect the induction time τ_1 in at least two ways: 1) the induction time may be enhanced by reluctance of the glass to phase separate, 2) phase separation may act to cause compositional changes of the phases. It is interesting to note that Tomozawa[143] observed an intercept in the crystal growth of Li_2O-SiO_2 glasses that phase separated. The intercept was similar in magnitude to the time necessary to complete phase separation. He identified the crystal growth induction time with the time to phase separate the glass.

However, this mechanism is not likely to be important in $BaO-SiO_2$ glasses at the growth temperatures used since phase separation was completed in a very short time compared with τ_1 (e.g. glass 30 phase separates at 780°C in less than 30 mins but τ_1 is approximately 200 mins). Also τ_1 was still substantial even for glasses that do not phase separate.

Comparing the Arrhenius plots for the two non-phase separating glasses in the low alumina group, (32 and 35G) the induction times are considerably higher for 32. This is probably because 32 has a slightly higher viscosity than 35G[136]. The other glass in the low alumina group, glass 26, phase separates readily and the matrix composition shifts towards $BaO2SiO_2$. The viscosity of this phase is reduced and τ_1 is lowered. However, τ_1 is still greater than that of 35G since the composition of the matrix does not reach the composition of 35G. This assumes that phase separation occurs to completion in times short compared with growth times, which is known to be the case. This argument cannot explain why τ_1 for 32 is higher than τ_1 for 26. There is, however, no corresponding anomaly in the growth rate results.

Consider now the results for glasses 28 and 30 which contain higher levels of alumina impurity. Both glasses have higher values of τ_1 than the glasses in the low alumina group. This is probably a reflection of the ability of alumina to increase the viscosity and so inhibit the nucleation of spikes. Glass 30 has a higher τ_1 than 28 and the comparison is analogous to that previously described for 26 and 32.

The activation enthalpies ΔH_τ given in Table (7.5) are similar in magnitude to the growth activation enthalpies (see Table (7.4)). However, the errors involved are much larger (ΔH_τ) and because of this no accurate comparison can be made. It seems that ΔH_τ is approximately the same for both phase separated and non-phase separated glasses (also high and low

alumina). Also, there is slight evidence that the $\log_{10} 1/\tau_1$ versus 1/T plot for glass 30 is curved.

Summarising, the main features of the log $1/\tau_1$ vs 1/T plots can be explained according to the viscosities of the glasses and their dependence on composition and temperature (and phase separation). However, some inconsistencies do appear when comparing glasses 26 and 32 and also 30 and 28, and there may be additional effects which have not been considered. One possibility is that the presence of a fine scale interconnected phase separation (as in 26 and 28) may cause the induction time for spike nucleation to decrease, perhaps by affecting ΔG_v and σ for spike nucleation. Further work is required to clarify this problem.

7.4 DISCUSSION OF THE NON-LINEAR GROWTH WITH TIME

All the glasses studied exhibited non-linear growth with time (i.e. non constant growth rates) at higher temperatures (Figures 7.18-7.21). For glasses 32, 26 and 30 the non-linear behaviour became noticable at 850°C and at a somewhat higher temperature for glass 28. In fact the effect was less apparent for glasses 26 and 28.

The occurrence of non-linear growth with time is not common in inorganic glass-forming systems. However, Williamson et al[146,147] have reported gradually increasing growth rates with time of wollastonite and anorthite in $CaO-MgO-Al_2O_3-SiO_2$ glasses containing iron oxide additions at the higher temperatures of investigation. When the iron oxide additions were replaced by vanadium oxides complete linear crystal growth occurred. Electron probe microanalysis indicated an iron oxide enriched layer at the interface of the growing crystal. The presence of Fe^{2+} and Fe^{3+} reduced the viscosity of the glass and increased the crystal growth rate. They also considered the possibility that material diffusion across the layer to the interface

may control the growth. However, this would lead to a gradually reducing crystal growth rate with time. They eliminated the possibility that changes in the molecular configuration of the glass, as the temperature is raised to crystallize the glass, could alter the growth rates since the relaxation times at these higher temperatures (>> Tg) are very small (< 1 sec). The effect of latent heat of crystallization is to establish a temperature gradient across the interface thus raising the temperature at the crystal face above that of the furnace. This could in theory lead to continuously increasing crystal growth rates. However, they commented that the slight magnitude of the resulting temperature gradient was not likely to produce greatly increasing growth rates.

Toropov and Tigonen[148] have also reported non-linear growth rates with time of anorthite in the system $CaO-Al_2O_3-SiO_2$.

Non-linear parabolic crystal growth was observed in devitrification studies of non-stoichiometric silica[149]. The parabolic dependence of cristobalite layer thickness on time was due to the rate of diffusion of oxygen or water through the material to the growing crystal face. Thus the crystal growth rate was dependent on the partial pressure of oxygen in the atmosphere. In the case of stoichiometric silica a constant growth rate was observed and oxygen diffusion was no longer necessary.

There are a number of possible reasons for the non-linear growth with time in the baria-silica glasses, which are as follows:-

(a) The presence of a component in the glass (major or minor) might cause the effect, as in the glasses studies by Williamson et al[146,147].

The growth of $BaO2SiO_2$ crystals in glasses containing less than 33⅓ mole% BaO may involve the rejection of SiO_2 at the crystal-glass interface. This would locally increase the viscosity and decrease ΔG, the thermodynamic driving force, in the vicinity of the interface thus

retarding growth. Thus rejection of impurities can cause a local decrease in growth rate near the interface. In practice this is unlikely to occur since the interface is not smooth but is composed of many fine crystal fibres in the spherulitic morphology. According to the theory of Keith and Padden[138] this morphology can arise due to the rejection of impurities. The planar interface becomes unstable in profile and small protuberances, which extend into the melt containing less impurity, grow at a faster rate. Eventually the whole spherulite grows with a constant rate with frequent non-crystallographic branching of the fibres. Such a mechanism has been suggested by Burnett and Douglas[15] to explain the spherulitic growth of barium disilicate in Na_2O-BaO-SiO_2 glasses. The small fibres (or spikes, as appropriate) grow linearly and the rejected SiO_2 is incorporated into the residual glassy phase between them. Hence there is no progressive build-up of SiO_2 'impurity' ahead of the growth front and the growth rates remain constant. In fact a build-up of silica would probably cause a progressive decrease in growth rate with time which is not observed. For the same reason, the presence of alumina impurity levels in the glass would not explain the observations assuming a build-up of alumina ahead of the growing spherulite, since alumina is known to decrease growth rates in barium disilicate glass.

There is also the possibility of other impurities affecting the growth rates with time. Thus small levels of iron are present in the glasses (Table (5.1)) and might affect the growth rates, as observed by Williamson et al[146,147]. A build-up of iron near the interface would produce a gradually increasing growth rate with time, provided addition of iron to these glasses increases the growth rate of barium disilicate. Unfortunately we have no data on the effect of small quantities of iron. However, small quantities of Na_2O or Li_2O are likely to cause significant

changes in growth rates as demonstrated by Rowlands[18] in the Li_2O(and Na_2O)-BaO-SiO_2 systems. Thus when 10 mol% Li_2O2SiO_2 is added to $BaO2SiO_2$ the growth rate of barium disilicate is increased at 750°C by about 7000 times. Thus trace impurities of alkali oxides might have a significant effect if rejected at the interface, by lowering the viscosity and exerting an increasing effect on growth with time. However, it may be argued that impurities such as these are unlikely to have any appreciable effect if the fibres in the interface undergo frequent branching since the impurities may be trapped between the fibres rather than accumulating ahead of the interface.

It should also be mentioned that Burnett and Douglas[15] also observed in some cases non-linear behaviour in the growth of barium disilicate in the Na_2O-BaO-SiO_2 system. However, this was a decrease in growth rate after longer periods and occurred when the spherulites began to approach closely together. The residual glassy phase was trapped between them, and the growth became controlled by long range diffusion rather than short range diffusion across the interface. This presumably occurred due to the gradual depletion of barium disilicate in the residual glass between the spherulites. No such decrease in growth rates was observed in the present experiment probably because the spherulites did not approach sufficiently closely.

(b) It is also possible that rejected Al_2O_3 or SiO_2 impurities in the glass may eventually crystallize and thus be unable to retard crystal growth further. Evidence has been presented (see Table (6.3) and section (6.1.2)) suggesting that cristobalite precipitates as a minor phase in some BaO-SiO_2 glasses at higher temperatures. Thus the gradual withdrawal of Al_2O_3 or SiO_2 from the glass could lead to gradually increasing crystal growth rates.

(c) The evolution of heat at the interface due to crystallization must also be considered. Heat flow effects are usually not important in glass-forming systems due to the relatively slow growth rates involved but are of great importance in, for example, metallic systems where they are responsible for the dendritic crystallization. It is not proposed to consider dendritic crystallization in detail but a brief discussion is relevant. A typical temperature profile across a crystal-liquid interface, in a situation where heat flow effects are important, is shown schematically in Figure (7.35)[151,150]. When the growth rate increases rapidly with undercooling (i.e. falling temperature) the interface shown is unstable with regard to small projections since undercooling increases with distance from the interface. The main growth will occur at the tip of the projection and not at the base and hence the projection will develop into a spike. Other spikes would form at distances determined by the radius of the zone affected by the first spike. Thus an array of spikes grow. The lateral growth of each is retarded by the latent heat of the others and so forward growth predominates. Branches may form which are in the same crystallographic orientation as the original spikes, as a result of corresponding instability of their lateral interfaces. Branching does not involve the nucleation of a fibre, probably with a different crystallographic orientation, as in the case of spherulitic growth. Such dendritic crystallization is important in metals and is probably also important in some glass-forming systems at higher temperatures near the liquidus. In this case growth rates increase with undercooling and thermal dendrites may result. However, at lower temperatures below the maximum in crystal growth rate, growth rates decrease with fall in temperature and for the probable temperature distribution (Figure (7.35)) then no instability would occur. This has been pointed out for the crystallization of a lithium disilicate glass[129] and also applies to the present baria-silica glasses.

Figure 7.35 Typical temperature profile at a crystal-glass interface (reference (150))

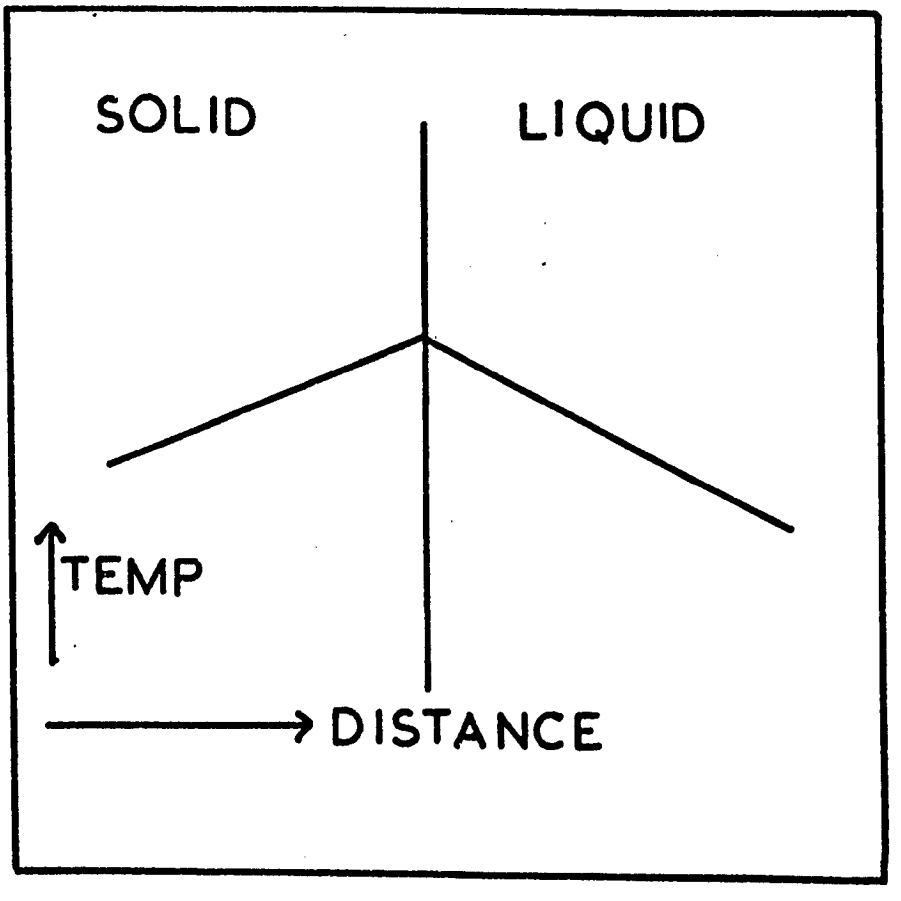
SOLID
LIQUID
TEMP
DISTANCE

Consider the question of the gradual increase in growth rates observed at some higher temperatures in the baria-silica glasses in relation to possible heat flow effects. In the temperature range involved, crystal growth rates were observed to increase with temperature. To explain the observations, the temperature of the interface would be required to gradually increase with heat treatment time.

This possibility has recently been considered theoretically by Hopper and Uhlmann[151] for a planar crystal-melt interface. Applying their analysis to the crystallization of sodium disilicate they showed that a significant rise in interface temperature should occur for an infinite system. However, for small samples (4 mm in thickness) the theory predicted no significant change in interface temperature with time. This theoretical result was confirmed experimentally. The results of Hopper and Uhlmann suggests that the heat flow is unable to explain the non-constant growth rates in baria-silica glasses, since only small sized samples were employed.

It may also be remarked that if heat flow effects are responsible for the non-linear growth, then it is likely that the effect would have been observed in many more systems (for example Li_2O-SiO_2) - whereas it has not.

(d) Another possible cause of the non-linear growth behaviour is a morphology change in the barium disilicate. MacDowell[16], Burnett and Douglas[15], and Rowlands[18] have all observed a break-up of the spherulites and recrystallization into lath-like crystals of the low form barium disilicate at higher temperatures. The temperature and times where non-linear growth became noticeable for the present glasses coincide approximately with the temperatures and times appropriate for lath formation, as indicated by the work of Rowlands. A morphology change in the spherulites near the interface would probably alter the growth kinetics, particularly if the fine crystal fibres or spikes at the interface developed into a coarser microstructure.

In summary, it is not possible to identify with certainty the cause of the non-linear growth behaviour observed. The most likely cause is the change in spherulite morphology that occurs at higher temperatures and longer times. Another possibility, for which there is less evidence, is the presence of small quantities of iron impurity in the glasses which might have a similar effect to that observed by Williamson et al[146,147].

Further work which might help to resolve this question would involve a more detailed study of lath formation in these glasses using optical and electron microscopy of samples showing non-linear growth, electron microprobe analysis of the interface region for impurities, particularly iron, and perhaps study of the effects of deliberate additions such as iron, on the growth rates.

CHAPTER EIGHT

THE EFFECT OF ELECTRIC FIELDS ON CRYSTAL NUCLEATION AND GROWTH IN GLASSES

CHAPTER EIGHT - THE EFFECT OF ELECTRIC FIELDS ON CRYSTAL NUCLEATION AND GROWTH IN GLASSES

8.1 THEORY OF FIELD INDUCED EFFECTS ON NUCLEATION

The influence of an electric field on nucleation will depend on its ability to alter σ, ΔG_D (the kinetic barrier) and ΔG (the thermodynamic driving force).

Kaschiev[11] has developed a theory that considers the effect of an electric and magnetic field on ΔG only. He presented the free energy change required for the formation of a spherical cluster of radius r in the form:

$$W = W_o + W_E$$

where W_o is the free energy change without an electric field and W_E is the free energy change due to the field. W_o has already been expressed in equation (3.1) as

$$W_o = - \frac{4\pi r^3 \Delta G}{3V_M} + 4\pi r^2 \sigma \qquad (3.1)$$

Kaschiev[11] has deduced that W_E is

$$- \frac{\varepsilon_M f(\lambda) E^2 r^3}{6} \qquad (8.1)$$

$$\text{where } f(\lambda) = \frac{(1 - \lambda)}{(2 + \lambda)} \quad , \quad \lambda = \frac{\varepsilon_C}{\varepsilon_M}$$

where ε_C and ε_M are the dielectric permittivities of the crystalline and glass phases. For the case where $\varepsilon_C < \varepsilon_M$, W_E is negative and nucleus formation is encouraged, and vice versa when $\varepsilon_C > \varepsilon_M$. On the other hand, Isard[12] has shown that under experimental circumstances where a field of constant magnitude is applied from a battery, W_E is positive and nucleus

formation is encouraged when $\varepsilon_C > \varepsilon_M$. He has also shown, by considering the introduction of a medium of dielectric permittivity $\bar{\varepsilon}$ (containing glass and crystals) in place of the original glass ε_M, that the equation of Kaschiev (eqn. (8.1)) is in error. A modified version is given below:

$$W_E = + \frac{\varepsilon_M f(\lambda) E^2 r^3}{2} \qquad (8.2)$$

A further complication arises when static fields and slowly alternating fields are applied across the glass. Under these circumstances charges build up at the interface. The local field intensity becomes dependent on the conductivities of the two phases if the field is static for a period of time longer than ε_M/χ_M or ε_C/χ_C, whichever is the smaller[12]. This difficulty can be easily accommodated by a substitution of conductivities χ for permittivities ε, i.e. $\lambda = \chi_C/\chi_M$.

Figure (8.1) demonstrates schematically how electric fields alter the free energy changes W, depending on the relative values of the dielectric permittivities.

In the presence of an electric field, equation (3.1) is modified to give:

$$W = - \frac{4\pi r^3}{3} [\Delta G_V + hE^2] + 4\pi r^2 \sigma \qquad (8.3)$$

and $$h = - \frac{3\varepsilon_M f(\lambda)}{8\pi} \qquad \Delta G_V = \frac{\Delta G}{V_M}$$

The critical values of r* and W* in the presence of an electric field are:

$$r^* = \frac{2\sigma}{[\Delta G_V + hE^2]}$$

Figure 8.1 Free energy change for nucleus formation as a function of nucleus radius,

a) when $\varepsilon_c < \varepsilon_m$

b) when $\varepsilon_c > \varepsilon_m$

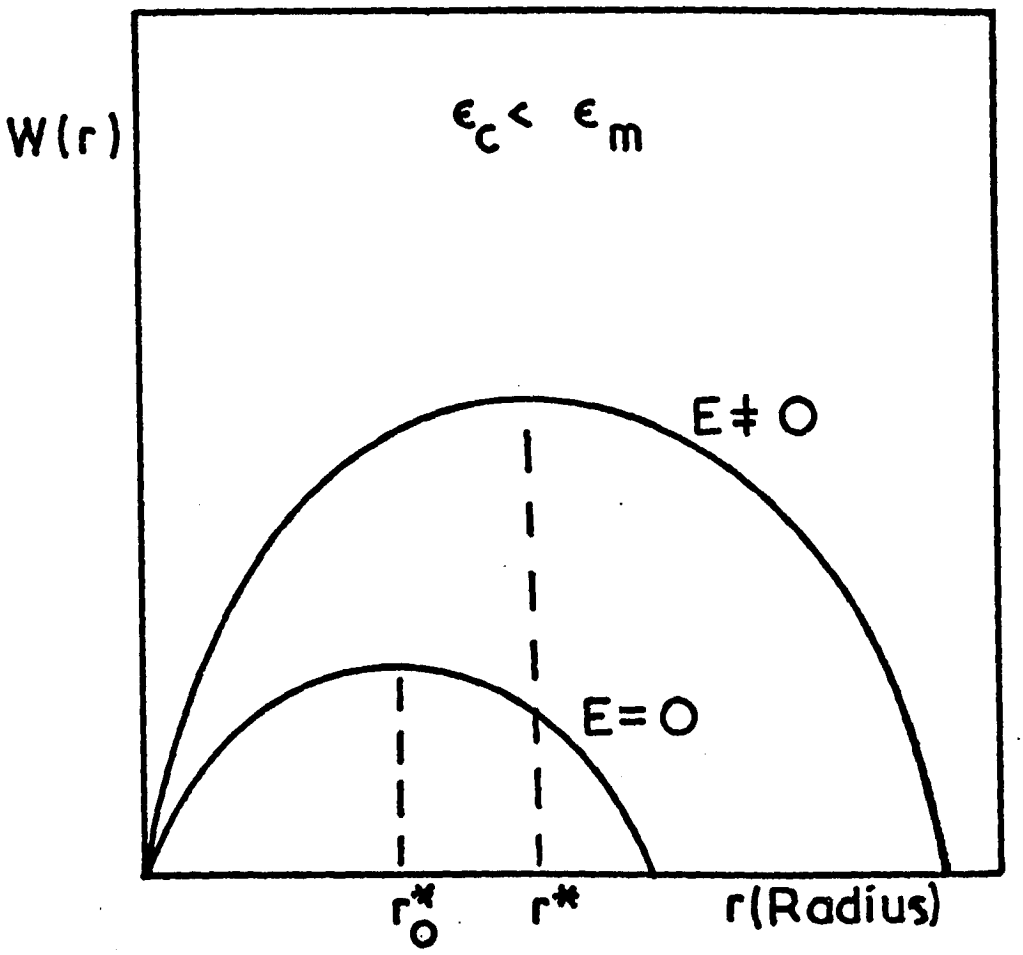
W(r)
$\epsilon_c < \epsilon_m$
E ≠ O
E = O
r_o^*
r^*
r(Radius)

a)

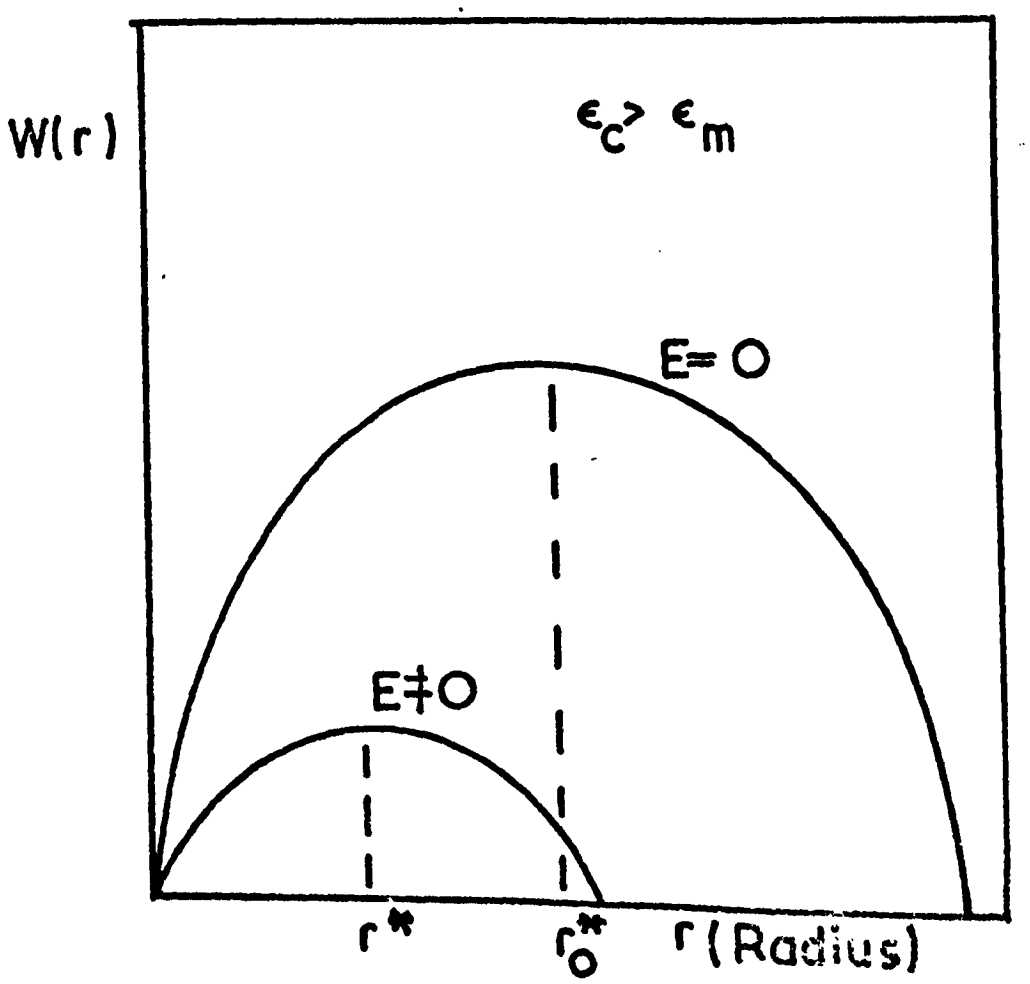
W(r)
$\epsilon_c > \epsilon_m$
E = O
E ≠ O
r^*
r_o^*
r (Radius)

b)

$$W^* = \frac{16\pi\sigma^3}{3[\Delta G_v + hE^2]^2} \tag{8.4}$$

Assuming that the pre-exponential factor and ΔG_D in the nucleation rate equation are constant during the application of a field, the classical nucleation equation becomes:

$$I = A \exp(-\frac{W^*}{kT}) \tag{8.5}$$

$$\text{where } A = \frac{NkTA^*}{h} \exp(-\frac{\Delta G_D}{kT})$$

Substituting equation (8.4) into equation (8.5):

$$I = A \exp\left[\frac{-B}{[\Delta G_v + hE^2]^2}\right] \tag{8.6}$$

$$\text{where } B = \frac{16\pi\sigma^3}{3kT} \tag{8.7}$$

When E = O equation (8.6) reduces to:

$$I_o = A \exp(\frac{-B}{\Delta G_v^2}) \tag{8.8}$$

where I_o is the nucleation frequency without a field. Expanding $[\Delta G_v + hE^2]^{-2}$ as a power series in equation (8.6):

$$I = A \exp(\frac{-B}{\Delta G_v^2}[1 - \frac{2hE^2}{\Delta G_v} + \ldots])$$

When $T < T_M$; i.e. $\Delta G_v > O$ and assuming $|hE^2| \ll \Delta G_v$, all terms beyond the second in the series can be neglected.

$$I = A \exp\left(\frac{-B}{\Delta G_v^2}\right) \exp\left(\frac{2hBE^2}{\Delta G_v^3}\right)$$

$$= I_o \exp\left(\frac{2hBE^2}{\Delta G_v^3}\right) \qquad (8.9)$$

Substituting $r^* = 2\sigma/\Delta G_v$ into equation (8.7):

$$B = \frac{2\pi \Delta G_v^3 \, r^{*3}}{3kT}$$

Substituting equation (8.7) into equation (8.9):

$$I = I_o \exp\left[\frac{4\pi r^{*3} h E^2}{3kT}\right]$$

Defining the critically sized field E_c as that required to increase or decrease the nucleation rate e times:

$$\frac{4\pi r^{*3} h E_c^2}{3kT} = 1$$

$$\text{or} \quad E_c = \left(\frac{3kT}{4\pi r^{*3} h}\right)^{\frac{1}{2}} \qquad (8.10)$$

A plot of I versus E indicates the great sensitivity of the field to changes in E once the critical field strength E_c is exceeded (see Figure (8.2)).

Kaschiev[11] has calculated that a critical field strength of 6.14×10^6 V cm^{-1} is necessary to influence the condensation of water vapour.

Figure 8.2 Dependance of the nucleation rate on the electric field strength,

a) when $\varepsilon_c > \varepsilon_m$

b) when $\varepsilon_c < \varepsilon_m$

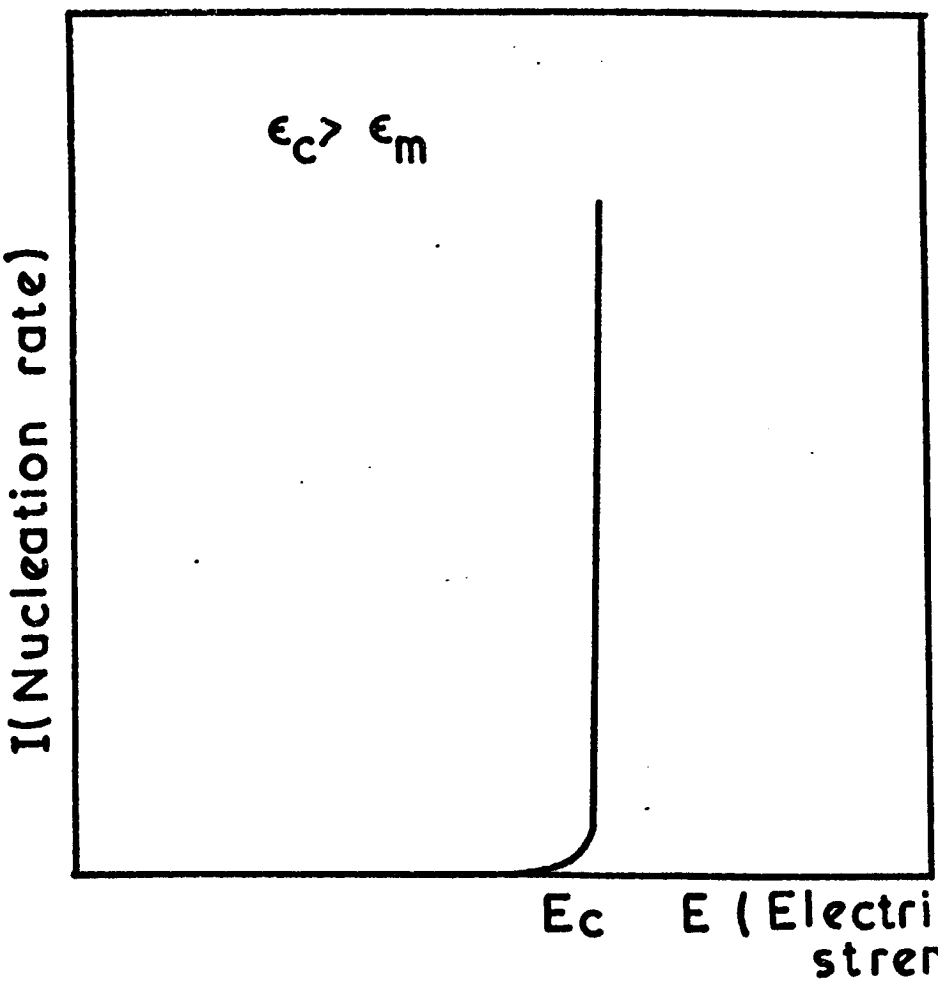
$\epsilon_c > \epsilon_m$
I (Nucleation rate)
Ec
E (Electric field strength)

a)

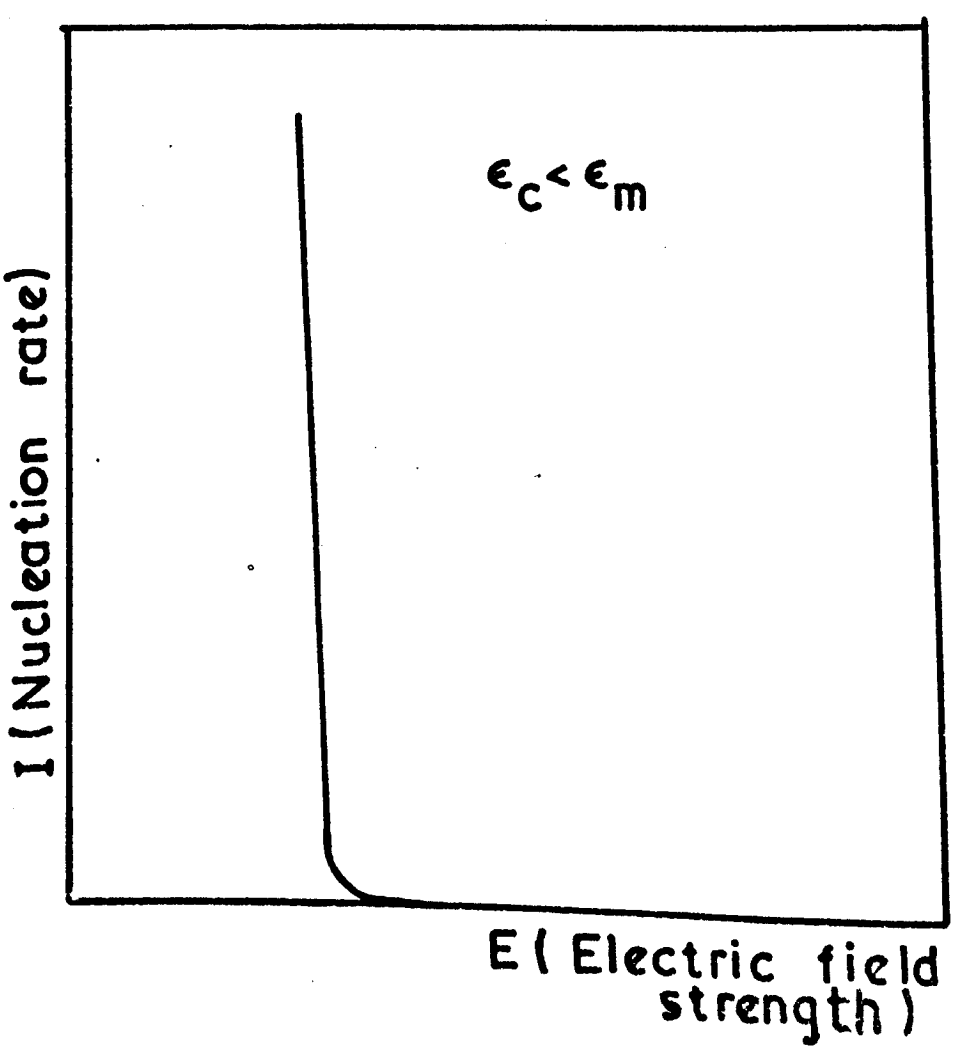
$\epsilon_c < \epsilon_m$
I (Nucleation rate)
E (Electric field strength)

b)

8.2 REVIEW OF GENERAL OBSERVATIONS OF FIELD EFFECTS ON PHASE TRANSFORMATIONS

A brief review of experiments designed to study the effects of electric fields on phase transformations is given below.

The effect of fields on dendritic growth of ammonium chloride on muscovite mica and glass substrates was studied by Motoc[152]. It was observed that the growth of crystalline needles occurred in the direction of the field. On removal of the field the needles developed branches which eventually detached themselves from the needles. An alternating field produced a similar effect. Under an a.c. field the dendritic growth was parallel to the field, the central stem being thickened. These effects were explained by assuming that the electric field increased the surface energy of the crystal. The application of the field acted to inhibit the formation of any perturbation so that the formation of needles rather than dendrities was favoured. Removal of the field caused the surface energy to decrease and encouraged the formation of branches.

Bartlett et al[153] and Crowther[154] have studied the growth of ice crystals in the presence of an electric field. They reported that a minimum value of the electric field was necessary to modify the growth. The crystals grew in the form of long thin needles. This was attributed to an increase in the molecular diffusion coefficient along the field direction, encouraging crystal growth in this direction. However, alternating fields and non-uniform static fields were not observed to modify the crystal growth rates.

Chopra[156] and Murayama et al[155] have reported increased coalescence and alignment of gold particles in a thin gold sheet along the direction of an electric field.

Peters et al[157], when applying a magnetic field during the isothermal martensitic transformation of a Ni-Mn alloy, observed a threefold increase in the transformation rates.

The application of electric fields is known to initiate memory switching in chalcogenide glasses. The voltage required to achieve the switch is known as the threshold voltage. The resistivity of the glass drops dramatically by 10^5 ohm cm or more and approaches that of a semiconductor[158]. The mechanism of switching is thought to be the precipitation of low resistivity phases (both crystalline and amorphous). This can be achieved by a) joule heating caused by the passage of a current. For example, it is thought that switching in GeTe glasses is associated with thermally induced crystallization of low resistance Te rich phases[160]. b) The effect of the field on free energy changes and diffusion may initiate crystallization or phase separation[161], and also encourage growth in the field direction. The alignment and coalescence of filament shaped particles in the direction of the field can produce low resistivity bridges across the material. For example, Thornburg and White[158,159] have demonstrated that an electric field can cause memory switching in an As_2Se_3 glass by such an alignment. In this sense the effect of the electric field is similar to that described earlier for non-glass-forming systems where crystals are encouraged to grow in certain directions.

Chandhari and Laibnwitz[162] have described the growth of crystalline filaments of a Te-rich phase from local field concentrations in a GeTe glass.

Geller et al[163] have investigated the power of electric fields to increase nucleation and growth of spherulites in a selenium glass. Their results showed a reduction of the activation energy for crystallization during the application of an electric field. It was thought that the field weakened the atomic structure and allowed the atoms more freedom of movement.

De Vekey and Majumdar[10] have studied the effect of 4 kV cm^{-1} static or alternating (50 Hz) electric fields on the phase separation morphology in a cordierite -based glass of composition CaO 4.5, SiO_2 48.9, Al_2O_3 22.2,

MgO 13.4, TiO_2 11.0 (wt %). The field was applied to a slab of glass at 690°C for 74 hours. An identical control sample was placed adjacent to the first sample. The electron micrographs of both samples revealed that the field had increased the size of the phase droplets although no change in number of droplets was detected.

Atkinson[164] was unable to confirm de Vekey and Majumdar's results on cordierite-based glass when using a field strength of 35 kV cm^{-1}. It is also interesting to note that Atkinson did not observe any increase in crystal nucleation and growth in a lithium silicate glass when a field was applied. However, because of excessive joule heating, he was unable to apply more than 250 V cm^{-1} to the glass.

MacKenzie and Brown[165,166] have recently studied the influence of an electric field on the crystallization of aluminosilicate glasses. They compared the areas and the positions of the main DTA crystallization peak obtained with and without a field. The heats of crystallization calculated from the peak areas were shown to decrease with increasing field strength. The peak was also observed to shift to lower temperatures, thus indicating that the field encouraged crystallization.

Summarizing, there are some claims from previous work that electric fields can modify the crystal nucleation and growth kinetics in various systems, including glasses. However, it is not clear how electric fields may affect the kinetics, if at all. For the experiments on glass, the systems used have tended to be rather complex, and also joule heating effects may have occurred. To attempt to clarify the situation we have used the relatively simple baria-silica system with some additions. This system exhibits internal crystal nucleation and has been fairly well characterised. Also, the internal electrical resistivity of the glass is relatively high. It is thus possible to apply fields of comparable strength to those employed

by de Vekey and Majumdar, and MacKenzie and Brown without excessive joule heating. The results of experiments designed to examine the field effect of crystal nucleation and growth kinetics in baria-silica glasses will be described shortly.

8.3 EXPERIMENTAL DETAILS

8.3.1 Preparation of magnesia aluminosilicate glass

As a starting point it was decided to carry out some experiments on a glass as close to that used by de Vekey and Majumdar[10] as possible. The batch composition was composed of 4.5 CaO, 48.9 SiO_2, 22.2 Al_2O_3, 13.4 MgO, 11.0 TiO_2 (all wt %) using the batch materials $Al(OH)_3$, TiO_2, Belgian sand, $CaCO_3$ and $MgCO_3$. The mixture was homogenised by rotation in a tumbler, then sintered at 1000°C for 24 hours in a mullite crucible. Melting was carried out in platinum in an electric furnace at 1480°C for six hours. Stirring was accomplished by bubbling air through the melt. This also ensured the oxidation of titanium ions in the glass. The melt was cast as rods and some as discs of 5 cms diameter, the latter being annealed in a muffle furnace at 660°C, and furnace cooled. The general appearance of the oxidised glass was a transparent yellow

8.3.2 The measurement of d.c. conductivity

A 3 cm square 1 cm thick slab of glass was cut from a disc and the largest area cross-section was coated with Johnson Matthey liquid bright platinum. The liquid layer was allowed to dry for one hour at room conditions and then fired at 500°C for one hour.

The electrode assembly is shown in Figure (8.3). All metal parts were made of heat resisting steel and the insulating rods of British

Figure 8.3 Electrode assembly used for electrical measurements

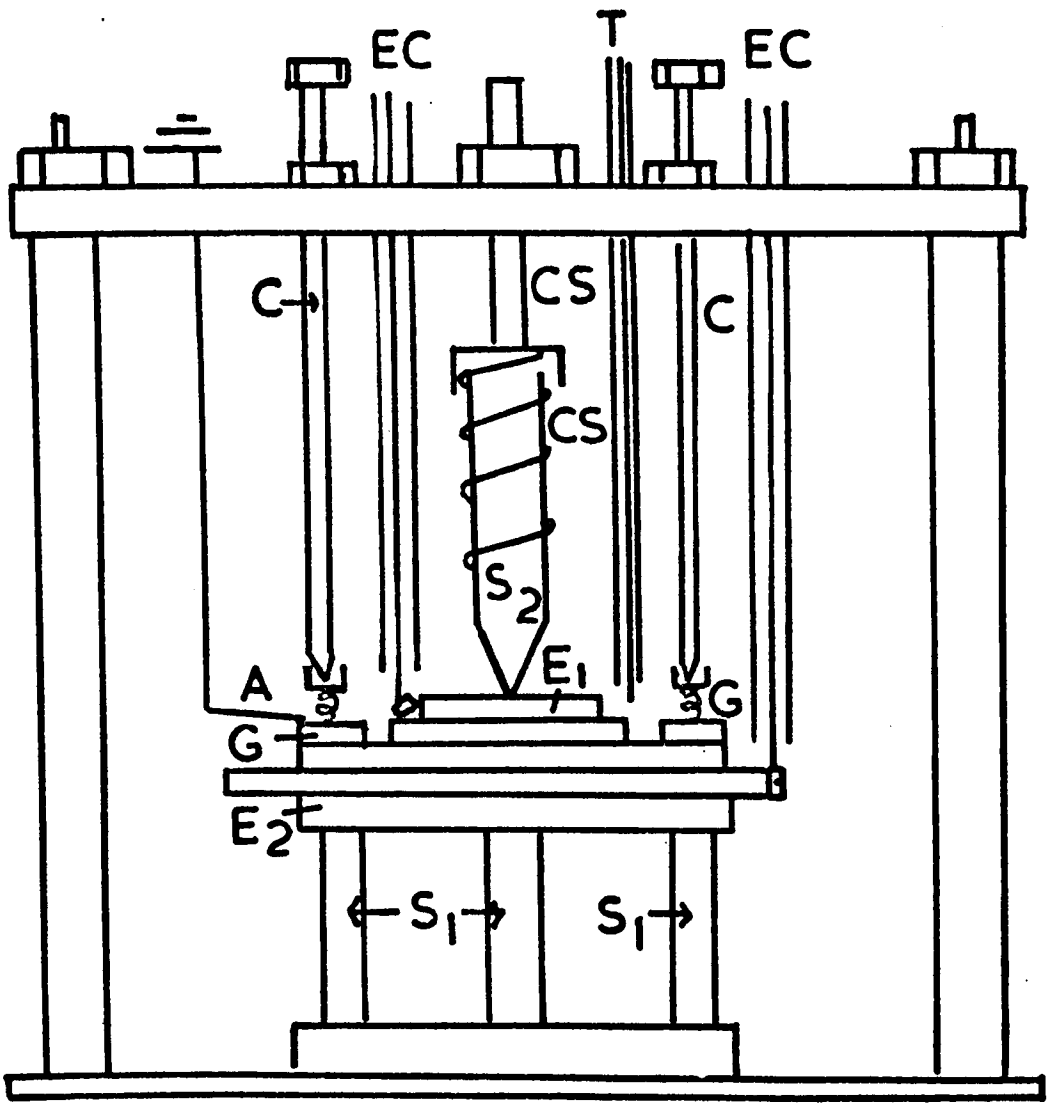

EC ELECTRICAL CONTACTS
T CHROME ALUMEL THERMOCOUPLE
C CLAMPING SCREWS
A ALUMINA CAPS TO ACCOMODATE C
S_1 FUSED SILICA RODS
S_2 CLAMPING SILICA ROD
CS CLAMPING SPRING/AND SCREW [FOR CENTRAL ELECTRODE]
G GUARD RING [EARTHED]
E_1 TOP ELECTRODE
E_2 BOTTOM ELECTRODE

Thermal Syndicate 'OS' quality fused silica. The assembly and specimen were enclosed in a metal container also made of heat resisting steel, the lid of which was pierced with holes for the electrical connections and the thermocouple. All metal parts, including the guard ring but excluding the electrodes, were earthed. The electrical leads were made of nichrome wire and insulated from the electrode assembly by fused silica tubes. The furnace consisted of a vertical cylindrical refractory tube wound with nichrome wire and enclosed in a metal case. The intervening space was packed with thermal insulation. The lower end of the inner tube was closed and a platform was erected to carry the electrode assembly so that the specimen was approximately in the centre of the furnace. The space above the electrode assembly was packed with firebrick. It was necessary to screen carefully the specimen and its electrode assembly and all the leads to the measuring instrument from external influence, particularly the 50 Hz mains supply. Accordingly, the inside of the furnace tube and platform was lined with an expanded metal screen, and on top of the furnace a cage of aluminium was constructed to screen the leads in the vicinity. A Sirect proportionality temperature controller, manufactured by CNS Industries Limited, regulated the temperature to within $\pm 1^{\circ}C$ for extended periods of time. The control and measuring thermocouples were insulated from the metal pot. The cold junction of the couple was immersed in a mixture of ice and water and the e.m.f. measured with a Cambridge sliding wire potentiometer.

An Ever Ready dry battery with a voltage selector was the source of an adjustable p.d. so that V_T, the p.d. measured by an Avometer across the Keithley electrometer and the glass, could be varied in discrete steps of 15 V from 0V to 60 volts.

The Keithley 610B electrometer was a versatile and very sensitive

instrument used to measure the currents flowing through the glass.

The electrical circuit is shown in Figure (8.4) and the resistance was calculated from the equation:

$$R_g = \frac{V_T - V_K}{i}$$

where V_K is the p.d. across the Keithley, i is the current flowing through the Keithley and the glass. The resistivity ρ and the conductivity χ can be calculated from:

$$\rho = \frac{1}{\chi} = \frac{R_g A}{\ell}$$

where A is the area of cross section and ℓ is the thickness of the glass.

The conductivity of the cordierite glass was determined as a function of temperature (Figure (8.5)).

8.3.3 Application of the field

The electrode assembly was modified slightly for the application of powerful fields. This change was necessary to accommodate a control sample in close proximity to the sample under the test. Thus any joule heating generated in the test specimen would be conducted through the control and the temperature of both control and test specimen would be comparable. The experimental arrangement shown in Figure (8.6) was devised in which the specimens discs T, M and B, 2 mm thick, were stacked with interleaving metal discs,and the field was applied to T and B while there was no field in the middle disc M. A comparison of nucleation rates in T and B with that in M was taken as a direct test of field effects alone, even if some joule heating occurred.

Figure 8.4 Electrical circuit for d.c. conductivity measurement

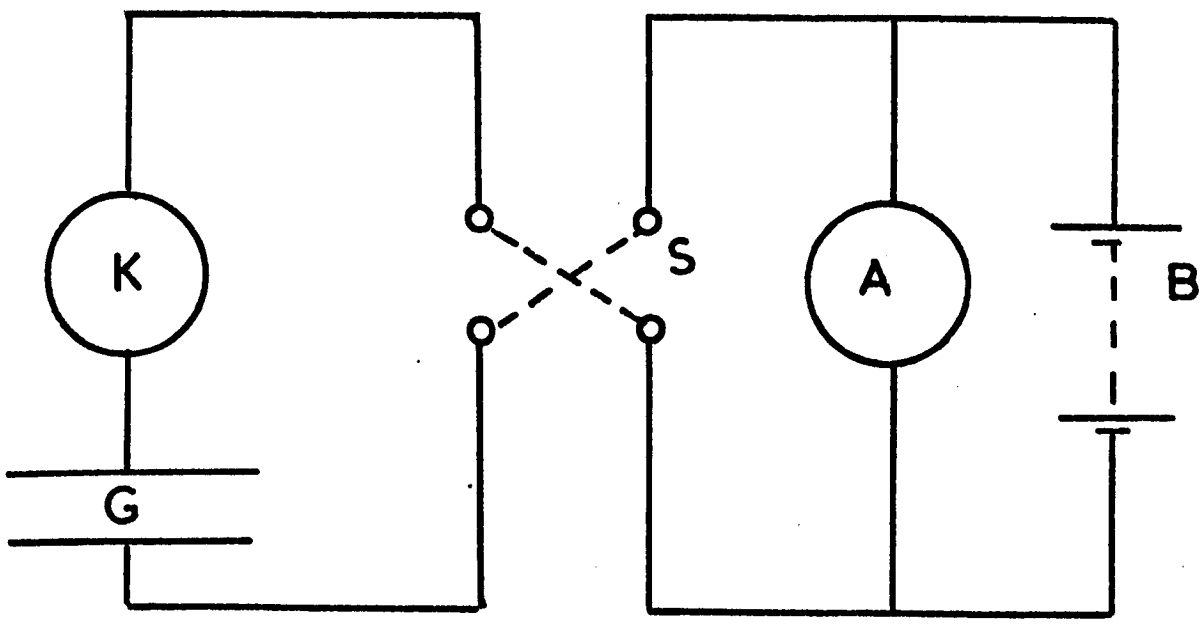

S TWO WAY SWITCH
B DRY CELL BATTERY
K KEITHLEY ELECTROMETER 610B
G GLASS AND ELECTRODE ASSEMBLY
A AVOMETER

Figure 8.5 Plot of $\log_{10} \chi$ (conductivity ohm^{-1} cm^{-1}) versus $\frac{1C^3}{T}$ ($°K^{-1}$) for magnesia aluminosilicate glass

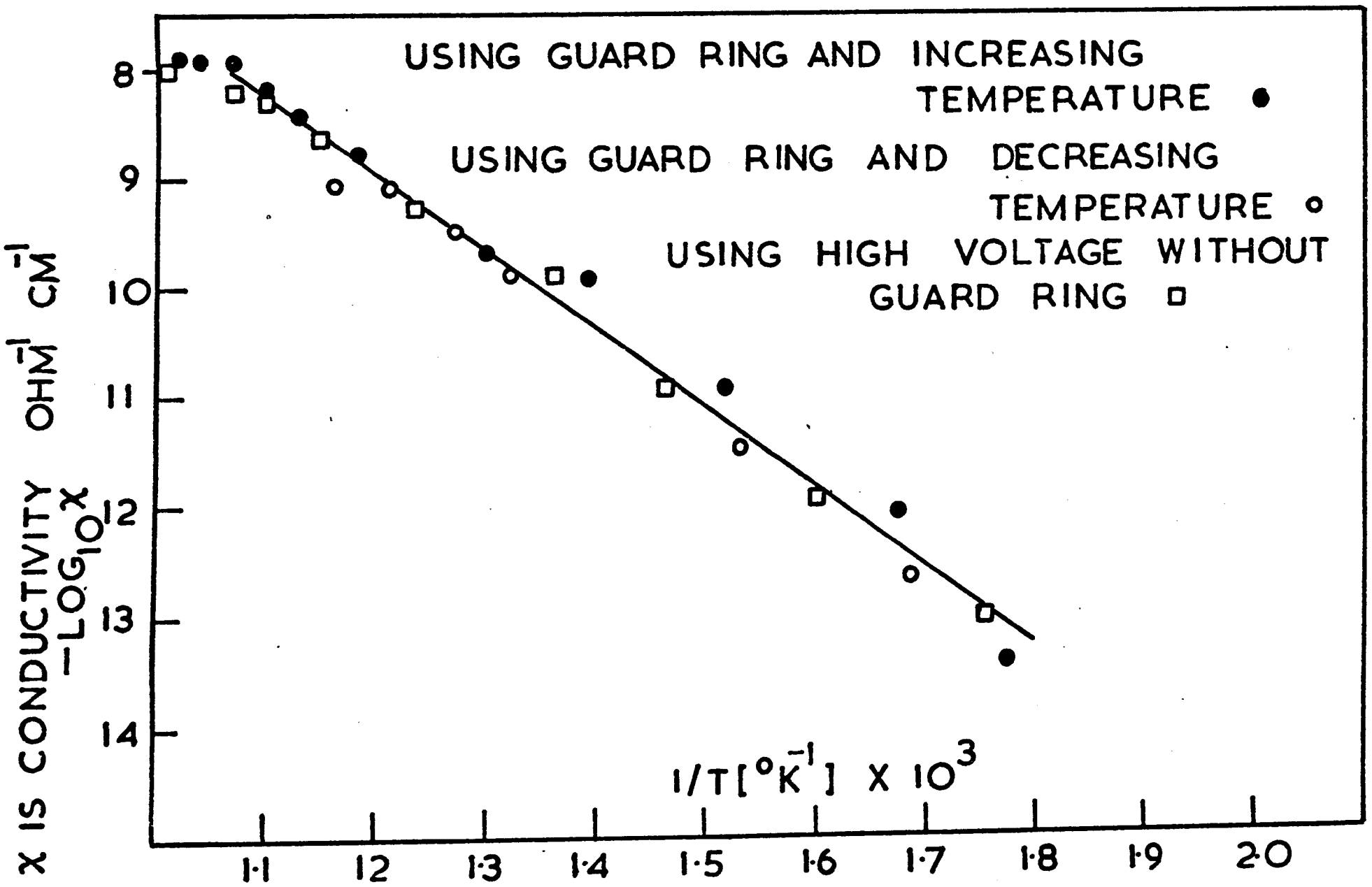
USING GUARD RING AND INCREASING TEMPERATURE ●
USING GUARD RING AND DECREASING TEMPERATURE ○
USING HIGH VOLTAGE WITHOUT GUARD RING □
χ IS CONDUCTIVITY OHM⁻¹ CM⁻¹
−LOG10 χ
8
9
10
11
12
13
14
1/T[°K⁻¹] X 10³
1·1
1·2
1·3
1·4
1·5
1·6
1·7
1·8
1·9
2·0

Figure 8.6 Part of the electrode assembly modified to accommodate a control specimen

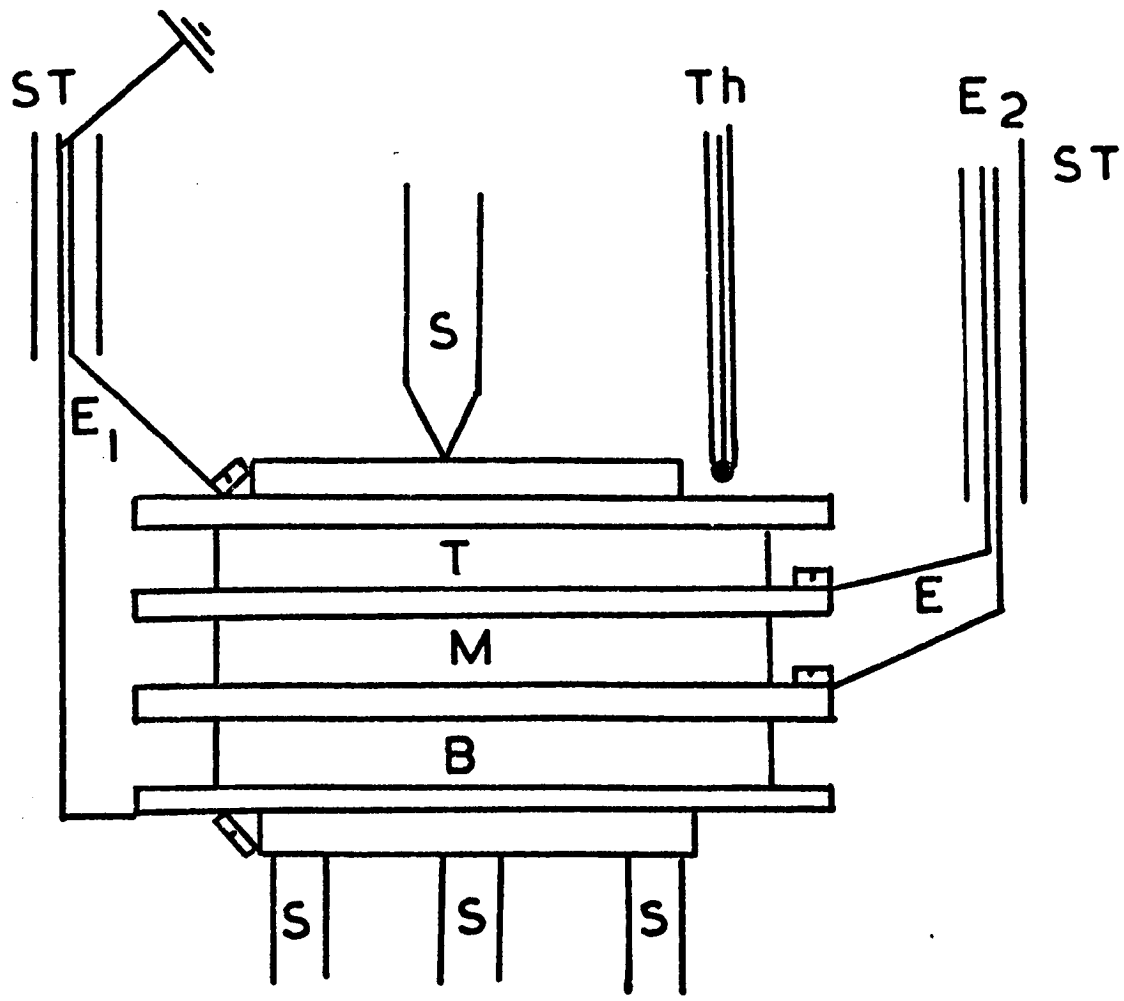

S FUSED SILICA RODS
ST FUSED SILICA TUBES
E_2 ELECTRODE CONTACTS
E_1 EARTHED CONTACT
E HIGH PONTENTIAL
Th THERMOCOUPLE
T TOP SAMPLE (FIELD APPLIED)
M CONTROL MIDDLE SAMPLE (NO FIELD APPLIED)
B BOTTOM SAMPLE (FIELD APPLIED)

The electrical circuit was altered slightly to accommodate a high resistance R_x ($R_x \ll R_{glass}$) to protect the Keithley instrument in the event of shorting.

Cordierite discs of 2 mm thickness and 3 cms diameter were used for the test runs. The resistivity of the glass at high applied voltages was similar to the predicted value from the log ρ versus 1/T plot (Figure (8.5)) constructed from the data obtained in the d.c. conducticity measurements using a guard ring. This established that the current was conducted through the glass over the entire electrode area. Thus it can be assumed that the field was applied through the volume of the glass and not across the surface.

The potential was supplied by an EHT set with an internal resistance of about ½ MΩ which delivered a smoothed d.c. voltage continuously up to 2000 volts.

Details of two runs are given in Table (8.1), The first run carried out at 720°C, using a p.d. of 4 kV cm^{-1}, was designed to follow closely the conditions used by de Vekey and Majumdar. In the first run, the magnitude of the field that could be applied was limited by electrical breakdown through the air between the metal electrodes at the temperature of the experiment. The second run was carried out at 800°C. The temperature 800°C was selected because phase separation and crystallization occurred rapidly and changes in the morphology caused by the field could be more easily detected. The maximum p.d. at 800°C was limited by the conductivity of the glass (avoiding excessive joule heating) and the internal resistance of the EHT generator.

The electrodes were inspected visually after completion of the run for evidence of electrolysis and the glass specimens were prepared for replication electron microscopy.

TABLE 8.1

DETAILS OF TWO RUNS ON A MAGNESIA ALUMINOSILICATE GLASS

Run	Time (mins)	Voltage difference across the sample volts cm^{-1}	Temperature °C
1	0	4000	721
	300	4975	720
	1520	4100	720
2	0	1500	802
	20	2450	800
	190	1950	799

8.3.4 Measurement of electric field influence on crystal nucleation and growth in $BaO-SiO_2$ glasses

Two $BaO2SiO_2$ batches that included 1 mol% Al_2O_3 and TiO_2 respectively were sintered, melted and cast into the form of discs about 4 cms diameter, and annealed in a muffle furnace at 620°C. These two glasses will be known as ABS_2 and TBS_2. The purpose of the small additions was to reduce the nucleation rates of the $BaO2SiO_2$ to values that could conveniently be measured after long heating times.

The electrical resistivity of slabs of the glass 2.25 cm^2 in cross-sectional area and 2 mm thick was measured without a guard ring and compared

with values published by Evstrop'ev and Kharyuzov[167], and Mashkovich and Varshal[168]. The similarity between the three sets of results showed that the guard ring was not necessary. (See figure (8.9)).

A Lynch bridge[169] was used to measure the a.c. conductivities and the dielectric permittivities ε of discs (2 mm thickness, 3 cms diameter) of the as-quenched $BaO-SiO_2$ glass, and also the glass ceramic formed from from the same glass by crystallizing at 700°C for 24 hours and then 1000°C for 24 hours. The permittivity values ε were employed in a calculation of the critical field strength using equation (8.10).

The apparatus used to apply and measure the large field was similar to that described previously with two exceptions. The resistivity of the $BaO-SiO_2$ glass was about fifty times lower than the corderite glass. Since the internal resistance of the EHT generator was about ½ MΩ, the greatest p.d. that could be applied was 50 volts - an unaceptably low value. The generator was replaced by an a.c. 5 kV transformer whose input was controlled by a variac. The alternating currents were measured on an Avometer.

After completion of a nucleation heat treatment with a high field applied, suitably sized samples from the top, middle and bottom sections were cut and the platinum removed. An appropriate heat treatment at 840°C developed the crystals to a size convenient for counting. One run was extended to allow the crystals to attain a size sufficiently large for observation in the electron microscope without an additional growth treatment. Surface replicas of the samples with and without a field were prepared and the diameters of the largest particles were measured. This subsidiary experiment allowed an assessment of the field effect on crystal growth to be made.

8.4 RESULTS AND DISCUSSION

8.4.1 The magnesia aluminosilicate glass

The micrographs (Figure (8.7)) show that liquid immiscibility occurred in magnesia aluminosilicate glasses at both 720 and 800°C but the phase boundaries were sharper at 800°C. Some crystals were observed at 800°C. In neither experiment could any differences be detected in the morphologies of the phase separation between the discs subjected to the field and that under no field, nor was any difference observed in the second experiment in the degree of crystallization.

In both experiments the current fell at first, indicating the occurrence of polarization (Table (8.1)). The decrease of the current observed during both experiments was relatively small and it is thought that only a small fraction of the total voltage was dropped across the surface polarised blocking layers. After a time the current rose to near the initial value. This possibly reflected a delayed diffusion of platinum ions into the glass. The appearance of the cathode platinum was marred by a greenish deposit, which under the microscope, presented the appearance of a mass of numerous crystals. The crystals may have formed by the crystallization of an alloy of sodium and platinum caused perhaps by overheating near the cathode. Deep craters also observed on the cathode, may be explained by non-uniformity of electrode application giving local melting or crystallization. It is interesting to note that MacKenzie and Brown[165,166] noted the appearance of numerous craters at the cathode during the electrolysis of an Al_2O_3-SiO_2 glass. They attributed these craters to the presence of water droplets formed locally by the recombination of hydroxyl ions and diffusing protons.

8.4.2 The baria silica glasses

The dielectric permittivities and conductivities are given in Figures (8.8), (8.9) and (8.10) for both glass and glass-ceramic.

The dielectric permittivity of the TBS_2 glass was constant within the temperature range (180 - 450°C) and approximately independent of the

Figure 8.7 Electron micrographs of liquid-liquid immiscibility and crystallization in a magnesia aluminosilicate glass

Top left: No field applied, 720°C, 1520 mins, Mag x47000

Top right: 4000 V cm^{-1} d.c. applied, 720°C, 1520 mins, Mag x47000

Bottom left: No field applied, 800°C, 2 hours, Mag x30000

Bottom right: 1500 V cm^{-1} d.c. applied, 800°C, 2 hours, Mag x38000

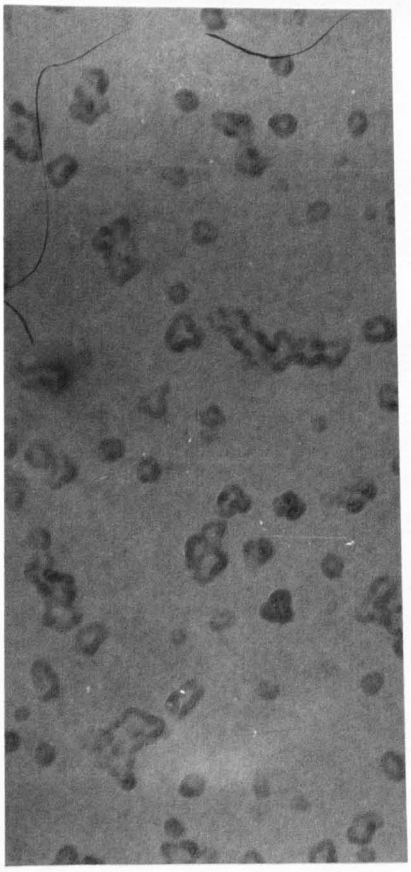

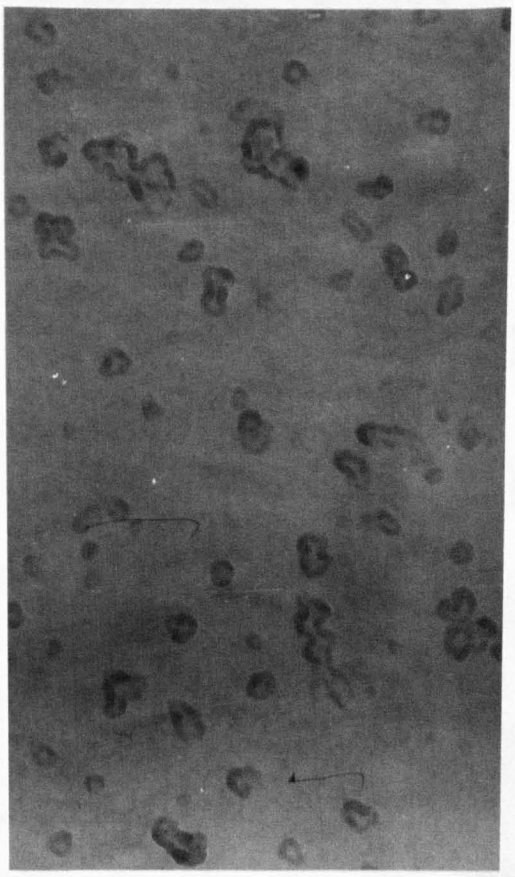

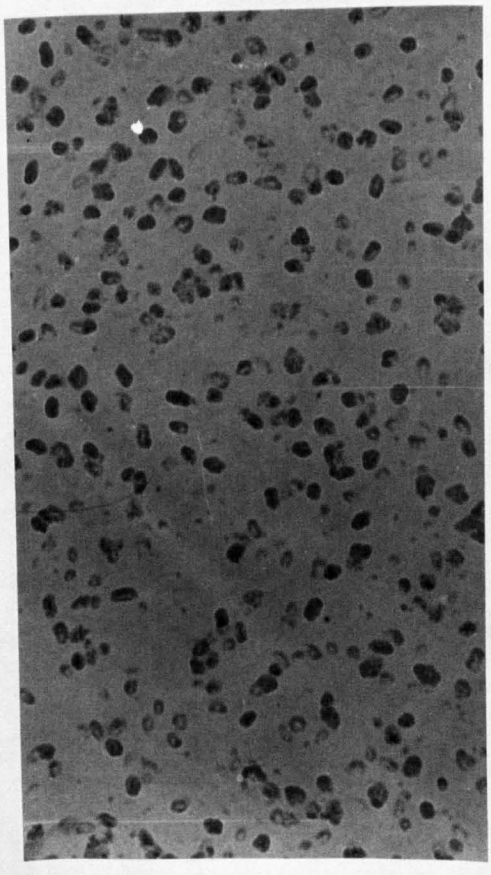

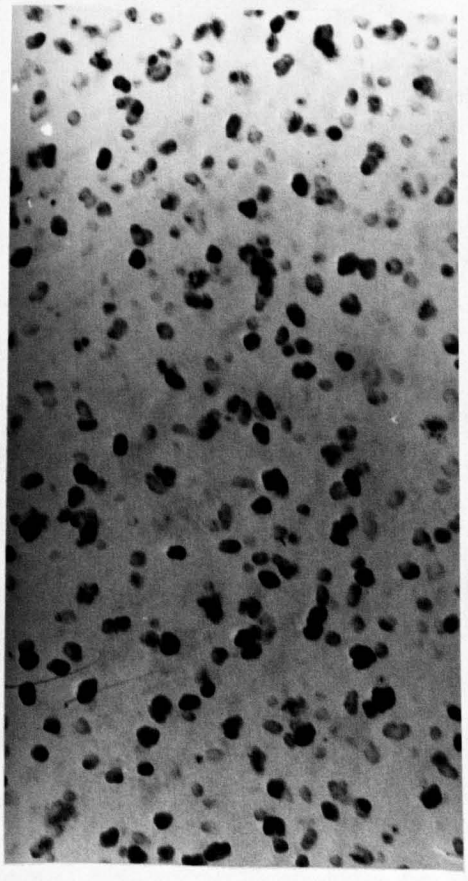

Figure 8.8 Plot of $\log_{10} \chi$ (conductivity ohm^{-1} cm^{-1}) versus $\frac{10^3}{T}$ ($°K^{-1}$) for ABS_2 glass and TBS_2 glass and glass-ceramic

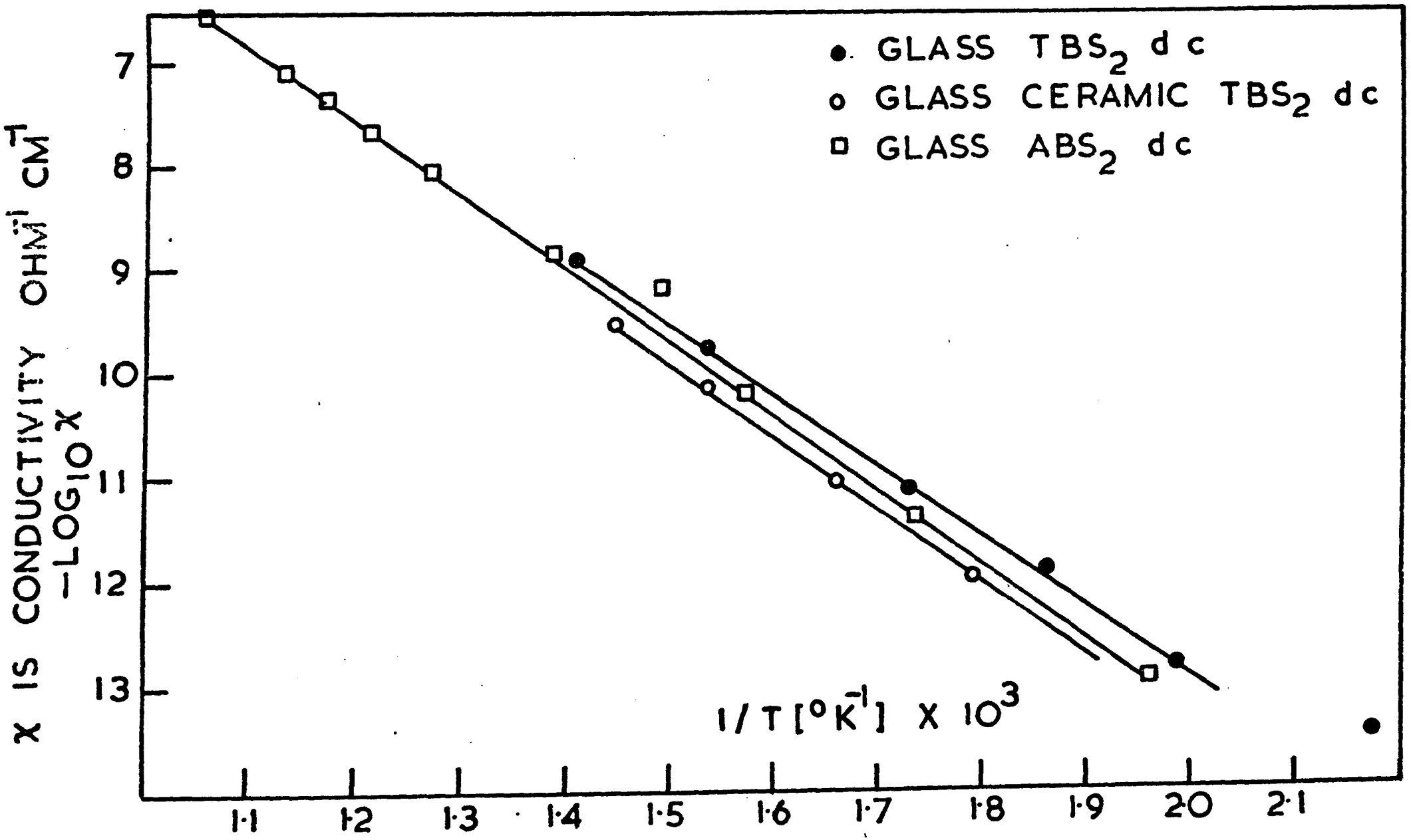
● GLASS TBS_2 d c
o GLASS CERAMIC TBS_2 d c
□ GLASS ABS_2 d c
χ IS CONDUCTIVITY OHM^{-1} CM^{-1}
$-\log_{10}\chi$
7
8
9
10
11
12
13
1/T [°K^{-1}] X 10^3
1·1
1·2
1·3
1·4
1·5
1·6
1·7
1·8
1·9
2·0
2·1

Figure 8.9 Plot of $\log_{10} \chi$ (conductivity $ohm^{-1}\ cm^{-1}$) versus $\frac{10^3}{T}$ ($^\circ K^{-1}$) for $BaO2SiO_2$ based glasses and glass-ceramics

Symbols		Data of Mashkocivh and Varshal[168] for $BaO2SiO_2$ glass
		Data of Mashkovich and Varshal[168] for $BaO2SiO_2$ glass-ceramic
	X	Data of Evstrop'ev and Khar'yozov for $BaO2SiO_2$ glass[167]
This work:	O	TBS_2 glass-ceramic d.c.
	●	TBS_2 glass d.c.
	Δ	TBS_2 glass a.c. 2×10^3 Hz
	▲	TBS_2 glass a.c. 10^4 Hz
	O	TBS_2 glass-ceramic a.c. 10^4 Hz
	O	TBS_2 glass-ceramic a.c. 2×10^3 Hz

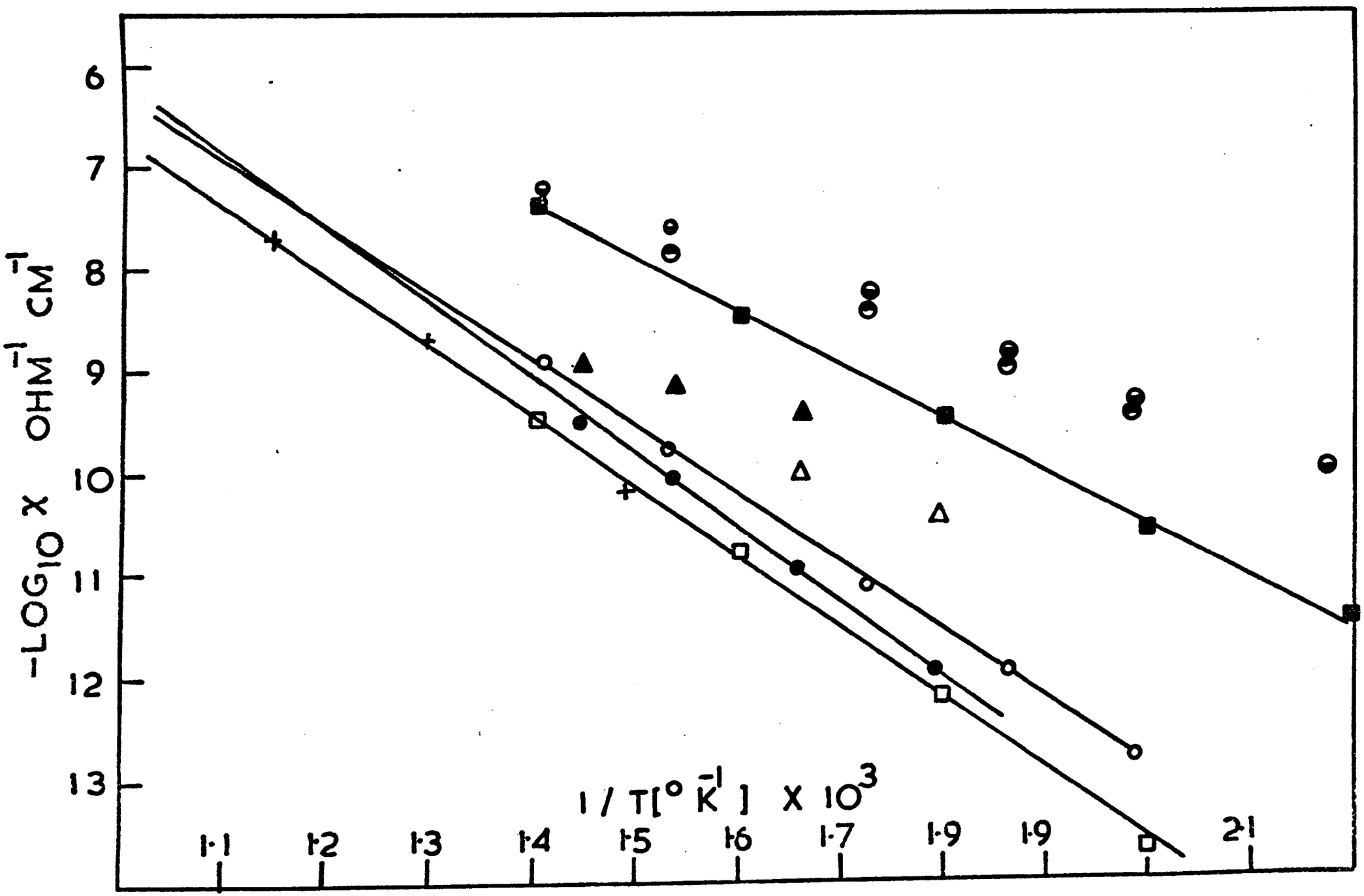
6
7
8
9
10
11
12
13
$-\log_{10} \chi$ OHM^{-1} CM^{-1}
1·1
1·2
1·3
1·4
1·5
1·6
1·7
1·9
1·9
2·1
1 / T[° K^{-1}] X 10^3

Figure 8.10 Plot of dielectric permittivity (ε) versus temperature ($^{\circ}C$) for TBS_2 glass and glass-ceramic

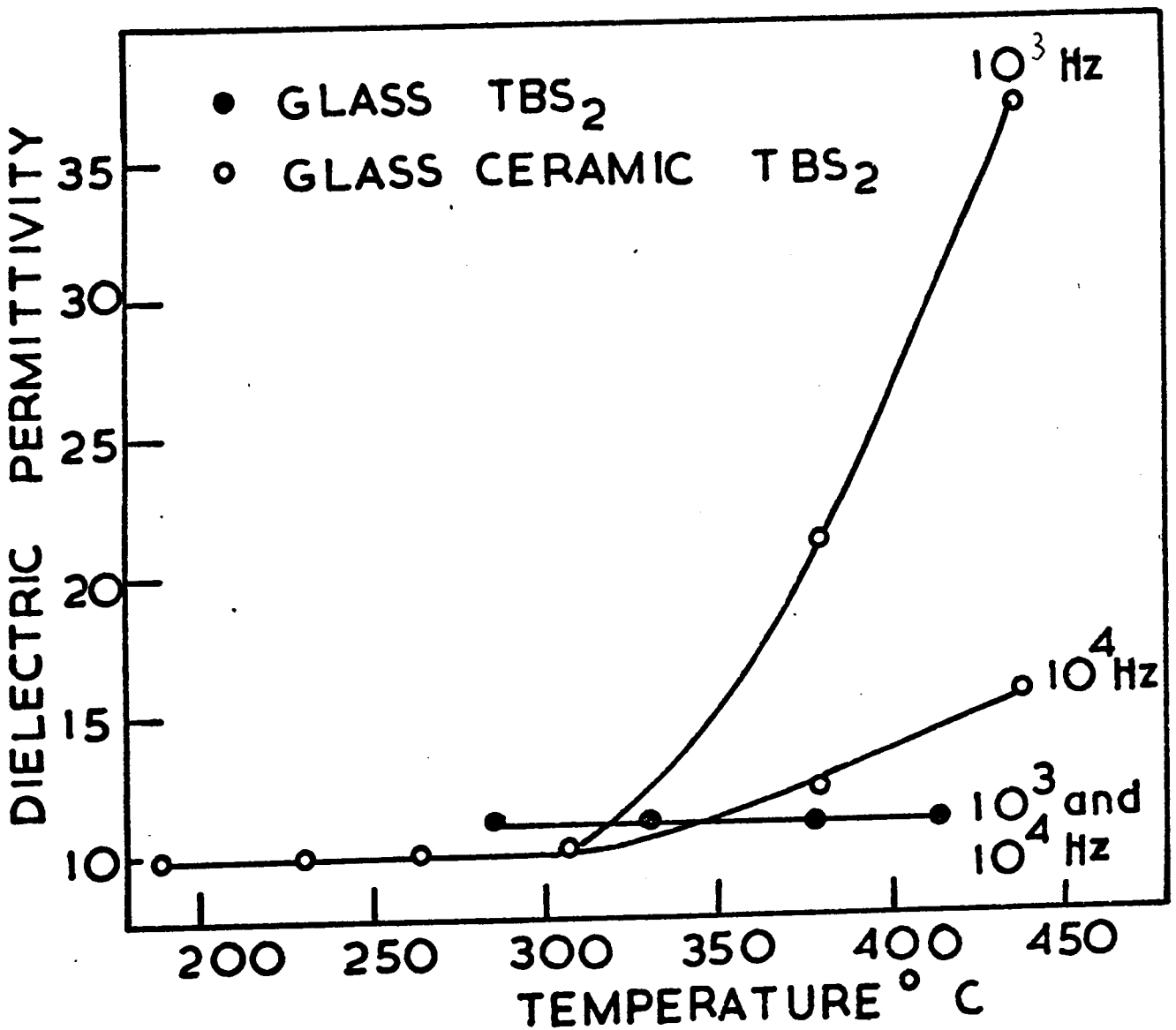
GLASS TBS2
GLASS CERAMIC TBS2
10^3 Hz
10^4 Hz
10^3 and 10^4 Hz
DIELECTRIC PERMITTIVITY
35
30
25
20
15
10
200
250
300
350
400
450
TEMPERATURE ° C

frequency used (10^3 to 10^4 Hz). The TBS_2 glass ceramic measurements exhibited values of permittivity that were constant at temperatures below 300°C but varied greatly with temperature and frequency above 300°C. This implied that a large dispersion occurred in the glass ceramic above 300°C.

The d,c, conductivities of both TBS_2 and ABS_2 glasses gave a linear plot of $\log_{10}X$ against reciprocal temperature which agreed closely with that of Mashkovich and Varshal[168] (see Figure (8.9)). The d.c. conductivities of the glass ceramic found by Mashkovich and Varshal were an order of magnitude hgher than those of the glass. The values found in the present work were only slightly above those for the glass but a very large dispersion was observed at very low frequencies. Thus the values found for 10^3 and 10^4 Hz were very similar to the d.c. values of Mashkovich and Varshal. The dispersion of the glass itself was very much smaller and at 50 Hz the a.c. conductivity was the same as the d.c. value. It is concluded that crystalline $BaO2SiO_2$ has a much higher conductivity (at 50 Hz) than the glass, approximating closely to the values found by Mashkovich and Varshal, but that the crystallized glass in the present work consisted of conducting crystal separated by insulating residual glass which showed a large Maxwell Wagner dispersion of conductivity and permittivity.

Most alkali containing glasses show an increase in resistivity during crystallization. The mobile alkali ions in the glass are incorporated within a crystal and are not as free to carry the current. Non-alkali glasses may contain alkali ion impurities that continue to fulfil an important role in conduction. Magnesia aluminosilicate glass, for example, was shown by Evstrop'ev et al[170], employing an isotope diffusion method, to conduct mainly by sodium ions. They also showed that alkali ion enrichment in the remaining vitreous phase in the glass ceramic explained

the overall rise in conductivity during crystallization.

Mashkovich and Varshal[168] repeated the experiment of Evstrop'ev et al on $BaO2SiO_2$ glass and found that the conductivity of the crystallized glass decreased only slightly on adding Na_2O and concluded that Na^+ in the residual glass phase of the glass ceramic cannot be carrying the current.

According to Evstrop'ev and Kharyuzov[167], the barium ions are the main current carriers in alkali-free barium silicate glasses. Mashkovich and Varshal suggested that the greater conductivity of the glass ceramic over the glass in the barium silicate system is not due to any residual glassy phase but is due to the mobility of electrons and the defects in the crystalline phase.

In the present work the activation energies for d.c. conductivities in the glass and glass ceramic are 15.2 and 13.8 kcals $mole^{-1}$ respectively (Figures (8.8) and (8.9). Mashkovich and Varshal obtained corresponding values of 14 and 10.5 kcals $mole^{-1}$. This suggests a lowering of the activation energy on crystallization.

The crystal nucleation and growth results on TBS_2 and ABS_2, with and without a field, are given in Table (8.2). The figures in brackets below the values obtained for discs T and B show the percentage change compared with the value for the field free disc M. It is seen that there is no consistent change produced by the field and that the percentage changes are less than the value of ±15% calculated for 95% confidence limits. It is concluded that there was no significant effect of the field on the rate of crystal nucleation in any of these runs. This is supported by the similar appearance of the optical micrographs (see Figure (8.11)). The sizes of the crystals are also not significantly altered by the field, indicating that the growth rates were not altered by the field.

Figure 8.11 a) Optical micrographs showing crystal density in a TBS_2 glass

Top left: 678°C, 1160 mins, no field applied, grown 840°C, Mag x600

Top right: 678°C, 1160 mins, 3.9×10^3 V cm^{-1} a.c. applied, grown 840°C, Mag x600

Figure 8.11 b) Electron micrographs showing size of crystals in an ABS_2 glass (with and without a field)

Bottom left: 706°C, 3310 mins, no field applied, Mag x37000

Bottom right: 706°C, 3310 mins, 2.2×10^3 a.c. applied, Mag x 37000

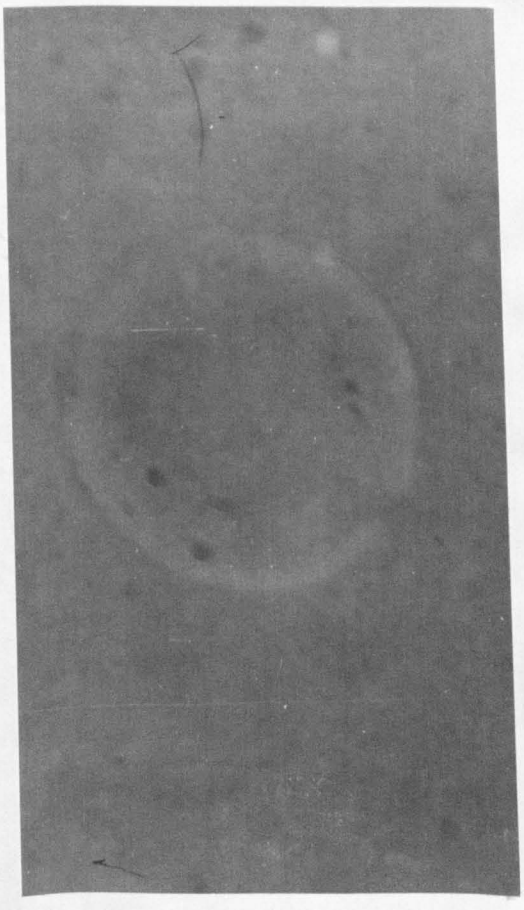

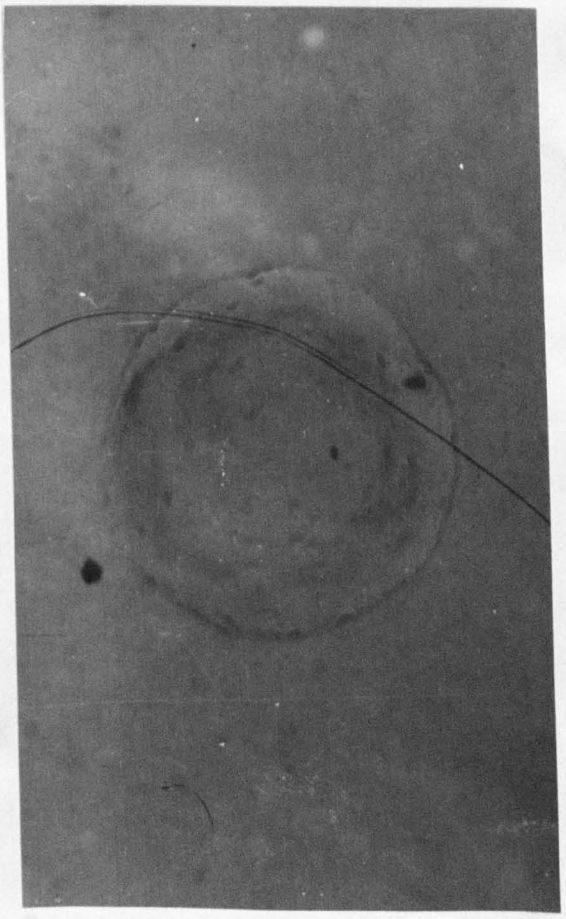

TABLE 8.2

HIGH FIELD EXPERIMENTS ON BARIA-SILICA GLASS

Run	Glass	Mean Field V cm^{-1}	Temp.°C	Time mins	Disc T	$N_V \times 10^{-8}$ cm^{-3} M	B
1	ABS_2	2.6×10^2 d.c.	685	185	6.13 (- 1.5%)	6.25	5.98 (- 8%)
2	ABS_2	2.4×10^3 a.c.	670	410	5.21 (+ 12%)	4.17	4.04 (- 12%)
3*	ABS_2	2.2×10^3 a.c.	706	3310	83.3 (+ 0%)	83.2	77.8 (- 6.5%)
4	TBS_2	3.9×10^3 a.c.	678	1160	12.8 (+ 0%)	12.8	13.5 (+ 5.5%)

* Run 3 size of pre-growth treatment spherulites (dia.)

With field 1.15×10^{-4} cms, without field 1.22×10^{-4} cms

Using the values of Mashkovich and Varshal[168] for the conductivity of the crystals and a permittivity (Figure (8.10)) of 10, the relaxation time ε_c/X_c is about 10^{-6} secs so that electrodynamic conditions apply to the experiments at 50 Hz and the conductivities control the field distribution. Using Mashkovich and Varshal's results for the conductivities of the glass ceramic at 685°C, the average temperatures of the runs, $f(\lambda) = - 0.64$. An estimate of the critical field E_c can be obtained from equation (8.10). Thus taking the enthalpy of fusion ΔH[18] as 8.6 kcals $mole^{-1}$, ...

the liquidus temperature as 1420°C and hence the undercooling at the average experimental temperature of 685°C as $\Delta T = 735°C$:

$$\Delta G_M = \frac{\Delta H_M \Delta T}{T_M} = 1.58 \times 10^{11} \text{ ergs mole}^{-1}$$

The interfacial energy between $BaO2SiO_2$ crystal and melt is $\sigma = 132 \pm 4$ ergs cm^{-2} [18] and the molar volume is 73.2 cm^{-3}. The critical radius r* without a field is given by:

$$r^* = \frac{2\sigma V_M}{\Delta G} = 1.225 \times 10^{-7} \text{ cms}$$

Equation (8.10) then gives $E_c = 1.43 \times 10^6$ V cm^{-1}. The calculation of E_c assumes the surface energy between the two phases is not altered by the field. This is quite reasonable in $BaO-SiO_2$ glasses since the field is likely to affect only the position of the mobile Ba^{2+} ions in the glass and not the rigid dimensional siliceous structure.

The calculated value of E_c is so large that no detectable effect could be produced by the fields of 10^3 to 10^4 V cm^{-1} which were used in the present experiments. Fields as high as 10^6 V cm^{-1} could not be applied continuously to $BaO2SiO_2$ glass at the temperature of nucleation since the power dissipation due to joule heating would be excessive. Furthermore, the value of E_c is of the order of the intrinsic breakdown strength of glass. If the undercooling was reduced by an order of magnitude the value of E_c would be reduced about 30 times; however, the rate of growth of spherulites, once nucleated, would then be so high that the rate of nucleation could not be determined reliably. Thus it would seem to be impossible to observe the change of nucleation rate due to a field predicted by classical thermodynamics for this system.

CHAPTER NINE

SUMMARY, CONCLUSIONS AND SUGGESTIONS FOR FUTURE WORK

CHAPTER NINE - SUMMARY, CONCLUSIONS AND SUGGESTIONS FOR FUTURE WORK

9.1 GENERAL

The importance of crystal nucleation, crystal growth and liquid-liquid immiscibility in the formation of glass ceramics was outlined. The thermodynamics of liquid-liquid immiscibility were discussed using free energy diagrams, and simple solution theories were considered. Theories of crystal nucleation and growth in glasses and the factors affecting crysallization were described. The possible influences of liquid-liquid immiscibility on crystal nucleation were outlined. This discussion was centred principally on the four points mentioned by Uhlmann[9]. Previous work designed to study the effect of liquid-liquid immiscibility on crystal nucleation in glasses were critically reviewed. It was concluded that the effect of immiscibility was far from understood and that further carefully chosen experiments were required to clarify the position.

9.2 CRYSTAL NUCLEATION STUDIES

Three experiments to examine the influence of liquid-liquid immiscibility on the kinetics of crystal nucleation in baria-silica glasses were performed.

In the first experiment six baria-silica glasses of different compositions were heat treated for one hour at a series of nucleation temperatures in the range 673-807°C followed by a growth treatment at a higher temperature. At lower temperatures (673-720°C) nucleation of barium disilicate crystals occurred in the glasses at quite different rates. However, from 720-807°C nucleation occurred in all the glasses at approximately the same rates. Liquid immiscibility was present in most of the glasses (except glasses 32 and 35G) heat treated at 720-807°C, but below 720°C all the glasses, with the exception of glasses 26 and 28, were free

from liquid immiscibility. The morphology of liquid phase separation was found to vary considerably with composition of the glasses. The occurrence of liquid immiscibility significantly affected the nucleation rates. Subsequently small quantities of alumina impurity were detected in the glasses. Experiment showed that 1 mole% Al_2O_3 could depress nucleation by approximately two orders of magnitude. A simple semi-empirical equation was derived to correct for the presence of the alumina. The crystal nucleation characteristics for each glass at lower temperatures were explained simply on the basis of their composition and proximity to the precipitating phase, barium disilicate. Nucleation theory predicts that nucleation behaviour in glasses should be sensitive to variation in composition. This is because the thermodynamic driving force ΔG for crystal nucleation, the crystal-liquid surface energy and the nucleation kinetic barrier are functions of composition.

The similar nucleation behaviour of the glasses at the higher temperatures could be explained most simply by a change in the composition of the baria-rich phase brought about by the phase separation process. This change to a composition richer in baria for the glasses within the immiscibility dome could cause an increase in ΔG, the thermodynamic driving force, giving an increase in crystal nucleation as a result of liquid immiscibility. There might also be a simultaneous decrease in the crystal-liquid interfacial free energy due to the composition change, which would also increase nucleation. In addition, a shift in composition to a more baria-rich phase might also decrease the kinetic barrier term and thus enhance crystal nucleation. This experiment did not enable the possibility to be ruled out entirely that hereogeneous nucleation effects might have occurred at the interfaces between the separated liquid phases but it was unlikely. Thus the different phase separation morphology of each glass was not reflected in the nucleation rates. It was also shown theoretically

that the heterogeneous nucleation mechanism was unlikely.

The effect of liquid phase separation in this system was to effectively increase the range of glasses which exhibited high nucleation rates by shifting the precipitating baria-rich phase closer in composition to barium disilicate (as determined by the immiscibility binodal curve). This general conclusion supported the work of Burnett and Douglas[15] who showed that immiscibility in the Na_2O-BaO-SiO_2 system effectively enhanced the region of internal nucleation in the system by a similar process to that described here.

To test the conclusions from experiment 1, two further experiments were carried out. In experiment 2, the development of liquid phase separation in glass 26 was found to have a marked influence on the rate of crystal nucleation. This was reflected in rapid changes of crystal nucleation rate during the early stages of phase separation. The phenomenon was most pronounced for quenched glasses that experienced rapid phase separation during the first few hours of heat treatment at 700°C. The nucleation time lag that occurred in glasses at low nucleation temperatures could not account for the results. No correlation was found between the nucleation curves and the interfacial areas or the number of droplets in the glass. Again, the results were explained successfully by a consideration of the composition changes that occur as a result of phase separation. These in turn influenced the thermodynamic driving force for crystal nucleation ΔG, the interfacial energy σ and the kinetic barrier, as described previously.

In experiment 3, similar conclusions were reached for glass 30. Unlike glass 26, a constant crystal nucleation rate occurred during the later stages of the experiment. It was shown that liquid immiscibility was completed at the beginning of the period of constant nucleation rate. The changes in crystal nucleation rate could be related to the development

of liquid immiscibility and the accompanying compositional changes as for 26. Again, no relation between morphology of phase separation and crystal nucleation rate was detected.

Attempts were made to deduce the mechanism by which crystal nucleation increased as the matrix composition shifted towards barium disilicate. Examination of the crystal growth rate data in the system suggested that changes in the kinetic barrier term in the nucleation equation during phase separation could account in part (but not whole) for the observed changes in nucleation rates. Calculations based on assuming ideal mixing between BaO and SiO_2 suggested that ΔG changes during phase separation might also account for a large part of the observed changes.

Further work on this system is needed to clarify the relative importance of the kinetic barrier, driving force and surface energy terms. Low temperature viscosity data would be useful to assess the effects during phase separation of a changing kinetic barrier. Experiments carried out on rapidly cooled glasses at lower temperatures (such as 700°C) could be particularly helpful in this respect in detecting changes in viscosity over extended periods of time, provided crystallization does not interfere with the results. To assess the influence of the driving force term more precisely detailed calculations are required using more realistic solution models. Charles[48] has calculated an unmixing curve assuming regular mixing between BaO and SiO_2. Unfortunately activity data of BaO was not known and the calculation could not be made for glasses richer in baria than the eutectic (~ 26 mole% BaO). Also, his predicted immiscibility dome was at appreciably higher temperatures than that observed experimentally by Seward et al[14]. Haller[28] has shown that regular mixing between $(SiO_2)_8$ and $BaO2SiO_2$ describes accurately, liquid immiscibility in the baria-silica system. Thus a more promising approach might be to estimate the liquid

free energy curves at 700°C and then calculate the ΔG effect on crystal nucleation during liquid phase separation.

A complete analysis of the phase separation effect should also include estimates of the magnitude of crystal-liquid interfacial energy changes during phase separation, although there is no direct means of doing this at present. Thus it may be only possible to estimate the effect of surface energy indirectly after elimination of the ΔG and kinetic barrier effects.

More generally, it would be appropriate to repeat the described investigation on other systems, i.e. systems that exhibit both phase separation and internal crystallization, such as Li_2O-SiO_2, Al_2O_3-SiO_2, and Na_2O-CaO-SiO_2, for comparison with the present results.

9.3 CRYSTAL GROWTH STUDIES

Early stage crystal growth in a BaO2SiO_2 glass was examined at 700°C using electron microscopy. The first crystalline particles to appear were small spheres, probably of h-BS_2. The spheres appeared after a negligible nucleation and growth induction time (~ ½ hr), and were composed of many small crystallites, approximately 100 Å in size, arranged radially.

After an induction time of 30-40 hours rapidly growing spikes began to grow from the spheres. The spikes were composed of a central spine, probably of ℓ-BS_2, and fine fibrillar crystallites growing laterally from the spine, probably composed of h-BS_2. The longitudinal growth rate of the spikes (spines) was about six times the radial growth rate of the sphere. The lateral growth rate of the spikes was similar to that of the spheres. The spikes continued to nucleate and grow until they formed a larger spherulite. The radial growth of the larger spherulites observed in the

optical microscope was identified with the longitudinal growth of the spikes. Also, the presence of an intercept time in crystal growth versus time plots for the spherulites was attributed to the spike (or spine) nucleation induction time during the early stages of growth.

All the glasses, both phase separated and non-phase separated, gave linear plots of spherulite radii versus time (constant growth rates) except at high temperatures (generally above 850-900°C), where curved plots were observed and growth rates increased with time. At low temperatures the plots gave intercepts on the time axis due to the induction time for formation of spikes already discussed above.

The linear growth plots were used to construct an Arrhenius plot of growth rate versus 1/T for each of the glasses. These Arrhenius plots were straight lines for all the glasses, with the exception of glass 30.

At the lower temperatures studied, the glasses undergoing phase separation had growth rates close to the glasses which did not separate and which were just outside the immiscibility boundary. However, at higher temperatures, the growth rates in the separated glasses tended to be much lower than the non-separated glasses. This was due to the variation in matrix (baria-rich) phase composition in the separated glasses with temperature (as determined by the immiscibility boundary), the shift being greater at lower temperatures. The same effect caused the slopes of the Arrhenius plots to be less for the phase separated glasses (apparent activation enthalpies ΔH_D about 95 kcals mol^{-1}) compared with the non-phase separated glasses (ΔH_D values about 120 kcals $mole^{-1}$).

The presence of alumina impurity was found to noticeably reduce the growth rates in some of the glasses although it had no effect on the measured ΔH_D.

The intercept time τ_1, attributed to the induction time for spike

formation, decreased with rise in temperature for all the glasses. The logarithm of the reciprocal of these times when plotted versus 1/T gave approximate straight lines. The activation enthalpies calculated from the slopes were similar to those obtained from the growth rates. It was suggested that the temperature dependence of the induction process was probably similar to the temperature dependence of the viscosity. However, the relative values of induction time for the glasses could not be explained in every case simply on the basis of variations in viscosity due to the different compositions and on the basis of changes in composition due to phase separation.

Further studies of the induction times for different glasses as a function of temperature might help to determine the factors affecting the induction process for spike formation. It would be useful to examine the effect (if any) of phase separation morphology on the intercept times by comparing glasses with coarse and fine scale phase separation. Low crystal growth temperature (700-720°C) should be employed for this work.

Possible reasons were discussed for the non-linear behaviour of crystal growth at higher temperatures in the baria-silica glasses. The presence of non-linear growth is of great interest since few examples have been observed in glass-forming systems. It was concluded that temperature changes in the vicinity of the crystal-liquid interface caused by the heat of crystallization were unlikely to explain the non-linear behaviour. Also, the existence of temperature profiles at the interface could not explain the crystallite branching processes responsible for the spherulitic morphology, since at the growth temperatures involved, growth rates decreased with increasing undercooling.

The effect of concentrations of major components (e.g. 'rejected' silica) or minor impurities (such as alumina or alkali) were also unlikely

to cause the non-linear growth behaviour. Thus rejected components or impurities, in most cases, probably did not build up ahead of the growth front but were entrapped within the residual glass between the growing spherulite fibres and were thus unable to influence growth. A possible exception was iron impurity, which has been shown to cause non-linear growth in another system[146,147]. Although the impurities did not cause non-linear growth they might have been responsible for the branching process causing the spherulitic morphology, in the manner suggested by Keith and Padden[139].

A possible reason for the non-linear growth could be the precipitation of cristobalite at higher temperatures causing a depletion of silica from the glass and an increase in the barium disilicate growth rate. However, the most likely reason was considered to be the occurrence of the spherulite to lath transformation of barium disilicate at the higher temperatures.

Further work is required to determine the cause of the non-linear growth. First, a more detailed study of the spherulite to lath transformation should be carried out using high resolution tansmission electron microscopy in conjunction with growth rate measurements. Secondly, electron probe microanalysis in the interface region might also indicate an accumulation of impurities, particularly iron. Further growth rate studies of the effect of deliberate additions of impurity would also be useful. Thirdly, it would be appropriate to extend the temperature profile analysis of Hopper and Uhlmann[150] described in section (7.4), to $BaO-SiO_2$ glasses. Also, experimental verification of the temperature profile could be achieved by observing the temperature variation of a thermocouple bead inserted in a glass adjacent to a crystal face.

There is considerable scope for further studies of the mechanism of spherulitic growth and the origin of the branching process. It would be of interest to study the crystallization of glasses with baria contents greater

than that of the disilicate composition, for comparison with the present results. The precipitation of other phases, such as $2BaO3SiO_2$ from baria-silica, could also be studied in detail. The effects of deliberate additions of small quantities of impurities on spherulite morphology (as studied by electron microscopy) and on growth kinetics, could provide further information on growth mechanisms and the factors controlling growth. In addition, it would be of interest to assess the effect of phase separation morphology on crystal growth in a silica-rich glass. At compositions near the baria-rich end of the immiscibility boundary, the phase separation morphology was shown not to have a large effect, probably because the baria-rich phase was continuous and the silica-rich phase was non-continuous (mainly droplets). However, for glass compositions much richer in silica, the baria-rich phase becomes non-continuous and may have an effect on the precipitation of barium disilicate crystals.

9.4 STUDIES OF THE EFFECTS OF ELECTRIC FIELDS

Static electric fields of approximately 4 kV cm^{-1} were found to have negligible effect on the phase separation and crystallization in a magnesia aluminosilicate glass. Similarly, the application of an alternating (50 Hz) electric field of approximately 4 kV cm^{-1} had no effect on the crystal nucleation and growth rates in a $BaO2SiO_2$ based glass. A calculation based on Isard's modification to Kaschiev's theory of field induced nucleation implied that a field of the order of 10^6 volts cm^{-1} was necessary to influence the nucleation rates. Extensive joule heating limited the magnitude of the applied field. However, this problem might be circumvented by employing a condenser system that discharges periodically and allows the resultant heat to be dissipated in the charging cycle. Thus a very large field could be applied intermittently to the glass.

Further work on the effects of electric fields should be carried out on glasses that possess the following characteristics: a) a high but measurable homogeneous nucleation rate, b) preferably simple compositions, c) as high an interfacial energy between crystals and liquid and as low a thermodynamic driving force as possible, to give a higher critical radius r*, d) a large difference in dielectric permittivity between crystals and glass - for example a high TiO_2 glass may precipitate high dielectric titanate crystals; e) a high electrical resistivity. Unfortunately, the requirement of high resistivity of the glass can only usually be satisfied at low temperatures where the size of the critical nucleus is small and E_c is large.

More success might be achieved if the kinetics of liquid phase separation were studied. A glass composition with a low miscibility temperature T_M will have a relatively larger r* for phase droplets at temperatures near Tg, where the electrical resistivity is also high.

APPENDIX

APPENDIX 5.1

CALCULATION OF N_v, THE NUMBER OF PARTICLES PER UNIT VOLUME

The following results were obtained for glass 32 nucleated for 4.5 hours at 700°C.

Mean Size of Particles in interval i $(\bar{D}_i = \frac{1}{Z_i})$ cm	Number of particles within size range i N_{A_i}	$N_{A_i} Z_i$ cm^{-1}
0.101	1	9.90
0.125	4	32.00
0.151	8	52.98
0.177	15	84.75
0.207	14	67.63
0.234	12	51.28
0.259	27	103.85
0.284	14	49.12
0.311	19	60.90
0.338	49	144.54
0.363	49	134.99
0.389	62	159.38
0.414	75	180.72
0.440	29	65.76
0.466	31	66.52
0.492	10	20.28
0.518	5	9.69
0.620	1	1.61

The area of the print was 284.14 cm^2 and the magnification of the print was 1008 times.

$$\sum_{i=1}^{n} N_{A_i} \bar{Z}_i = 1295.9$$

Substituting into equation (5.1)

$$N_v = \frac{2}{\pi} \times \frac{1295.9}{284.12} \times (1008)^3$$

$$= 2.97 \times 10^9 \ cm^{-3}$$

APPENDIX 5.2

CALCULATION OF THE ERRORS IN N_v, THE NUMBER OF PARTICLES PER UNIT VOLUME

A print depicting a typical area from glass 30 heated first at 780°C for one hour (to give phase separation) and then at 700°C for 9.25 hours (to give crystal nucleation) was divided into 14 equal areas of 15.2 cm^2. The number of particles N_A in the total area considered (i.e. 14 x 15.2 or 212.8 cm^2) was 361, about the average number of particles counted in a typical N_v calculation.

The values of N_v determined for each area are given below:

1.608, 1.460, 2.590, 1.185, 1.732, 1.552, 1.468, 2.085, 1.790,

1.930, 2.130, 1.272, 2.080, 1.475 (all N_v x 10^{-9} cm^{-3}).

Assuming the values are normally distributed, the standard deviation of n data is given by

$$\text{S.D.} = \frac{\sum_{i=1}^{n} (x_i - \bar{x})^2}{n - 1}$$

where x is the property (e.g. N_v, V_f, S_T etc.) whose statistical error is to be determined.

Standard error of the mean (S.E.) = $\frac{\text{S.D.}}{\sqrt{n}}$

The 95% confidence limits lie within the range:

$$\bar{x} \pm 2 \text{ S.E.}$$

In this example, $\bar{N}_v = 1.708 \times 10^9$

$\therefore$ S.D. = 0.50×10^9

S.E. = 0.134×10^9

$\therefore$ 95% confidence limits in N_v are 1.430×10^9 and 1.987×10^9 with the mean at 1.708×10^9, i.e. the 95% confidence limits are approximately ±16% of the mean.

A similar calculation was carried out on glass 30 heated, first at 780°C for one hour (to give phase separation) and then at 700°C for six hours to give crystal nucleation. Twelve areas of size 21.2 cm^2 were chosen, containing a total of 345 particles.

The mean value of N_v was 9.65×10^8 cm^{-3} and the 95% confidence limits were 8.2×10^8 and 11.11×10^8. In this case the confidence limits were approximately ±15% of the mean.

APPENDIX 5.3

CALCULATION OF VOLUME FRACTIONS

The following results were obtained for volume fractions in glass 26 phase separated at 900°C for 10 minutes, and are the number of grid points in a 16 point grid that fell within the dispersed phase:

.7, 4.5, 5. 6.5, 7.5, 6.5, 7.5, 8, 4.5, 5, 4, 6.5, 5.5, 6,

3.5, 4, 5.5, 7, 3.5.

The volume fraction for 20 trials is 31.25%.

Using equation (5.2), we can approximately calculate the number of counts necessary to limit the 95% confidence limits to within ±10% of the mean. The error required is:

$$0.313 \pm .031$$

i.e. $\sigma = .016$ and

$$N = \frac{0.313(1 - .3.3)}{(.016)^2} = 872 \text{ points}$$

or 55 trials

Thus 60 trials were used to estimate the volume percentages.

APPENDIX 5.4

CALCULATION OF THE INTERFACIAL AREA OF DISPERSED PHASE

The following data gives the number of interfaces that an arbitrary 10 cm line intersects on the two dimensional section (print).

20, 15, 16, 10, 11, 19, 8, 12, 10, 8, 15, 13, 15, 11, 12, 17, 11, 13, 11, 16, 19, 15, 13, 15, 15, 15, 14, 14, 14, 14, 11, 17, 12, 19, 10, 7, 17, 18, 15, 13. Average = 13.75.

The average number of interfaces per cm of line is 1.375. The magnification of the print is 70470 times and hence the number of intersections that are made per cm is

$$96800 = N_T$$

Substituting into equation (5.3) the surface area S_v is:

$$2 \times 96800 = 1.938 \times 10^5 \text{ cm}^2 \text{ cm}^3$$

The procedure used to calculate the 95% confidence limits is similar to that described in Appendix (5.2). The 95% confidence limits for the surface areas is 1.795×10^5 and 2.080×10^5 cm^2/cm^3 i.e. ±8% of the mean.

APPENDIX 5.5.

CALCULATION OF THE BEST STRAIGHT LINE FOR A LOG_{10}(GROWTH RATE) VERSUS $1/T^{\circ}K$ PLOT

Call $\frac{1}{T} = x$ and $\log_{10}$(growth rate) = y

$(x) \times 10^4$	y	$xy \times 10^3$	$x^2 \times 10^{-7}$
9.132	-6,09626	-5.5671	8.33934
9.328	-6.62206	-6.177	8.70115
9.551	-7.28233	-6.9553	9.12216
9.794	-7.84283	-7.6812	9.59224
8.711	-5.15243	-4.4882	7.58815
8.576	-4.84285	-4.1532	7.35477
8.873	-5.62342	-4.9896	7.87301
8.361	-4.58503	-3.8335	6.99063
8.197	-4.38405	-3.5936	6.71908
8.039	-4.15243	-3.3381	6.46255

$\bar{x} = 8.8562 \times 10^{-4}$ $\quad \bar{y} = -5.658371$ $\quad \sum x^2 = 7.87431 \times 10^{-6}$

$\bar{x^2} = 7.84322 \times 10^{-7}$ $\quad \sum xy = -.0507772$

Assuming that x is not subject to error, the best straight line by the method of least squares is given by

$$y - \bar{y} = m(x - \bar{x})$$

where m(slope) $= \dfrac{\sum xy - n\bar{x}\bar{y}}{\sum x^2 - n\bar{x}^2}$ (5.5A)

and n is the number of observations (in this case n = 10).

Substituting the data into equation (5.5A) the best value of m is 48970 K^{-1}. The activation enthalpy is

slope x 1.98×10^{-3} Kcals $mole^{-1}$

= 97.94 Kcals $mole^{-1}$

APPENDIX 6.1

According to theory, the nucleation rate is:

$$I = \frac{NkT}{h} \exp(-\frac{W^*}{kT}) \exp(-\frac{\Delta G_D}{kT})$$

Let us assume that addition of small quantities of alumina affect the free energy term in W^* but not σ or ΔG_D

$$I_1 \alpha \exp(-\frac{W^*}{kT})$$

where I_1 is the nucleation rate in pure glass. Henceforth, subscripts 1 2 refer to the pure glass and the impurity-containing glass respectively.

$$\frac{W^*}{kT} = \frac{16\pi\sigma^3 V_M^2}{3kT\Delta G_1^2} \sim \frac{A}{T\Delta G_1^2}$$

Also $$\frac{W_2^*}{kT} \sim \frac{A}{T\Delta G_2^2}$$

For a pure glass, the driving force for crystallization is

$$\Delta G_1 \sim - \frac{\Delta H \, \Delta T}{T_M'}$$

where ΔH is the enthalpy of fusion

ΔT is the undercooling

T_M' is the melting temperature

Assuming that small quantities of impurity depress the liquidus ideally, the driving force for crystallization

$$\Delta G_2 \sim \frac{\Delta H \, \Delta T}{T_M} - RT \ln Y$$

$$= \Delta G_1 - RT \ln Y$$

where Y is mole fraction of $BaO2SiO_2$

$$\therefore \quad \frac{W_2^*}{RT} = \frac{A}{T(\Delta G_1 - RT \ln Y)^2}$$

$$= \frac{A}{T \, \Delta G_1^2} \left(1 - \frac{RT \ln Y}{\Delta G_1}\right)^{-2}$$

On expanding, and assuming that $RT \ln << \Delta G_1$ for small additions of alumina (i.e. $Y \sim 1$):

$$\frac{W_2^*}{RT} \sim \frac{A}{T \, \Delta G_1^2} \left(1 + \frac{2RT \ln Y}{\Delta G_1}\right)$$

Comparing the nucleation rates I_1 (for pure glass) and I_2 (for impurity contaminated glass):

$$\frac{I_2}{I_1} = \frac{\exp\left(-\frac{A}{T \, \Delta G_1^2}\left[1 + \frac{2RT \ln Y}{\Delta G_1}\right]\right)}{\exp\left(-\frac{A}{T \, \Delta G_1^2}\right)}$$

$$= \exp\left(-\frac{A}{\Delta G_1^3}\left[2R \ln Y\right]\right)$$

$$\ln I_2 - \ln I_1 = -\frac{A}{\Delta G_1^3} (2R \ln Y)$$

$$\sim - B \ln Y$$

where $B = \dfrac{A\, T_M^{\,3}}{\Delta H_f^{\,3} (\Delta T)^3}$ ~ constant for a given ΔT

$$\ln I_2 - \ln I_1 \sim - B(1 - Y) \text{ if } Y \sim 1$$

$$\therefore \ln I_1 = \ln I_2 + B\, Y_A$$

where Y_A is mole fraction of impurity (alumina)

REFERENCES

1. Stookey, S.D. (1956), Brit. Pstent No. 752,243.

2. McMillan, P.W. (1964), 'Glass Ceramics', Academic Press, London.

3. Berezhnoi, A.I. (1970), 'Glass Ceramics and Photo Sitalls', Plenum Press, New York.

4. Pincus, A.G. (1971), 'Advances in nucleation and crystallization of glasses', p. 210 American Ceramic Society, Columbus, Ohio.

5. Beall, G.H. (1971), ibid, p. 251.

6. Ohlberg, S.M., Golob, H.R. and Strickler, D.W. (1962), 'Symposium on nucleation and crystallization in glasses and melts', edited by Reser, M.K., Smith, G. and Insley, H., p. 55. American Ceramic Society, Columbus, Ohio.

7. Vogel, W. and Gerth, K., ibid, p. 11.

8. Cahn, J.W. (1969), J. Am.Ceram.Soc., 52, p. 118.

9. Uhlmann, D.R. (1970), Disc. of the Faraday Society, Remarks, 118.

10. De Vekey, R.C. and Majumdar, A.J. (1970), Nature, 225, No.5228, p. 172.

11. Kaschiev, D. (1972), Phil. Mag., 25, p. 459.
(1972), J.Crystal Growth, 13/14, p. 128.

12. Isard, J.O., (1977), Phil. Mag., 35, p. 817.

13. Roth, R.S. and Levin, E.M. (1959), J.Res.Nat.Bur.Standards, 62, p. 193.

14. Seward III, T.P., Uhlmann, D.R. and Turnbull, D. (1968), J.Am.Ceram. Soc., 51, p. 278 and p. 634.

15. Burnett, D.G. and Douglas, R.W. (1971), Phys. Chem. Glasses, 12, p. 117. and idem (1970), Disc. Faraday Soc., 327-10-11, GaS, Paper 19.

16. MacDowell, J.F. (1965), Proc. Brit. Ceram. Soc., No.3, p. 101.

17. Freiman, S.W., Onada, G.Y. and Pincus, A.G. (1972), J.Am.Ceram.Soc., 55, p. 354.

18. Rowlands, E.G. (1976), 'Nucleation and crystal growth in the lithia-baria-silica system', Ph.D. thesis, University of Sheffield.

19. Turnbull, D. (1956), Solid State Physics, Vol.3, Academic Press, New York.

20. Cottrell, A.H. (1948), 'Theoretical Structural Metallurgy', p. 139, Arnold Press, London.

21. Darken, L.S. and Gurry, R.W. (1953), 'Physical Chemistry of Metals', McGraw Hill, New York.

22. Hildebrand, J.H. (1929), J.Am.Chem.Soc., 51, p. 66.

23. Levin, E.M. (1970), 'Phase Diagrams', Vol.3, p.143, edited by Alper, A.M., Academic Press, London.

24. Kracek, F.C. (1930), J.Am.Chem.Soc., 52, p. 1440.

25. Rawson, H. (1967), 'Inorganic glass-forming systems', Academic Press, London.

26. Moriya, Y., Warrington, D.H. and Douglas, R.W. (1967), Phys. Chem. Glasses, 8, p. 19.

27. Andreev, N.S., Goganov, D.A., Porai-Koshits, E.A. and Sokolov, Y.G. (1964), 'The Structure of Glass', Vol.3, p. 47, ed. Porai-Koshits, E.A., Consultants Bureau, New York.

28. Haller, W., Blackburn, D.H. and Simmons, J.H. (1974), J.Am.Ceram.Soc., 57, p. 120.

29. Hardy, H.K. (1953), Acta. Met., 1, p. 202.

30. Burnett, D.G. (1967), 'Liquid-liquid immiscibility in the soda-lime-silica glass-forming system', Ph.D. thesis, University of Sheffield.

31. Lumsden, J. (1952), 'Thermodynamics of Alloys', Institute of Metals, London.

32. Hammel, J.J. (1967), J.Chem.Phy., 46, p. 2234.

33. Van der Toon, L.J. and Tiedema, T.J. (1960), Acta Met., 8, p. 711.

34. De Fontaine, D. and Hilliard, J.E. (1965), ibid, 13, p. 1019.

35. Prigogine, I. and Defay, R. (1962), 'Chemical Thermodynamics', p. 418, Longmans, London.

36. Eskola, P. (1922), Am. J. Sci., 5th Series, 4, p. 345.

37. Greig, J.W. (1927), Am. J. Sci., 5th Series, 13, p. 27.

38. Douglass, R.M. (1958), Am. Miner., 43, p. 517.

39. Katscher, H., Rissert, G. and Liebau, F. (1973), Zeut. für Krist., 137, p. 146.

40. Oshlschlegal, G. (1971), Glastechn. Ber., 44, p.194 and (1975), J. Am.Ceram.Soc., 58, p. 148.

41. Katscher, H. and Liebau, F. (1965), Naturwiss, 52, p. 512.

42. Katscher, H. (1969), Acta Crystallog., 25, p. 107.

43. Katscher, H. and Liebau, F. (1966), Acta Crystallog., 21, p. 58.

44. Levin, E.M. and Cleek, G.W. (1958), J.Am.Ceram.Soc., 41, p. 175.

45. Cahn, J.W. and Charles, R.J. (1965), Phys. Chem. Glasses, 6, p. 181.

46. Toropov, N.A., Salakhov, S. Ya and Bondar, I.A. (1956), Bull. Acad. Sci. USSR, Div. chem. Sci., 6, p. 641.

47. Charles, R.J. (1967), Phys. Chem. Glasses, 8, p.185.

48. Argyle, J.F. and Hummel, F.A. (1963), Phys. Chem. Glasses, 4, p.103.

49. Benson, G.C. and Shuttleworth, R. (1951), J. Chem. Phys., 19, p. 130.

50. Cahn, J.W. and Hilliard, J.E. (1958), 28, p. 258.

51. Idem, ibid, (1959), 31, p. 688.

52. Volmer, M. and Weber, A. (1926), Z. Phys. Chem., 119, p. 227.

53. Becker, R. and Doring, W. (1935), Ann. Phys., 24, p. 719.

54. Christian, J.W. (1969), 'The theory of transformations in metals and alloys', Pergamon Press.

55. Turnbull, D. (1950), J. Chem. Phys., 18, p. 198.

56. Kaschiev, D. (1969), Surface Science, 14, p. 209.

57. Hillig, W.B. (1962), 'Symposium on nucleation and crystallization in glasses and melts', edited by Reser, M.K., Smith, G. and Insley, H., p. 77, American Ceramic Society, Columbus, Ohio.

58. Cahn, J.W. (1961), Acta Met., 9, p. 795.

59. Idem, ibid, (1962), 10, p. 179.

60. Idem, ibid, (1962), 10, p. 907.

61. Idem, J. Chem. Phys. (1965), 42, p. 93.

62. Seward III, T.P. (1970), 'Phase diagrams', Vol.1, p. 295, edited by Alper, A.M., Academic Press, London.

63. Fine, M.E. (1964), 'Introduction to phase transformations in condensed systems', Macmillan, London.

64. Russel, K.C. (1970), 'Phase transformations', p. 219, edited by Aronson, H.I., Am. Soc. Metals distributed by Chapman and Hall, London.

65. James, P.F. (1974), Phys. Chem. Glasses, 15, p. 95.

66. Matusita, K. and Tashiro, M. (1973), J. of Non-Crystalline Solids, 11, p. 471.

67. Turnbull, D. and Fisher, J.C. (1949), J. Chem. Phys., 17, p. 71.

68. Hillig, W.B. and Turnbull, D. (1956), J. Chem. Phys., 24, p. 914.

69. Hillig, W.B. (1966), Acta Met., 14, p. 1868.

70. Jackson, K.A. (1958), 'Nature of solid-liquid interfaces', in "Growth and perfection of crystals", Wiley, New York.

71. Frank, F.C. (1950), Proc. Roy. Soc., A 201, p. 586.

72. Zener, C. (1949), J. App. Phys., 20, p. 950.

73. Vergamo, P.J. and Uhlmann, D.R. (1970), Phys. Chem. Glasses, 11, p. 30.

74. Wagstaffe, F.E. (1969), J. Am. Ceram. Soc., 52, p. 650.

75. Meiling, G.S. and Uhlmann, D.R. (1967), Phys. Chem. Glasses, 8, p. 62.

76. Magill, J.H., and Plazek, D.J. (1967), J. Chem. Phy., 46, p. 3757.

77. Greet, R.J. (1967), J. Cryst. Growth, 1, p. 195.

78. De Luca, J.P., Eagan, R.J. and Bergeron, C.G. (1969), J. Am. Ceram. Soc., 52, p. 322.

79. Matusita, K. and Tashiro, M., (1973), J. Ceram. Ass. Japan, 81, p. 500.

80. Leontjewa, A. (1941), Acta Physiocochim. ARSS, 14, p. 245.

81. Dietzel, A. and Wickert, H. (1956), Glastech. Ber., 29, p. 1.

82. Morley, J.G. (1966), Glass Tech., 6, p. 77.

83. Eagan, R.J., De Luca, J.P. and Bergeron, C.G. (1970), J. Am. Ceram. Soc., 53, p. 214.

84. Burnett, D.G. and Douglas, R.W. (1970), Phys. Chem. Glasses, 11, p. 125.

85. Ohlberg, S.M. and Hammel, J.J. (1965), Paper 32, 7th Int. Congress on glass, Brussels.

86. Ohlberg, S.M. and Hammel, J.J. (1965), J. App. Phys., 36, p. 1442.

87. Greenwood, G.W. (1956), Acta Met., 4, p. 243.

88. Lifshitz, I.M. and Slyozov, V.V. (1961), J. Phys. Chem. Solids, 19, p. 35.

89. Wagner, C. (1961), Z. Elektrochem., 65, p. 581.

90. Haller, W. (1965), J. Chem. Phys., 42, p. 686.

91. McCurrie, R.A. and Douglas, R.W. (1967), Phys. Chem. Glasses, 8, p. 132.

92. Uhlmann, D.R. (1971), 'Advances in nucleation and crystallization of glasses', p. 91, Am. Ceram. Soc., Columbus, Ohio.

93. James, P.F. and McMillan, P.W. (1970), Phys. Chem. Glasses, 11, p. 59; ibid, (1970), 11, p. 64.

94. Zarzycki, J. and Naudin, F. (1967), ibid, 8, p. 11.

95. Neilson, G.F. (1972), ibid, 13, p. 70.

96. Mahoney, R., Srinivasan, G.R., Macedo, P.B., Napolitano, A. and Simmons, J.H. (1974), ibid, 15, p. 24.

97. Oehlschlegal, G. (1971), Glastech. Ber., 44, p. 194, and (1975), J. Am. Ceram. Soc., 58, p. 148.

98. Tanikawa, H. and Tanaka, H. (1967), Osaka Kogya Gijutsu Shikensho Kiho, 18, p. 230.

99. The structure of glass (1964), edited by Porai-Koshits, E.A., Vol.3, Consultants Bureau, New York.

100. Stookey, S.D., 'Catalysed crystallization of glass in theory and practice', (1959), Glastech. Ber., 32K, V International Glass Congress, Heft V.

101. Roy, R. (1960), J. Am. Ceram. Soc., 43, p. 670.

102. Kalina, A.M., Filipovich, V.N., Kolesova, V.A. and Bondor, I.A. (1964), The structure of glass, vol.3, p. 53, edited by Porai-Koshits, E.A., Consultants Bureau, New York.

103. Buzhinskii, I.M., Sabaeva, E.I. and Khomyakov, A.N. (1964), ibid, p. 133.

104. Vogel, W. (1966), Glass Tech., 7, p. 15.

105. Idem, (1965), VII International Congress on glass, Paper 33, Brussels.

106. Idem, (1971), Structure and crystallization of glasses, Pergamon Press.

107. Maurer, R.D. (1962), J. App. Phys., 33, p. 2132.

108. Idem (1962) 'Symposium of nucleation and crystallization in glasses and melts', p. 55, Am. Ceram. Soc., Columbus, Ohio.

109. Doherty, P.E., Lee, P.W. and Davis, R.S. (1967), J. Am. Ceram. Soc., 50, p. 77.

110. Bayer, G. and Hoffman, W. (1966), Glass Tech., 7, p.94.

111. Takusagawa, N. and Saito, H. (1970), J. Ceram. Soc. Japan, 78, p. 411.

112. Leger, L. and Bray, J. (1968), Silicate Industriel, 33, p. 257.

113. Kawazawa, T., Nakai, A. and Kawazoe, H. (1972), J. Ceram. Soc. Japan, 80, p. 456.

114. Hummel, F.A., Tien, T.Y. and Kim, K.H. (1960), 43, p. 31.

115. Partridge, G. and McMillan, P.W. (1963), Glass Tech., 4, p. 173.

116. Phillips, S.V. and McMillan, P.W. (1965), Glass Tech., 6, p. 46.

117. James, P.F. Unpublished data.

118. Harper, H., James, P.F. and McMillan, P.W. (1970), Disc. of the Faraday Soc., 50, p. 206.

119. Harper, H. and McMillan, P.W. (1972), Phys. Chem. Glasses, 13, p. 97.

120. Nakagawa, K. and Izumitani, T. (1969), Phys. Chem. Glasses, 10, p. 179.

121. Tomozawa, M. (1972), Phys. Chem. Glasses, 13, p. 161.

122. Matusita, K. and Tashiro, M. (1973), Phys. Chem. Glasses, 14, p. 77.

123. Idem (1974), Phys. Chem. Glasses, 15, p. 106.

124. Mukerjee, S.P. and Rogers, P.S. (1967), Phys. Chem. Glasses, 8, p. 81.

125. Lyng, S. (1968), Glass Tech., 9, p. 179; also
Lyng, S., Markali, J., Krogh-Moe, J. and Lundberg, N.H. (1970) Phys. Chem. Glasses, 11, p. 6.

126. Kokubo, T., Yamashito, K. and Tashiro, M. (1973), 81, p. 132.

127. Blinov, V.A. (1969), J. Mat. Sci., 4, p. 461.

128. Barry, T.I., Clinton, D., Lay, L.A., Mercer, R.A. and Miller, R.P. (1969), J. Mat. Sci., 4, p. 596; and
Idem, (1970), ibid, 5, p. 117.

129. James, P.F. and Keown, S.R. (1974), Phil. Mag., 30, p. 789.

130. James, P.F. and McMillan, P.W. (1968), Phil. Mag., 18, p. 863.

131. Fullman, R.L. (1953), Trans. Metall. Soc., A.I.M.E., 197, p. 447.

132. De Hoff, R.T. and Rhines, F.N. (1961), Trans. Metall. Soc., A.I.M.E., 221, p. 975.

133. De Hoff, R.T. (1968), 'Quantitative Microscopy', McGraw-Hill, New York.

134. Hilliard, J.E. and Cahn, J.W. (1961), Trans. Metall. Soc. A.I.M.E., 221, p. 344.

135. Smith, C.S. and Guttman, L. (1953), J. of Metals, Trans, A.I.M.E. p. 81.

136. Bockris, J.O.M., MacKenzie, J.D. and Kitchener, J.A. (1955), Trans Faraday Soc., 55, p. 1734.

137. Scholes, S. (1970), Disc. of the Faraday Soc. Remarks, 6A.

138. Keith, H.D. and Padden, F.J. (1963), J. App. Phys., 34, p. 2409.

139. Morse, H.W. and Donnay, J.D.H. (1933), 18, p. 66.

140. Peddle, C.J. (1927), 'Defects in glass', p. 114-124, Glass publication Limited.

141. Holland, A.J. and Prestin, E., (1937), J. Soc. Glass Tech., 21, p. 395.

142. Bowen, N.L. (1918), J. Am. Ceram. Soc., 1, p. 594; and Idem, (1919), ibid, 2, p. 261.

143. Tomozawa, M. (1973), Phys. Chem. Glasses, 14, p. 112.

144. Ogura,T., Hayami, R. and Kadota, M. (1968), J. Ceram. Assoc. Japan, 76, p. 277.

145. Cullity, B.D. (1967), 'Elements of X-ray diffraction', Addison-Wesley publishing company, inc.

146. Williamson, J. Tipple, A.J., and Rogers, P.S. (1968), J. Iron Steel Inst., 206, p. 898.

147. Idem, (1969), J. Mst. Sci., 4, p. 1069.

148. Toropov, N.A. and Tigonen, G.V. (1965), Inorg. Mater., 1, p. 711; and ibid, (1965), 1, p. 1821.

149. Wagstaffe, F.E., Brown, S.D. and Cutter, I.B. (1964), Phys. Chem. Glasses, 5, p. 76.

150. Hopper, R.W. and Uhlmann, D.R. (1973), J. Cryst. Growth, 19, p. 177.

151. Chalmers, B. (1964), 'Principles of Solidification', Wiley and Sons Inc., New York.

152. Motoc, C. (1972), J. Cryst. Growth, 12, p. 309.

153. Bartlett, J.T., Van den Heuval, A.P. and Mason, B.J., (1963), J. App. Math. Phys. (Z.A.M.P.) 14, p. 599.

154. Crowther, A.G. (1972), 'The growth of ice crystals in electric fields', Ph.D. thesis, UMIST, Manchester.

155. Murayami, Y., Kashiwagi, K. and Matsumoto, M. (1971), J. Phys. Soc. Japan, 31, p. 303.

156. Chopra, K.L. (1966), J. App. Phys., 37, p. 2249.

157. Peters, C.T., Bolton, P. and Miodiownik, A.P. (1972), Acta Met., 20, p. 881.

158. Thornburg, D.D. and White, R.M. (1972), J. App. Phy., 43, p. 4609.

159. Thornburg, D.D. (1973), J. Electronic Mat., 2, p. 3.

160. Takamori, T., Roy, R. and McCarthy, G.J. (1970), Mat. Res. Bull., 5, p. 529.

161. Tomlinson, J.L. (1972), J. Electronic Mat., 1, p. 357.

162. Chaudhari, P. and Laibriwitz (1972), Thin Solid Films, 12, p. 239.

163. Geller, I.K., Kolomiets, B.T., Popov, A.I. and Balakhtov, G.M. (1972), Neorg. Mater., 8, p. 1005.

164. Atkinson, D.I.H. (1975), Ph.D. Thesis, University of Warwick.

165. MacKenzie, K.J.D. and Brown, I.W.M. (1975), J. Thermal Analysis, 7, p. 619.

166. Idem, (1975), ibid, p. 3.

167. Evstrop'ev, K.K. and Rhar'yozov, V.A. (1961), Dokl. Akad. Naul. SSSR, 136, p. 140.

168. Mashkovich, M.D. and Varshal, B.G. (1969), Neorg. Mater., 5, p. 335.

169. Lynch, A.C. (1957), Proc. Inst. Elec. Engrs, 104B, p. 363.

170. Evstrop'ev, K.K., Pavlova, G.A. and Pavlovskii, V.K. (1966), Zh. Prik. Khim, 39, p. 452.

171. Lewis, M.H. and Smith, G. (1976), J. Mat. Sci., 11, p. 2015.